STUDY AND DESIGN OF CRYOGENIC PROPELLANT ACQUISITION SYSTEMS. VOLUME 2: SUPPORTING EXPERIMENTAL PROGRAM

MCDONNELL-DOUGLAS ASTRONAUTICS CO.,
HUNTINGTON BEACH, CALIF

DEC 1973

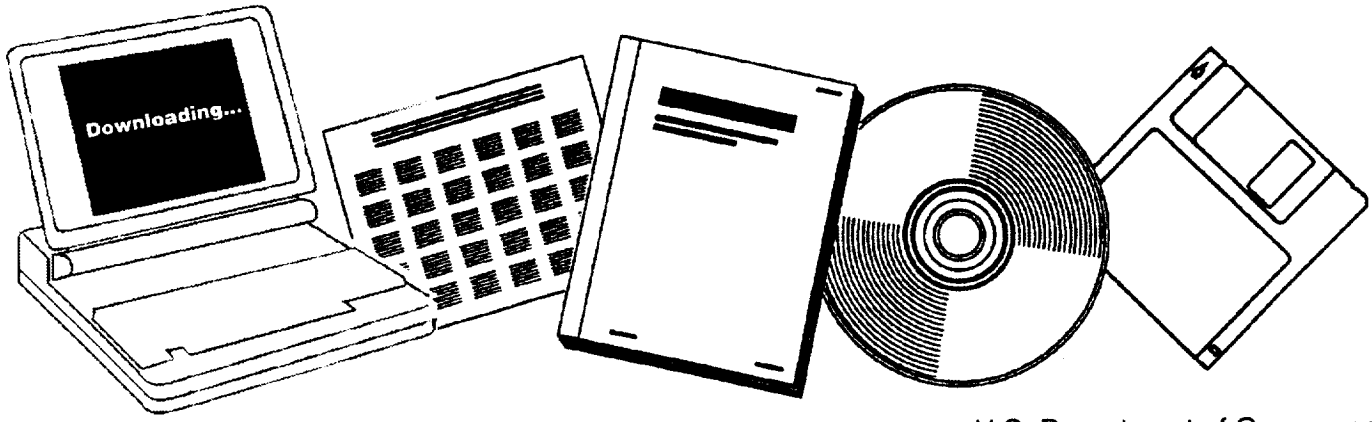

Tailored to Your Needs!

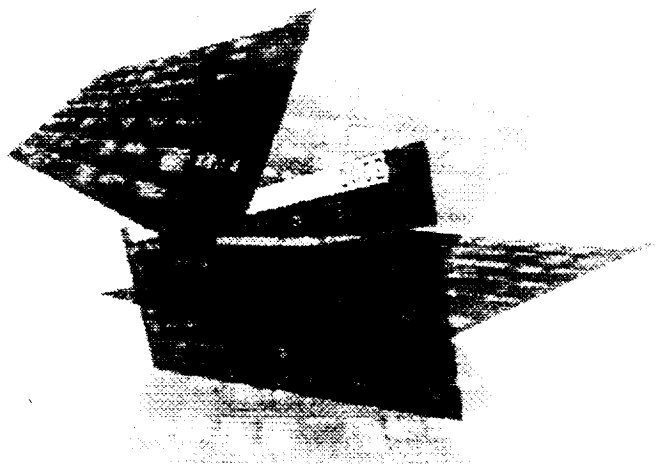

Selected Research In Microfiche

SRIM® is a tailored information service that delivers complete microfiche copies of government publications based on your needs, automatically, within a few weeks of announcement by NTIS.

SRIM® Saves You Time, Money, and Space!

Automatically, every two weeks, your SRIM® profile is run against all *new* publications received by NTIS and the publications microfiched for your order. Instead of paying approximately $15-30 for each publication, you pay only $2.50 for the microfiche version. Corporate and special libraries love the space-saving convenience of microfiche.

NTIS offers two options for SRIM® selection criteria:

Standard SRIM®–Choose from among 350 pre-chosen subject topics.

Custom SRIM®–For a one-time additional fee, an NTIS analyst can help you develop a keyword strategy to design your Custom SRIM® requirements. Custom SRIM® allows your SRIM® selection to be based upon *specific subject keywords*, not just broad subject topics. Call an NTIS subject specialist at (703) 605-6655 to help you create a profile that will retrieve only those technical reports of interest to you.

SRIM® requires an NTIS Deposit Account. The NTIS employee you speak to will help you set up this account if you don't already have one.

For additional information, call the NTIS Subscriptions Department at 1-800-363-2068 or (703) 605-6060. Or visit the NTIS Web site at *http://www.ntis.gov* and select SRIM® from the pull-down menu.

U.S. DEPARTMENT OF COMMERCE
Technology Administration
National Technical Information Service
Springfield, VA 22161 (703) 605-6000
http://www.ntis.gov

MDC G5038

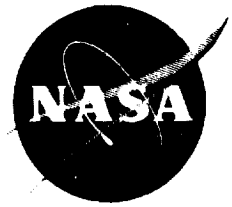

STUDY AND DESIGN OF CRYOGENIC PROPELLANT ACQUISITION SYSTEMS

VOLUME II
SUPPORTING EXPERIMENTAL PROGRAM

Final Report
December 1973

by

G. W. Burge
J. B. Blackmon, Ph.D.

McDonnell Douglas Astronautics Company
Huntington Beach, California 92647

Prepared for

NATIONAL AERONAUTICS AND SPACE ADMINISTRATION
Marshall Space Flight Center
Huntsville, Alabama
Contract NAS8-27685

FIGURES

TABLES

SECTION 1. INTRODUCTION

As the feed system studies reported in Volume I evolved, areas were identified where critical experimental information was needed either to define a design criteria or to establish the feasibility of a design concept or a critical aspect of a particular design. Such data requirements fell into three broad categories: (1) basic surface tension screen characteristics; (2) screen acquisition device fabrication problems; and (3) screen surface tension device operational failure modes. To explore these problems and to establish design criteria where possible, extensive laboratory or bench test scale experiments were conducted. In general, these proved to be quite successful and, in many instances, the test results were directly used in the system design analyses and development. In some cases, particularly those relating to operational-type problems, areas requiring future research were identified, especially screen heat transfer and vibrational effects. Some of this work was reinforced by MDAC Independent Research and Development projects and is covered to a limited extent.

In Section 2 of this volume, each experiment undertaken is discussed in detail according to the categorization defined above. Test results are specified along with test conditions and test apparatus design. Results are discussed and evaluated. In Section 3 of this report, the overall results are discussed, and, where appropriate, the developed design criteria or procedures resulting from this experimental research are summarized and qualified as necessary. Areas requiring future research are specifically identified.

SECTION 2. TECHNICAL DISCUSSION

In the following section, the experimental projects conducted in support of this program are described and discussed as identified in Section 1.

A. Screen Characteristics Definition Projects

Four individual experimental projects were conducted to further define basic surface tension device screen characteristics. These included: (1) screen bubble point measurements with saturated LH_2; (2) screen element flow loss evaluation; (3) pleated screen flow loss and bubble point measurements; and (4) measurements of the effects of basic screen flexure on bubble point performance. These are discussed below.

1. Basic Screen Bubble Point Performance with LH_2. Surface tension devices made from fine-mesh screen materials have been found to provide improved head retention and expulsion capabilities because of the relatively high surface-tension pressure that can be supported across the small effective pore size of the screen. The retention performance of these screen materials is expressed by a bubble-point property which is the pressure differential across the screen at which gas breaks through the wetted screen and enters the liquid. The bubble point characteristics of given screen materials are therefore basic input required for the design of a screen acquisition device. At this point in the program, data on screen bubble point characteristics with LH_2 were limited, and a series of tests to expand this data base was initiated. The limited LH_2 bubble-point tests reported in Reference 1 were available. During those tests where GH_2 was used as a pressurizing media, the data were repeatable and in agreement with predictions based on isopropyl alcohol bubble-point tests with the same screen samples. The predictions were based on a LH_2 surface tension of 1.95 dyne/cm at 20.2°K. However, the results with GHe were erratic and not adequately predictable. In general, the retention was increased when GHe was present. It was believed that this increase in retention was a result of local cooling and corresponding surface increase, due to the pressure of the helium. These tests provided no means to control the GHe partial pressure behind each of the screen samples. and it was hypothesized that the data scatter is related to the uncontrolled scatter in GHe partial pressure. The apparatus shown schematically in Figure 1 was designed in an attempt to provide a controlled and known GHe partial pressure. The apparatus was also designed so that the screen was in a position where it can be viewed directly through the dewar window. Close observation of the screen is required to detect the point of initial pore failure as opposed to gross (multipore) failure detected in the referenced tests.

Each of six screen samples was bubble tested in turn, using the same procedure. The dewar was filled with LH_2, completely submerging the samples

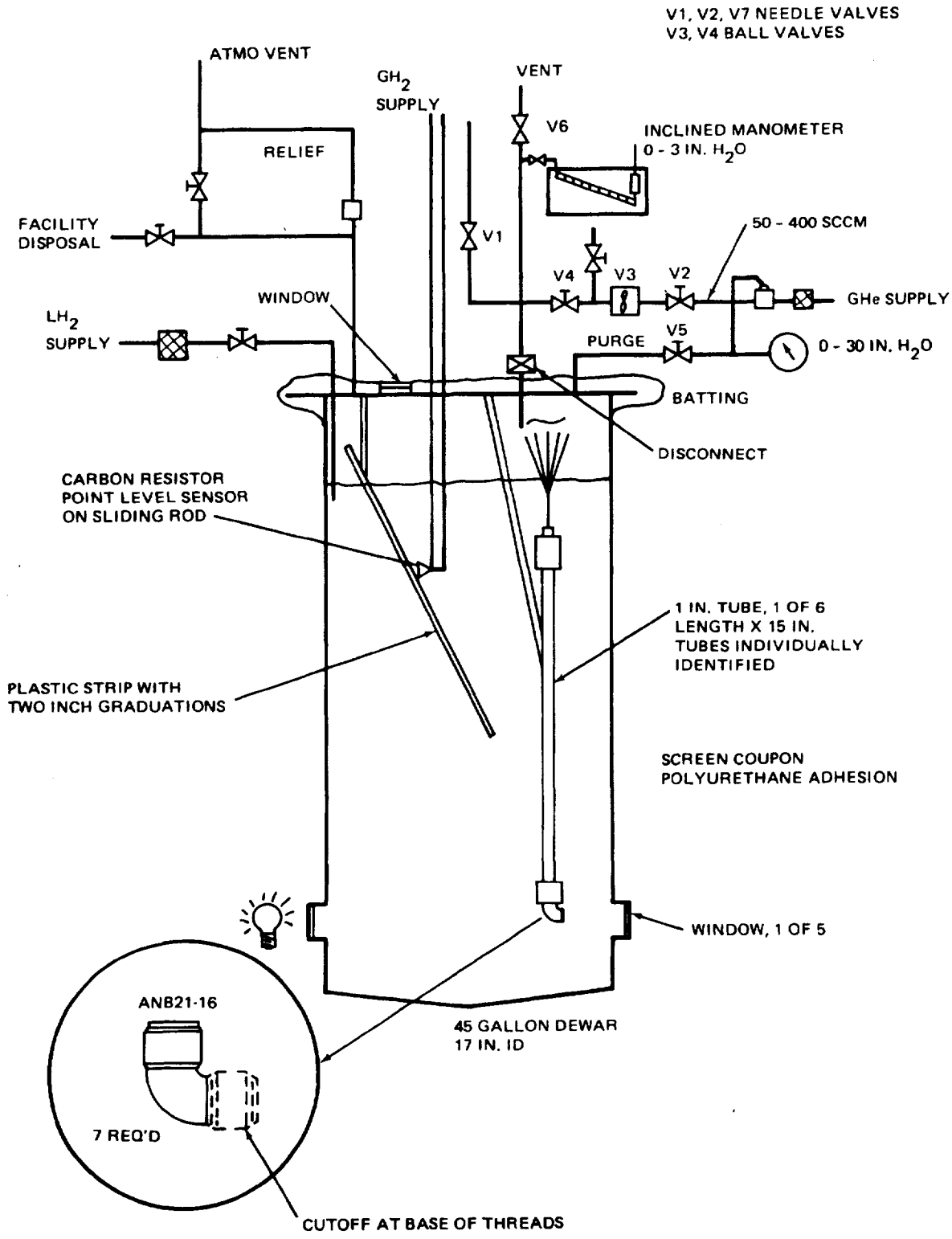

Figure 1. Bubble-Point Test Apparatus

and bank of 2.54 cm tubes that serve as individual accumulators behind each screen (Figure 2). The dewar was vented to atmosphere. Liquid level was monitored with a carbon resistor point level sensor with a graduated plastic strip serving as a redundant level detector. The 2.54 cm tube connected to the screen of interest was filled with LH_2 by venting through valve V6. GHe was used to displace this liquid through the screen at a rate measured by a flowmeter. In this fashion, the tube is charged with a known amount of GHe, at which point continued pressurization takes place slowly with GH_2 through valve V1. At the point of screen failure, the ΔP across the screen is indicated at the manometer. This pressure and the accumulator volume is combined with the amount of GHe present to yield the total amount of gas present at breakdown.

Prior to testing with LH_2, each screen assembly was tested with isopropyl alcohol as a baseline value and for later correlation with the LH_2 test results. The five screen specimens (165 x 800, 200 x 600, 200 x 1400, 325 x 2300, 450 x 2750) were each 2.85-cm in diameter and adhesively-attached to individual elbows on the lower end of short sections of 2.5-cm-diameter aluminum tubes suspended within the LH_2. The tubes created a region where the composition of the pressurizing gas could be controlled. Breakdown of the screen was observed by viewing through one of four windows in the lower portion of the dewar. A 25-cm inclined water manometer monitored the pressure differential between the gas pressure within the tube and the dewar ullage. Both GH_2 and GHe were used for pressurizing each tube in turn. A flowmeter was used to monitor the rate of GHe addition.

CR190
SSC 042486

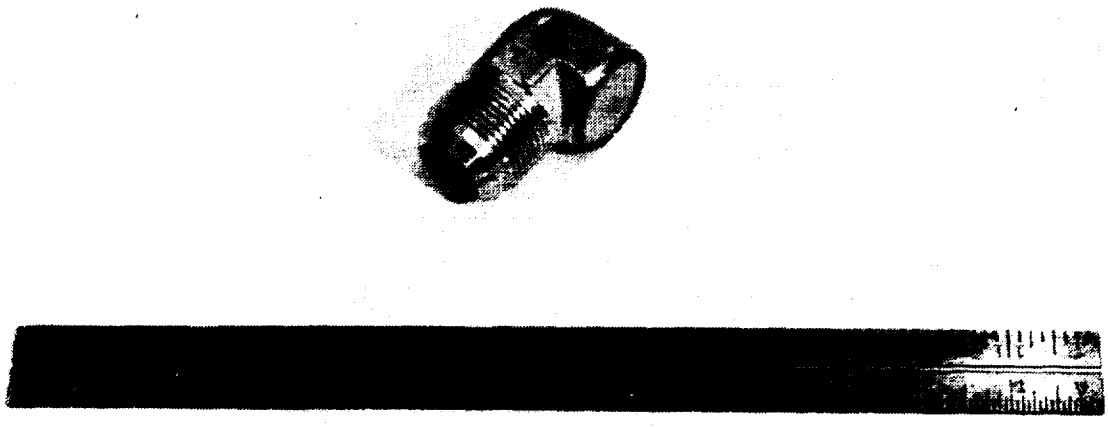

Figure 2. Screen Element and Holder

A single bubble point measurement consisted of first filling one of the five tubes with LH_2 and then displacing a portion of this liquid with a measured amount of GHe. The line sizes and lengths were selected so that at least 95 percent of the GHe added was located within the aluminum tube attached to the screen being tested (the remainder resided in the lines leading to the aluminum tube). Following the addition of GHe, the pressure within the tube rose slowly due to LH_2 evaporation as the GHe cooled to the liquid temperature. The LH_2 was completely displaced from the tube within a period of 1 to 10 minutes, at which time the pressure rose rapidly until screen failure occurred. The more rapid pressure rise was probably due to the fact that the ullage volume was no longer increasing as it was when the liquid was still being displaced. The gas volume suddenly became fixed with no significant reduction in the rate of GH_2 evolution. This rapid rise precluded an accurate measurement of the pressure at screen failure. Subsequently, the tube was vented during that phase when the tube emptied to modulate the rate of pressure rise. This technique, however, resulted in the loss of an unknown quantity of GHe which prevented the partial pressure from being accurately computed. Under equilibrium conditions, the partial pressure of the GHe will be the difference between the total pressure and the hydrogen vapor pressure. For nonequilibrium conditions, both the measured amounts of GHe and the partial pressure determinations will give only approximate values of the conditions at the screen interface.

The same throttling technique discussed above was used when presurizing the screen with GH_2 alone. The results of the bubble point tests with GH_2 are shown in Figure 3. The bubble point was calculated by subtracting the

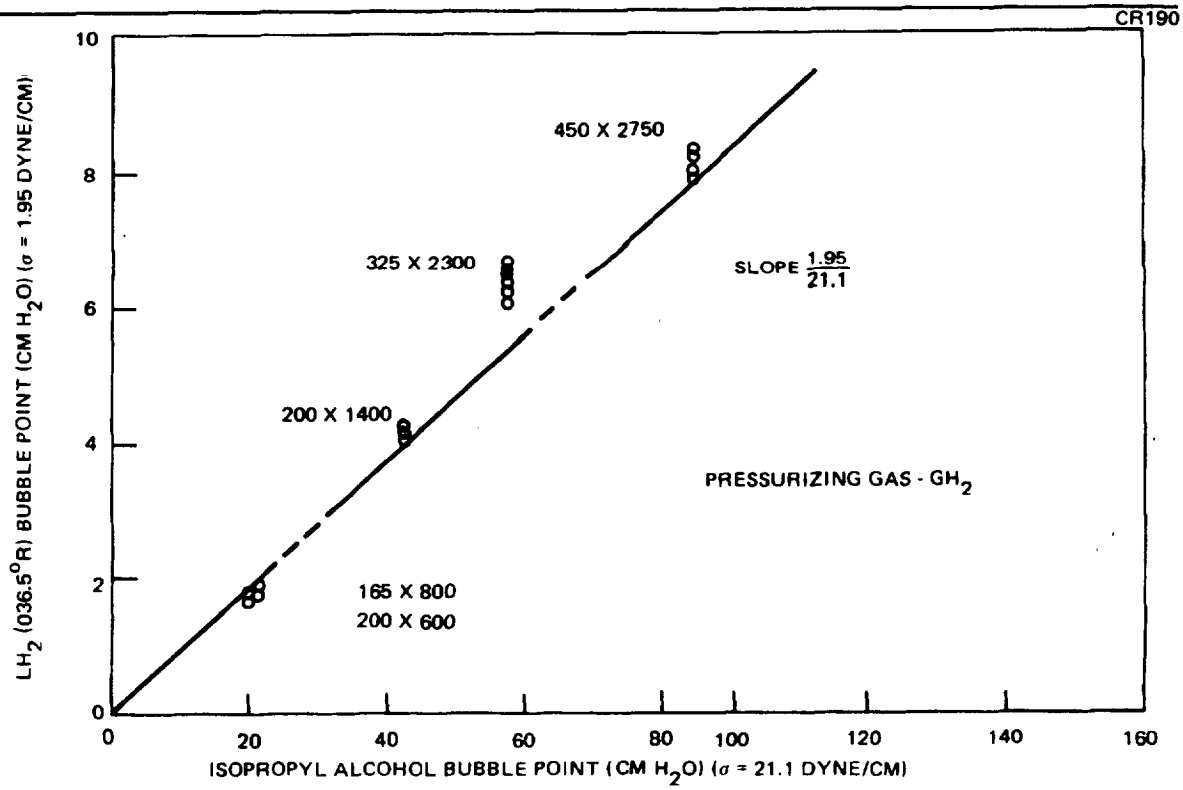

Figure 3. Measured Screen Bubble Points with LH_2/GH_2

LH_2 head from the manometer reading at the point of breakdown. The expected correlation between the isopropyl alcohol and LH_2 data is based on the following values for surface tension:

LH_2 at 20.2°K	1.95 dyne/cm
Isopropyl alcohol at 296°K	21.4 dyne/cm

Four of the five screens are in good agreement with the expected correlation of the two sets of bubble point data based on the ratio of the respective surface tensions. The 325 x 2300 mesh was rechecked in alcohol to verify that the exceptional behavior in LH_2 was not simply caused by a spurious measurement in alcohol. The result was the same. Test data for one of the screens tested with varying amounts of GHe is shown in Figure 4. The data scatter prevents the possibility of drawing definite conclusions regarding the influence of GHe on the bubble point. There appears to be a trend in the data

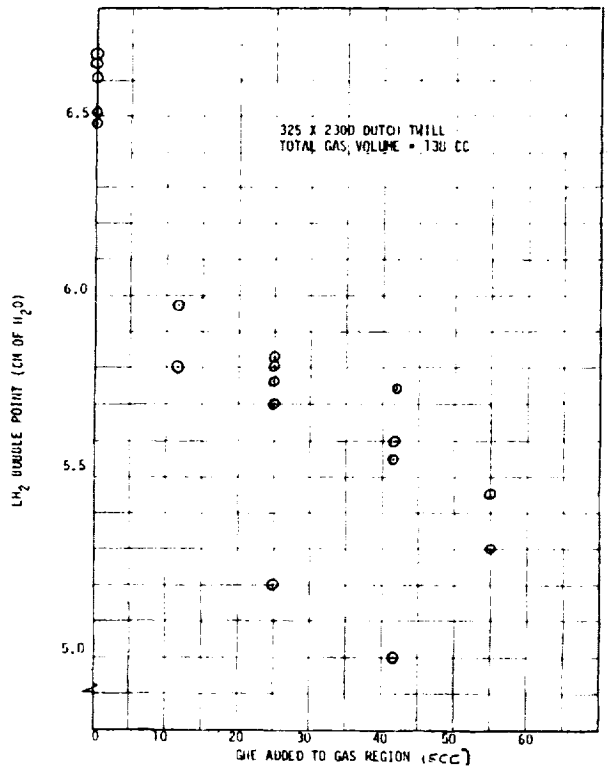

Figure 4. LH_2 Bubble Point With Helium Present

shown in Figure 4; adding GHe to the gas region tends to decrease the bubble point. However, except for one data point showing breakdown at a pressure difference of 5 cm of H_2O (water column), all of the bubble point pressures exceed the predicted bubble point value based on isopropyl alcohol data. The data scatter may be explainable in terms of heat transfer, since the larger the amount of helium introduced into the gas region, the higher the heat flux to the screen would be, which could cause a reduction in bubble point.

A limited number of retests was attempted. In these tests, LN_2 prechillers were used to cool the incoming helium and thus minimize the

pressure rise rate, but these did not yield usable results. This testing was terminated, and it was generally assumed that the LH_2 bubble point could be conservatively estimated based on alcohol bubble point test results, regardless of the pressurizing gas. However, the development of an experiment to validly measure bubble point with LH_2 and helium pressurant would be most desirable to resolve the question of helium effects on screen bubble point performance.

2. Screen Element Flow Loss Tests. While fine mesh screens enhance the retention capability of a surface tension device, it is only with a corresponding increase in the resistance to the flow of liquid through the screen. The screen channels and collection ducts of a retention subsystem must be sized so that viscous, dynamic, and hydrostatic losses within the passage are minimized. The sum of these losses must not exceed the bubble-point pressure for the basic screen used on the channels at any point to ensure that pressurant does not enter the suction line. Therefore, the basic screen element must offer minimal resistance to flow.

An MDAC numerical program (acquisition channel sizing code) is available for analyzing specific retention-system configurations. The program uses correlation equations devised by Armour and Cannon (Reference 2) to calculate the pressure loss accompanying flow through the screen into the screen channel but does not consider losses through screen backup materials and any interaction effects. Since backup perforated sheet is being considered to support the more flexible basic screen material, flow losses associated with these configurations had to be determined in the series of tests described below. The objectives of this test program are to determine the pressure drop through representative screens of various weaves for a wide range of Reynolds numbers, to determine the effects of backup perforated sheet behind these same screens, and to determine means to minimize these effects. Three sizes of screen and nine different backup configurations were tested using both gaseous nitrogen (GN_2) and helium (He) as the working fluid.

a. Test Setup. The basic components in the test setup are a flow tube designed to contain the test element, a pressurized gas supply, a gas filter, a manometer to measure the pressure drop across the test element, a vertical open-end water manometer to measure the static pressure immediately upstream of the test element, a variable area flowmeter calibrated for both GN_2 and He, and associated lines and valves. The apparatus was fabricated in the Propulsion Subsystem Laboratory at Huntington Beach, California, and is shown in Figures 5 and 6.

The setup is shown schematically in Figure 7. The flow tube consists of two identical halves which are bolted together at their flanged ends. Each flange contains a soft gasket which seals the test element between the bolted flanges for testing and establishes a well-defined flow area through the screen.

Pressure taps are drilled through each flange so that static pressures may be measured 1 cm upstream and downstream of the element. Two flow-unit tube sizes (see Figure 6) are available to allow for a greater range of flow velocities within the limits of the flowmeter. Pressurized supplies of both GN_2 and GHe were used to provide a wide range of Reynolds numbers. An inclined manometer was used to measure pressure drops of less than 5 cm

CR190
SSC 041325

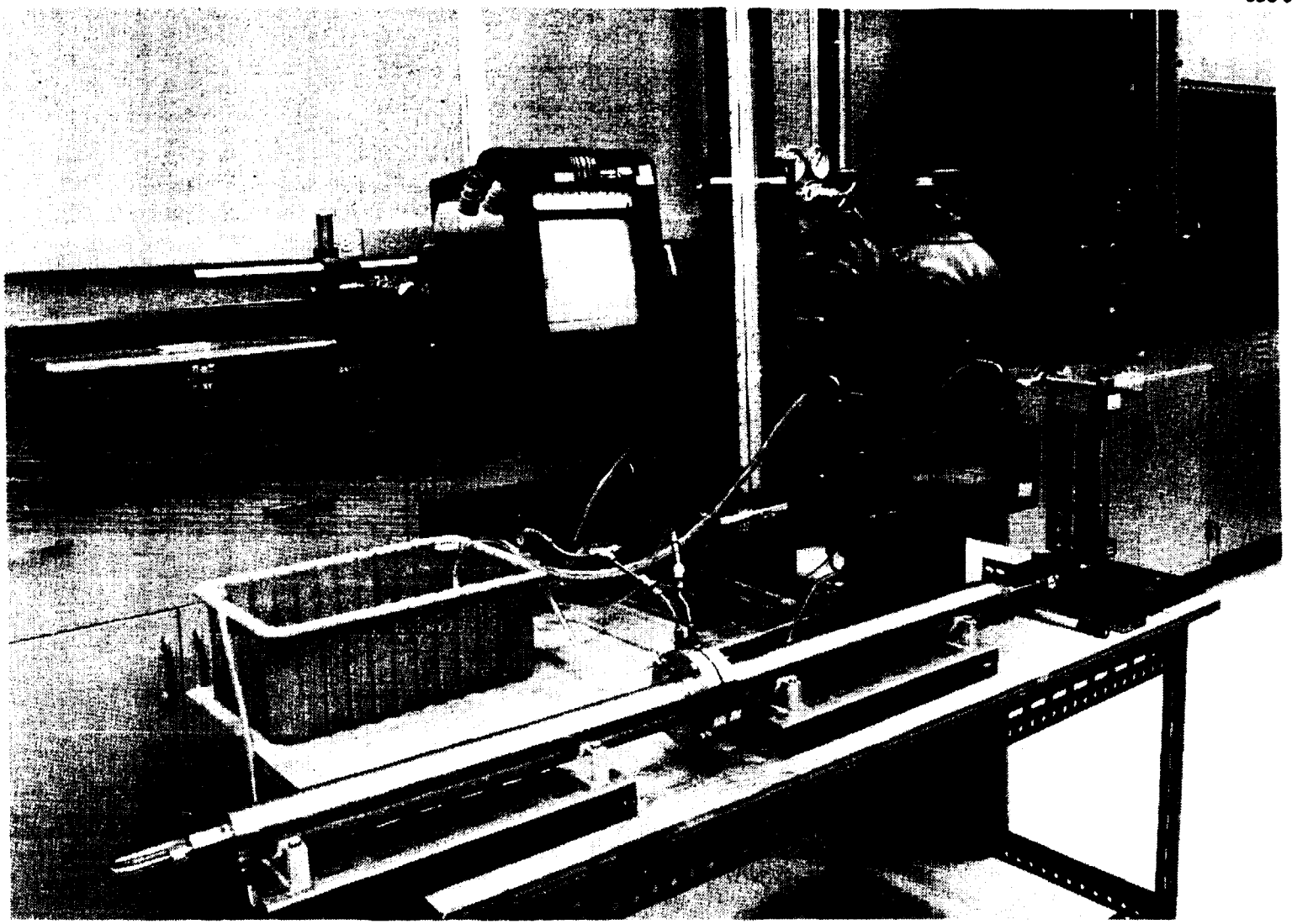

Figure 5. Flow Loss Test Setup

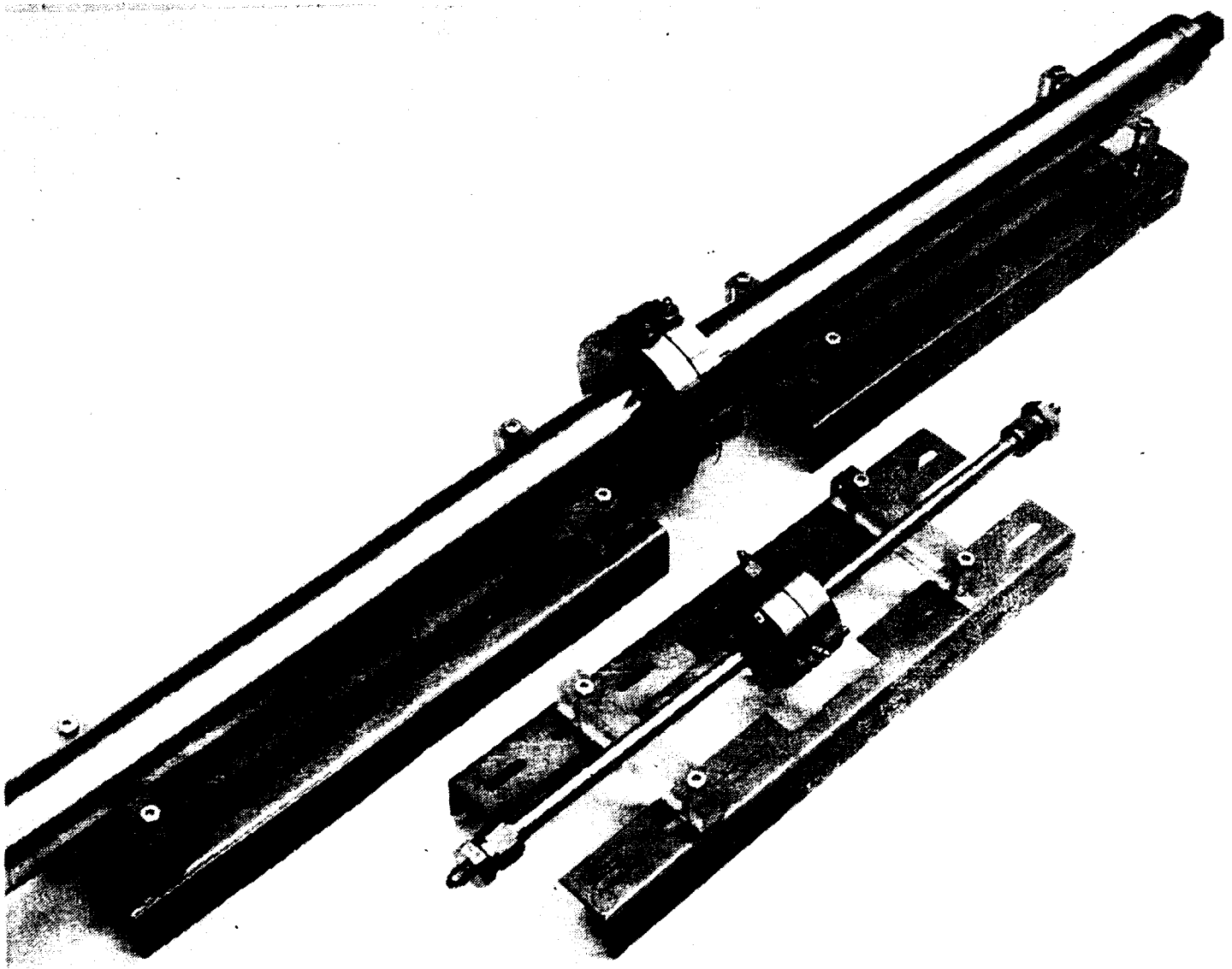

Figure 6. Flow Loss Test Device

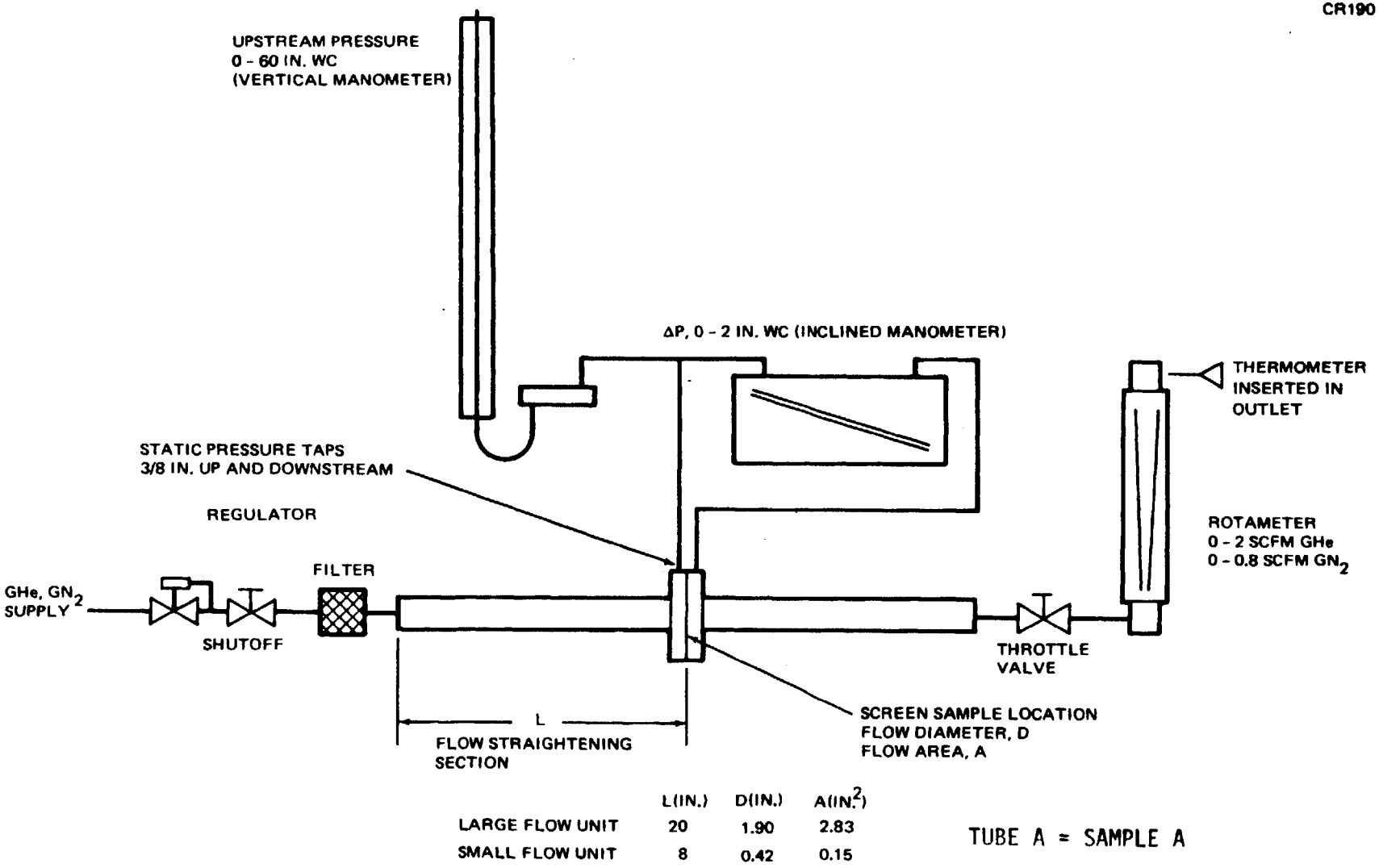

Figure 7. Screen/Backup Pressure Drop Test Apparatus

of water, whereas a 102 cm vertical manometer was used to measure those greater than 5 cm of water.

b. Summary and Results. The characteristics of the three types of stainless-steel, dutch-twill screens and of the nine perforated sheets (see Figure 8) which were used as screen backup materials are summarized in Tables 1 and 2, respectively. More than 20 data points were recorded for each of the three basic screens to represent the full range of Reynolds numbers possible with the available combinations of two inert gases and two flow areas. The effects of the perforated sheets as screen backup material were determined using the larger flow tube according to the schedule shown in Table 3.

The basic screen data are plotted in terms of a flow friction factor in Figure 9 as suggested by Armour and Cannon (Reference 2), and in terms of a dimensionless pressure loss (Poiseuille number, P_o) in Figure 10. The data points are uniformly lower than the Armour and Cannon correlation curve in Figure 9, which indicates that the correlation equation is conservative by a factor slightly greater than 2. Note, however, that the correlation is successful in aligning the data points for the three screens. It was further noted that the flow losses associated with gaseous helium were slightly less than those for gaseous nitrogen. Specific tests were run to compare 165 x 800 and 200 x 600 mesh material with the results shown in Figure 11, which showed that the 165 x 800 has a slightly higher flow loss even though the two meshes have the same bubble point. The Poiseuille number, P_o, is a convenient parameter for comparing pressure losses because it remains nearly constant for a specific screen in the laminar flow regime (see Figure 10). The laminar flow regime extended to a Reynolds number of approximately 1.0. The results of the GDC study (Reference 3) were presented in this manner for a number of screens which included the 200 x 1,400 mesh size. The GDC values of D and B (defined in Table 1) were normalized so that their data can be compared with those from the MDAC tests. GDA used a pore diameter apparently based on bubble point data, which gave a maximum diameter of 22.8 microns, whereas the manufacturer's rating for pore diameter is 10 microns, and is more appropriate as a flow loss characteristic diameter. The screen thickness, B, used by GDA was slightly different from the value used in this study, but the effect on the data correlations is neglible. These changes were made to compare GDA and MDAC data directly.

The pressure drop across a screen/perforated sheet combination representative of a screen element as mounted in a complete acquisition device is greater than that across the screen alone, as expected. The effects of the nine perforated sheets were compared on the basis of a pressure loss ratio, $\Delta P/\Delta P_o$, where ΔP is the average combined pressure loss (averaged over all data points for a specific screen) and ΔP_o is that for the basic screen alone. This parameter is plotted in Figure 12 against the fractional open area, F_A, of the perforated sheet. The plot indicates that a correlation would involve something more complicated than simply F_A. Pressure losses associated with flow through the perforated sheets alone were not measurable with the instrumentation at hand, which indicates that the loss across a combination is not merely additive but is strongly affected by the flow paths between and parallel to the screen and sheet. It was hypothesized that this effect could be reduced by inserting a lightweight (aluminum) coarse mesh spacer between the two elements to provide less severe flow paths, rather

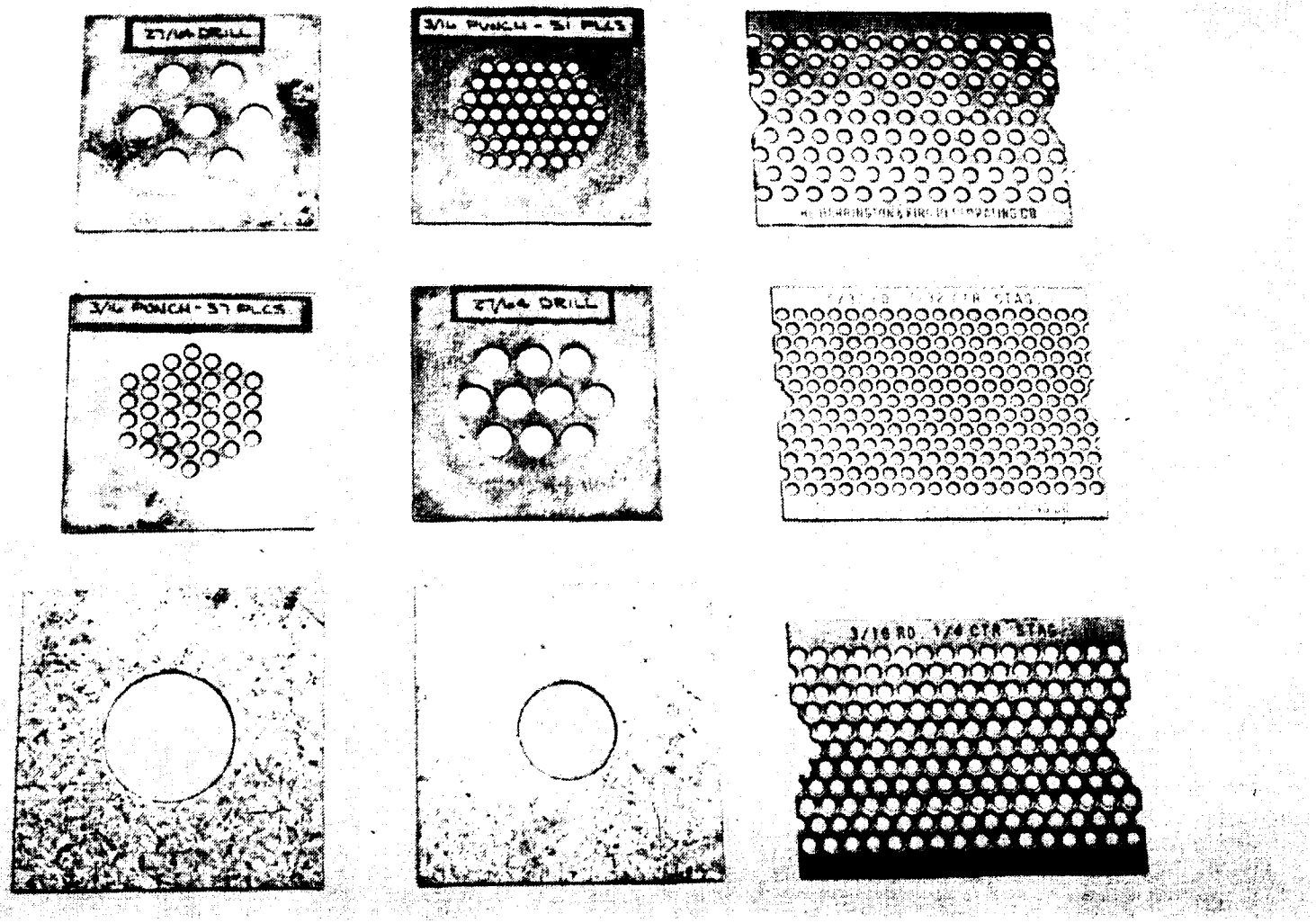

Figure 8. Perforated Plate Test Samples

Table 1

CHARACTERISTICS OF STAINLESS STEEL DUTCH TWILL SCREENS TESTED

Mesh (wires/in.)	200 x 1,400	250 x 1,370	325 x 2,300
Wire diameter (in.)	0.0028/0.0016	0.0022/0.0015	0.0015/0.0010
Pore diameter, D(ft)	7.14×10^{-5}	5.67×10^{-5}	4.83×10^{-5}
Screen Thickness, B(ft)	5.00×10^{-4}	4.50×10^{-4}	2.92×10^{-4}
Surface area per unit volume, $A(ft^{-1})$	19,930	22,443	33,598
Void fraction, ϵ	0.248	0.204	0.245
Tortuosity factor, Q	1.3	1.3	1.3

*See Appendix A for definition of terms.

Table 2

CHARACTERISTICS OF PERFORATED BACKUP SHEETS

Identifier	Open Area Fraction, F_A	Hole Size (in.)	Description
1	0.623	1-1/2	Single Hole
2	0.510	3/16	1/4 in. Center-to-Center
3	0.496	3/16	51 Holes
4	0.495	27/64	10 Holes
5	0.460	5/32	7/32 in. Center-to-Center
6	0.361	3/16	37 Holes
7	0.350	1-1/8	Single Hole
8	0.345	3/16	7 Holes
9	0.330	27/64	5/16 in. Center-to-Center

Table 3. Test Matrix for Screen/Perforated Sheet Combinations

Screen Mesh	Gas											
	GN_2										GHe	
200 x 1,400		x								x		
250 x 1,370	x	x	x	x	x	x	x	x	x	x	x	x
325 x 2,300		x								x		
	1	2	3	4	5	6	7	8	9	2	3	4

Perforated Sheet Identifier

than squeezing the elements together, as done in the reported tests. Various spacers were evaluated in the test program to determine if such a solution is possible. The results are shown in Figure 13 for 250 x 1,370 mesh, a 11 x 11 spacer mesh, and three perforated plates. As indicated, the flow loss now falls on the values for the fine mesh alone. Thus, the coarse mesh spacer does eliminate the high pressure drop problem for the screen element. Additional data showing flow loss with and without spacers are given in Appendix A.

Robusta type screen mesh were reported to exhibit low flow losses, and these were therefore evaluated toward the end of the exploratory test program. The results for four screen mesh (850 x 155, 720 x 140, 280 x 70, and 175 x 50) were evaluated using the procedures and apparatus applied to the tests discussed above. These results are summarized in Figure 14. It was found that the Robusta weaves did not have an unusually attractive flow resistance. Corresponding plain or twilled Dutch weaves with the same bubble points had as low or lower flow resistance in the laminar range.

3. Pleated Screen Tests. Pleating of the basic screen in a surface-tension acquisition device offers the potential of increasing the area available for liquid flow by a factor of as much as 3 or 4, with a corresponding dramatic reduction in flow loss through the screen. The reduction in loss is reflected in a higher operational head retention safety factor for the acquisition device. This advantage must be weighed against several detrimental factors brought about by pleating, such as increased screen weight and increased complexity in screen attachment. Another potential disadvantage that may offset the increase in safety factor is a potential reduction in the surface tension capability of the screen because of changes in the pore size distribution brought about solely by the pleating process. To quantitatively evaluate this effect, the bubble point was measured for various pleated-screen elements. Eighteen screen samples were pleated by a Rabofsky pleating machine to determine what degradation in bubble point occurs. Each 5 x 15-cm flat sample was initially bubble-point checked using isopropyl alcohol as a test fluid. Each sample was then pleated using a pleating blade radius of 0.038-cm, 0.047-cm pleat height and pitch of approximately

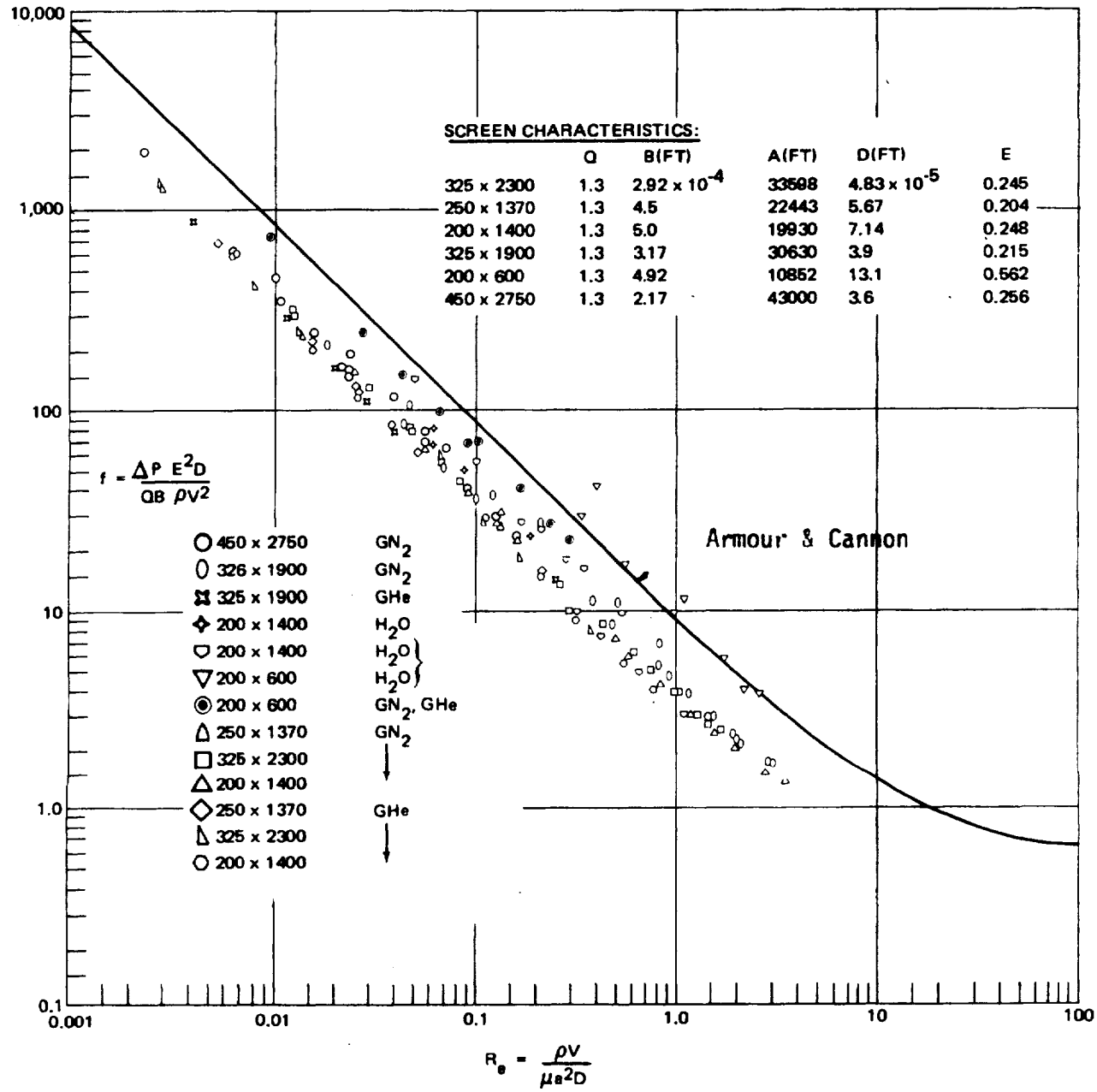

Figure 9. MDAC Flow Loss Data Correlation for Dutch Twill Screen

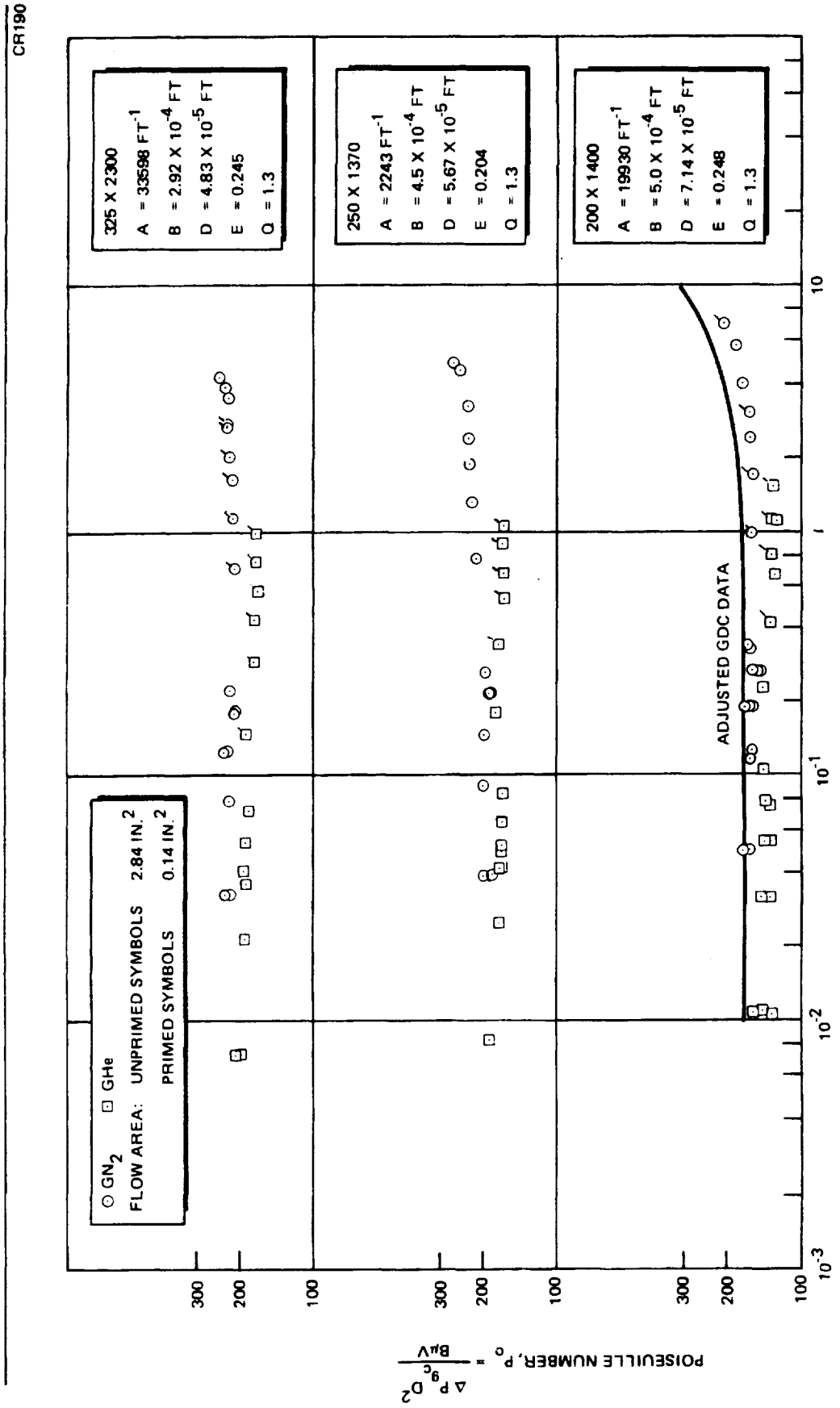

Figure 10. MDAC Flow-Loss Data for Dutch Twill Screen

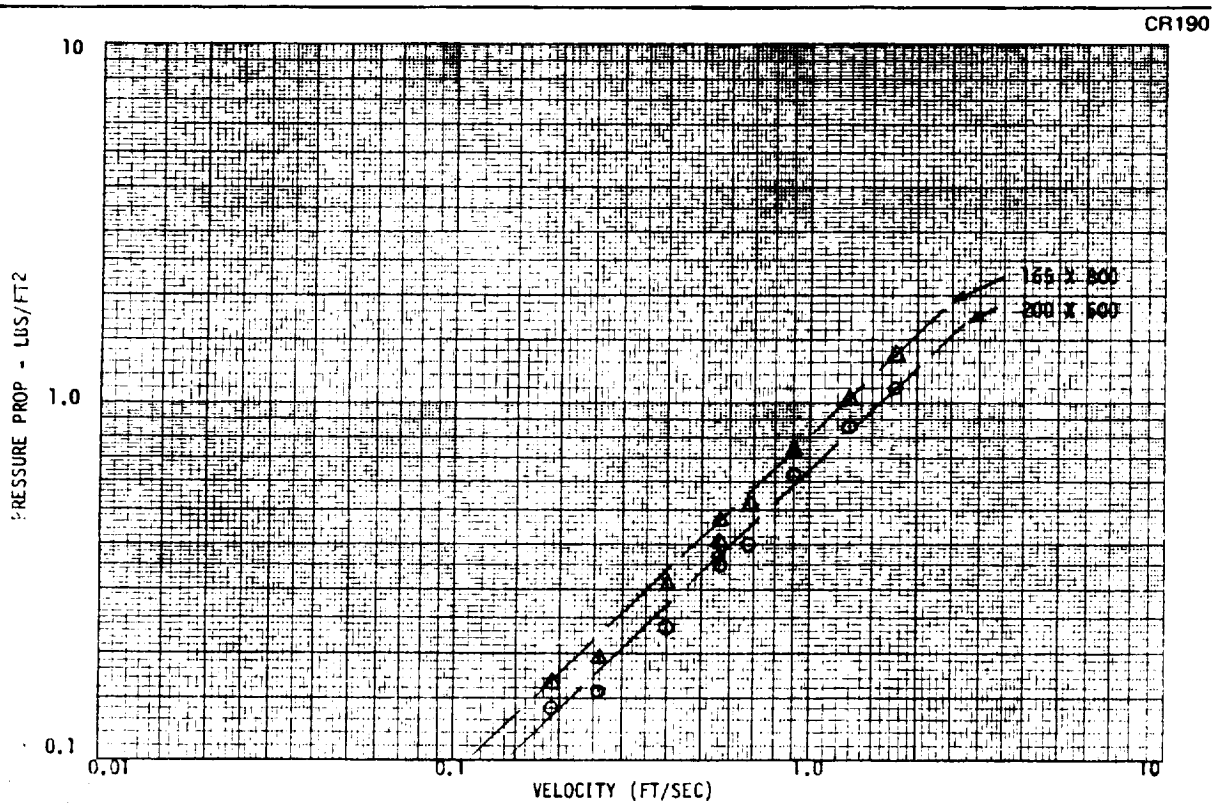

Figure 11. Laminar Flow Losses for Candidate Screen Mesh

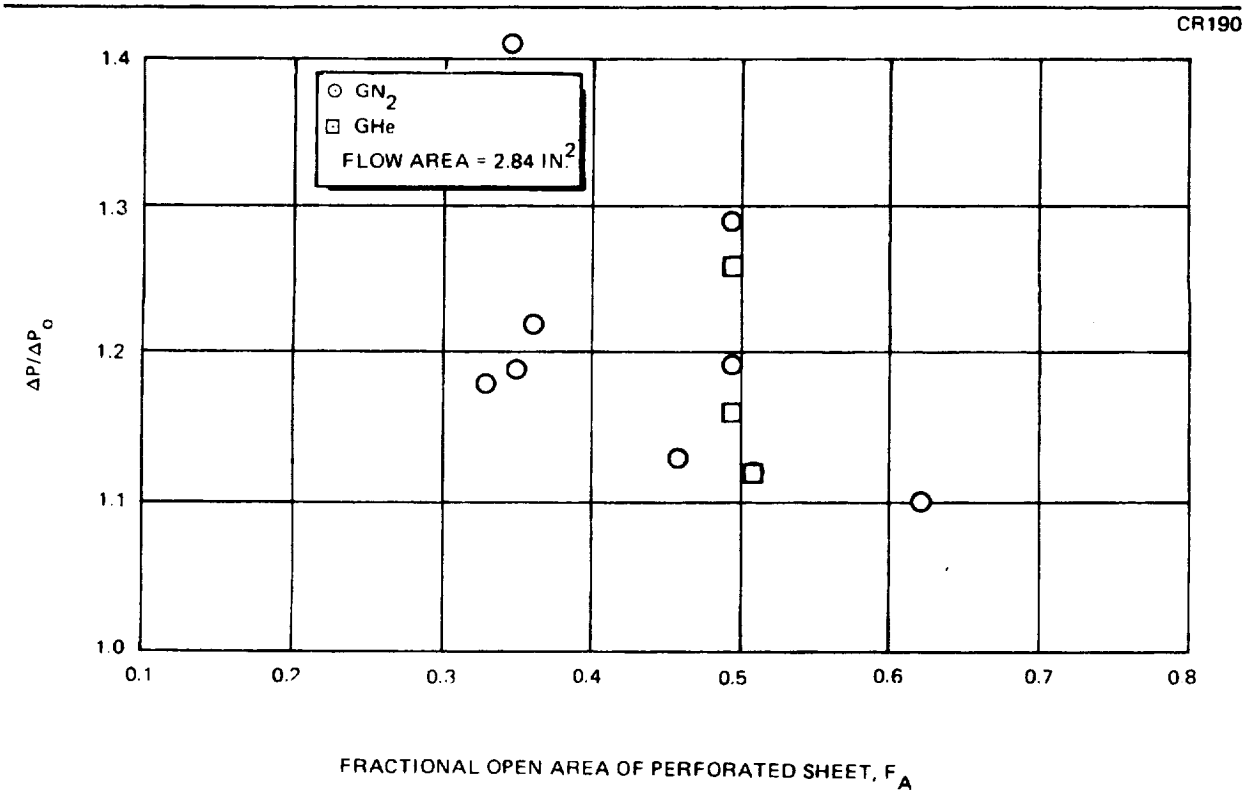

Figure 12. Effects of Perforated Backup Sheets on Screen Pressure Loss

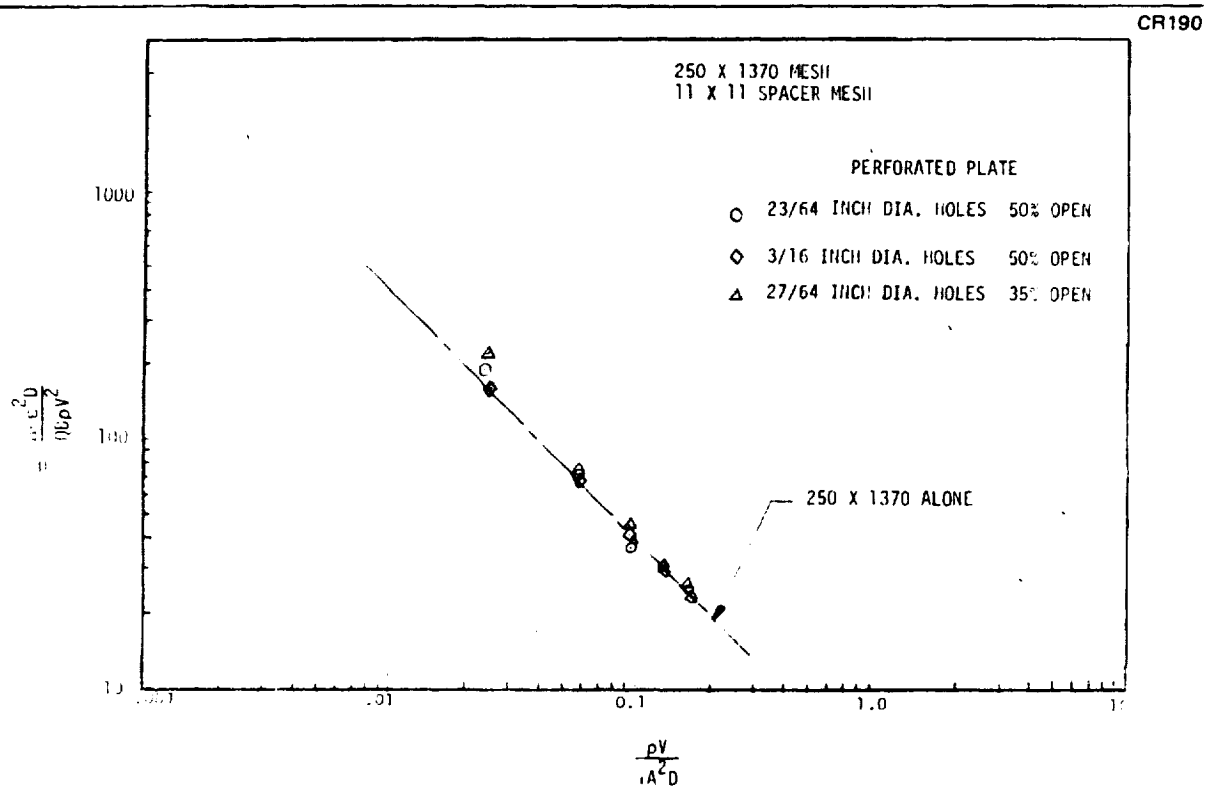

Figure 13. Influence of Coarse Mesh Spacer on Flow Loss

4 pleats/cm (pitch is a variable dependent upon the wire count and size for a given set of counter weights on the pleater). The type of pleat used is representative of that which may be used in an acquisition device. Pleating took place in both perpendicular and parallel orientation to the warp direction in the screen to identify any effects caused by the anisotropy of the screen. The screen samples (unsintered) are as follows:

Screen Mesh	No. Samples	
	Pleat Parallel to Warp	Pleat Perpendicular to Warp
1. 325 x 2,300	2	0
2. 250 x 1,370	2	2
3. 200 x 1,400	2	2
4. 200 x 600	2	2
5. 80 x 700	2	2

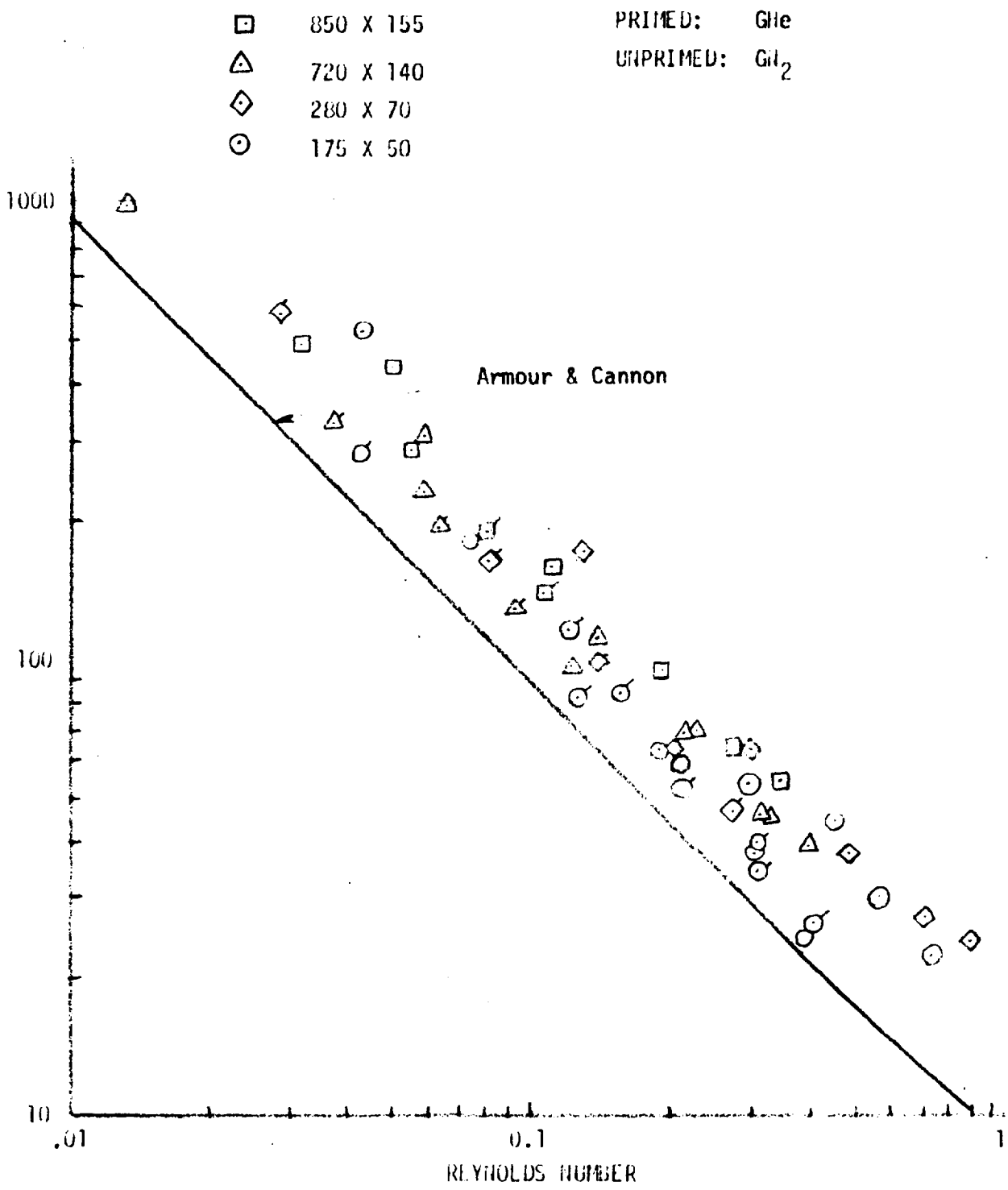

Figure 14. Flow Losses With Robusta Screen Material

The mesh thickness ranged from very thin (0.0090-cm, 325 x 2,300) to relatively thick (0.025-cm, 80 x 700); all samples being dutch-twill weaves. After pleating, each sample was glued into a plastic frame (see Figure 15) using a commercial epoxy. Glueing permits the edge of the screen to be sealed to a supporting frame without introducing added physical damage which may effect the pore sizes.

The bubble points for the various pleated screens were measured using alcohol with the results shown in Figure 16. Note that the measured degradation relative to the unpleated screen is very small - less than 20 percent in the worst case.

Flow loss tests were also conducted with four 250 x 1370 pleated screen samples. Two of the 5.1 x 15.3 cm specimens were made with the long dimension parallel to the warp wire and the other two parallel to the shute wire. Pleating took place across the shorter dimension. Pleating parallel to the warp direction results in a more rigid screen. These screens were bonded into the plexiglass frames and flow-tested in the apparatus described in Section 2. The completed units are shown in Figure 17. Tests were conducted with GHe and GN_2. The test results in terms of the Armour and Cannon correlation are shown in Figure 18. All tests fell in the laminar flow regime. For the correlation, the flow area was taken as the total screen area. The result indicates that the pleating did not measurably alter the pressure drop for the screen element. Based on the bubble point and flow loss tests, it is concluded that pleating can be effectively used to increase retention performance. Table 4 shows the typical potential retention safety factor improvement possible with pleating as related to the pleated-to-unpleated area ratio.

4. Influence of Screen Deflection on Retention Performance. Screens used in propellant acquisition devices will be subjected to cycle loadings during periods of outflow and liquid motion. It is not practical to completely restrain the screen, since this tends to limit flow and increase device weight. The primary consequence of screen flexing is possibly a reduction in the screen bubble point because of broken wires or movement of wires in the screen, thus causing a change in the effective pore size in a local region.

A series of bench tests was initiated to investigate the sensitivity of candidate screen bubble-point pressure to cyclic screen deflections. These tests were carried out using the welded screen assemblies built for the fabrication feasibility tests described in Section B1 and the bubble-point apparatus designed to accommodate these samples. 250 x 1350 mesh was used in all cases. The apparatus was modified by the addition of the small electric motor and eccentric drive shown in Figure 19. An attachment was made to the center of the welded screen assembly as it is clamped in the bubble-point apparatus. The motor and variable speed control introduce a vertical deflection in the center of the screen having a frequency of approximately 1 Hz. The bubble point of the screen was checked in isopropyl alcohol while the deflections were being applied. Initially, the deflection amplitude was quite low (0.3 cm). A large number of oscillations (minimum 1,000) were input at this amplitude while checking the bubble point at regular intervals and noting any new locations when the screen was observed to fail. Both fusion-welded and roll-spot-welded screen assemblies were tested. Figure 20 shows the imposed amplitudes and cycles. The 12.7 cm square

CR190
SSC 042487

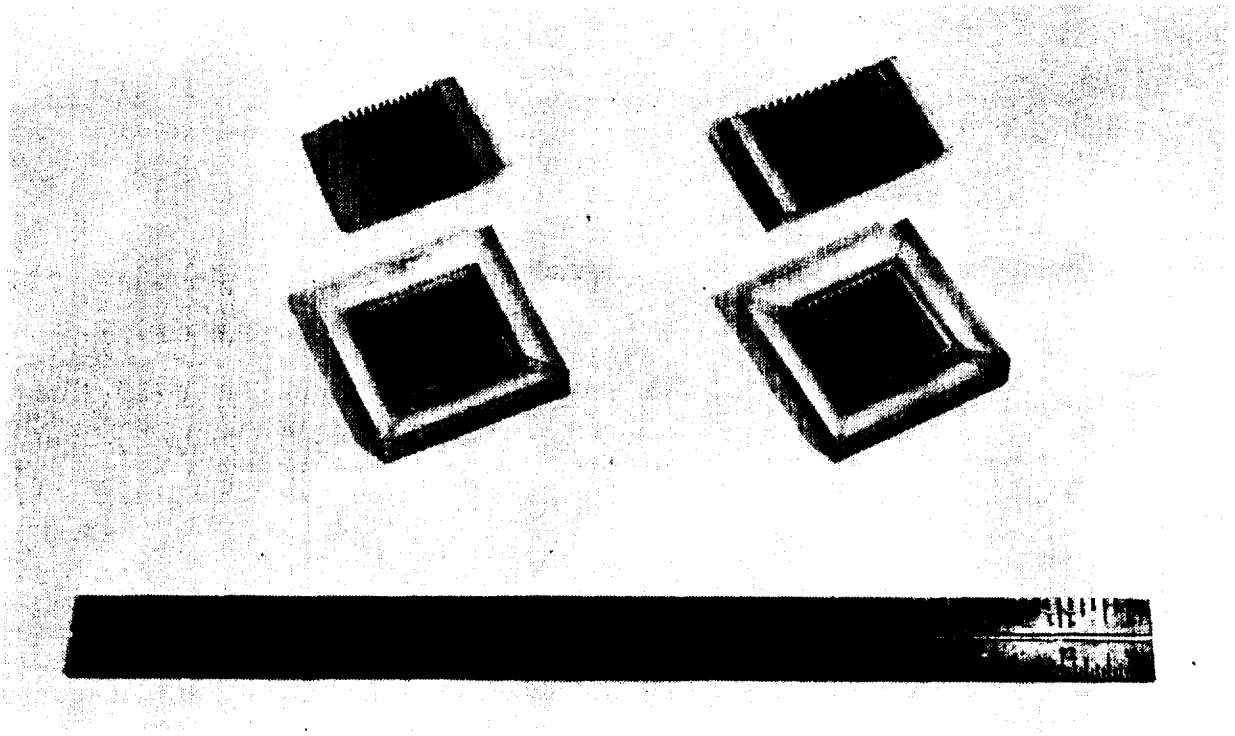

Figure 15: Pleated Screen Sample

CR190

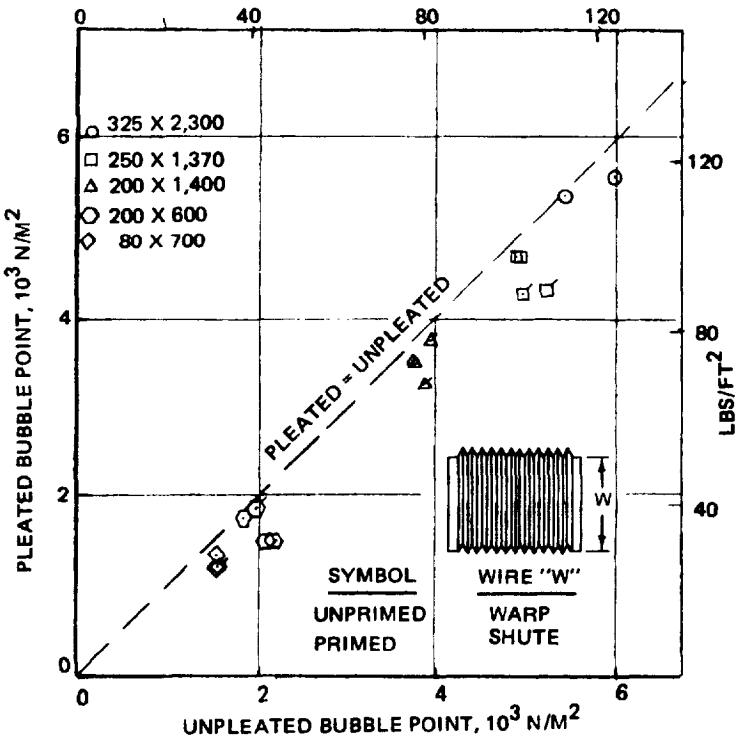

Figure 16. Bubble Point Performance of Pleated Screens

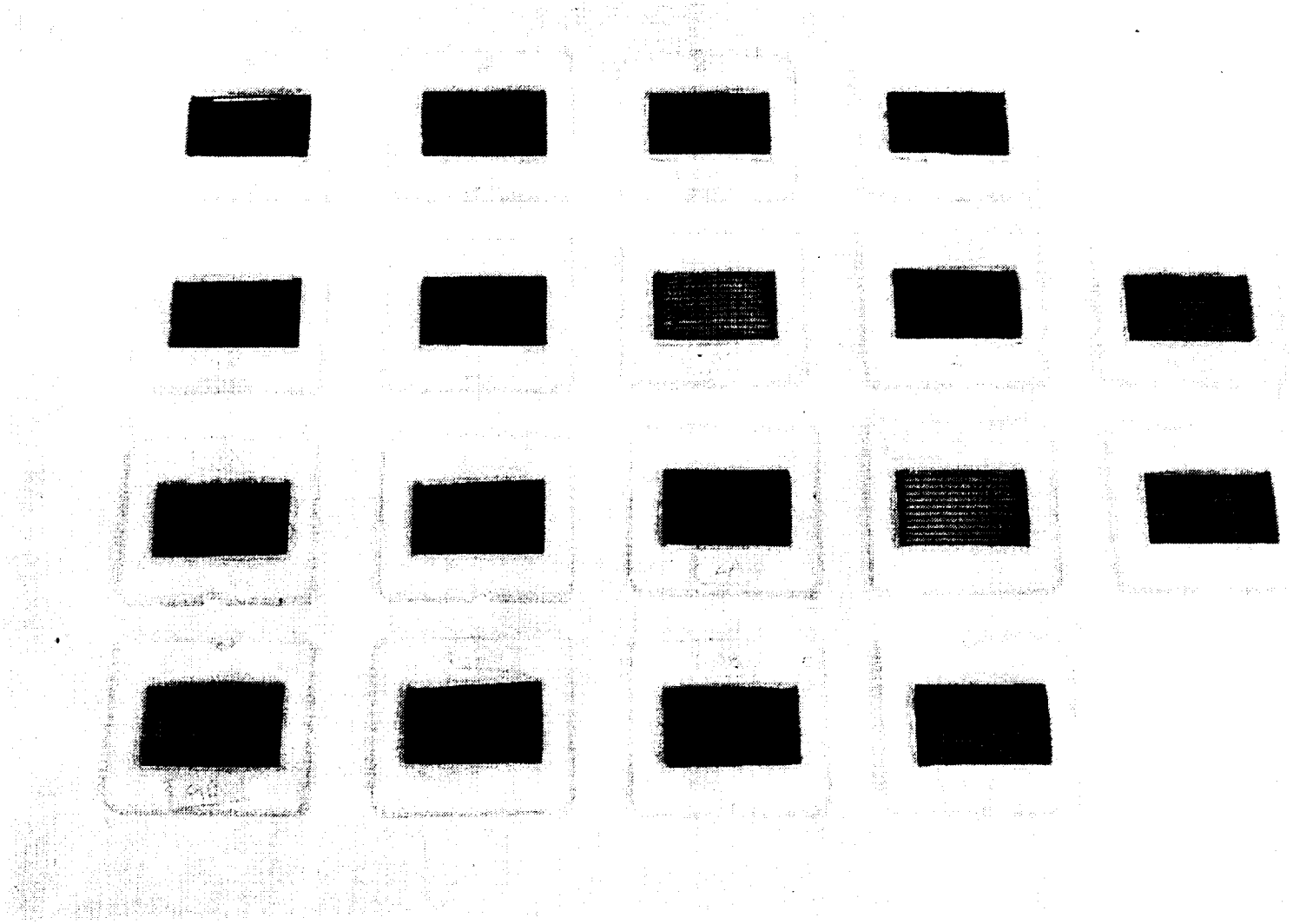

Figure 17. Pleated Screen Installed in Test Frames

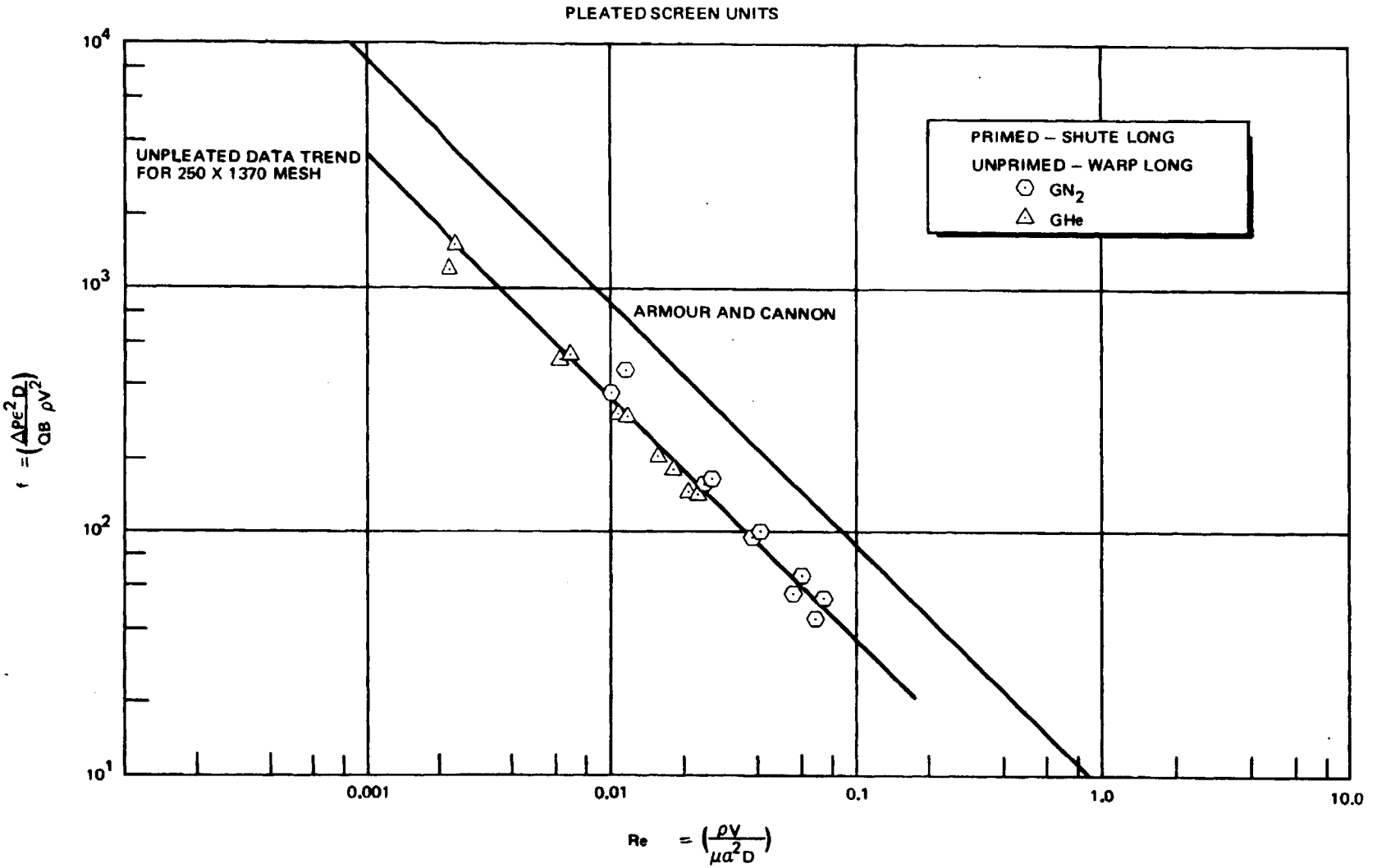

Figure 18. Pleated Screen Flow Loss Measurements

Table 4

INFLUENCE OF PLEATING ON RETENTION CAPABILITY

	Channel Flow Retention Safety Factors*		
	Pleated Area/Unpleated Area		
Screen Mesh	1	2	4
200 x 1400	0.697	0.959	1.165
250 x 1370	0.705	1.114	1.504
325 x 2300	0.883	1.307	1.703

LO_2 Tank - Bottom channel (CSS/APS design)

Screen 1/4 covered

.46M/sec^2 positive acceleration (on-orbit)

*Channel not optimized for a specific minimum acceptable safety factor.

screen element samples were tested over a wide range of conditions with amplitude ranging from 0.11 to 0.51 cm and cycles up to 13,800 with no significant degradation in bubble point. One of the fusion-welded samples failed at the forcing arm attachment point at 2550 cycles, but none of the other samples indicated damage. Although these tests were intended to be only qualitative, it is obvious that the screen material is quite able to sustain extreme deflection cycling with no retention performance degradation. Thus, this does not appear to be a significant design or operation problem, reinforcing the contention that screen acquisition devices are essentially load-cycle independent in normal operation.

B. Fabrication Feasibility Demonstration

Large screen surface tension acquisition devices have not been fabricated to any extent; to establish the feasibility of the design concepts, basic fabrication demonstration tests were conducted. These included basic screen welding tests, screen element attachment tests, duct coupling leak tests, and solid channel fabrication tests.

1. Screen Welding Demonstration Tests. After a survey of possible fabrication procedures that could be used to attach the screens to the supporting members within the acquisition device, two techniques were selected for experimental evaluation. The objective was to develop and demonstrate simple attachments that would form a leak-tight joint with a minimum of preparation and tooling. The two selected processes were the GTA fusion-weld (gas tungsten arc) and roll spot-welding (with spot welding as a subcategory).

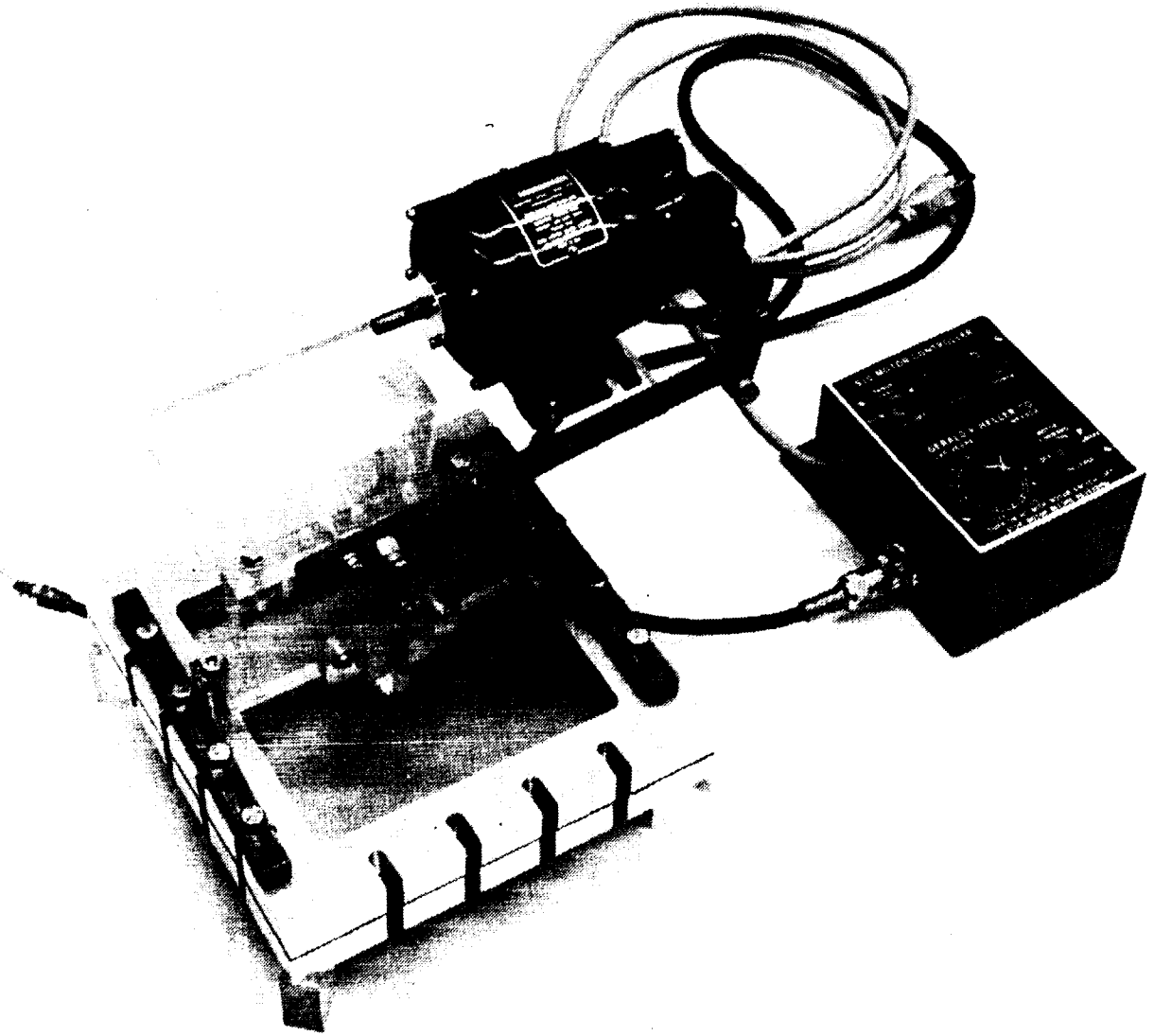

Figure 19. Screen Deflection Test Apparatus

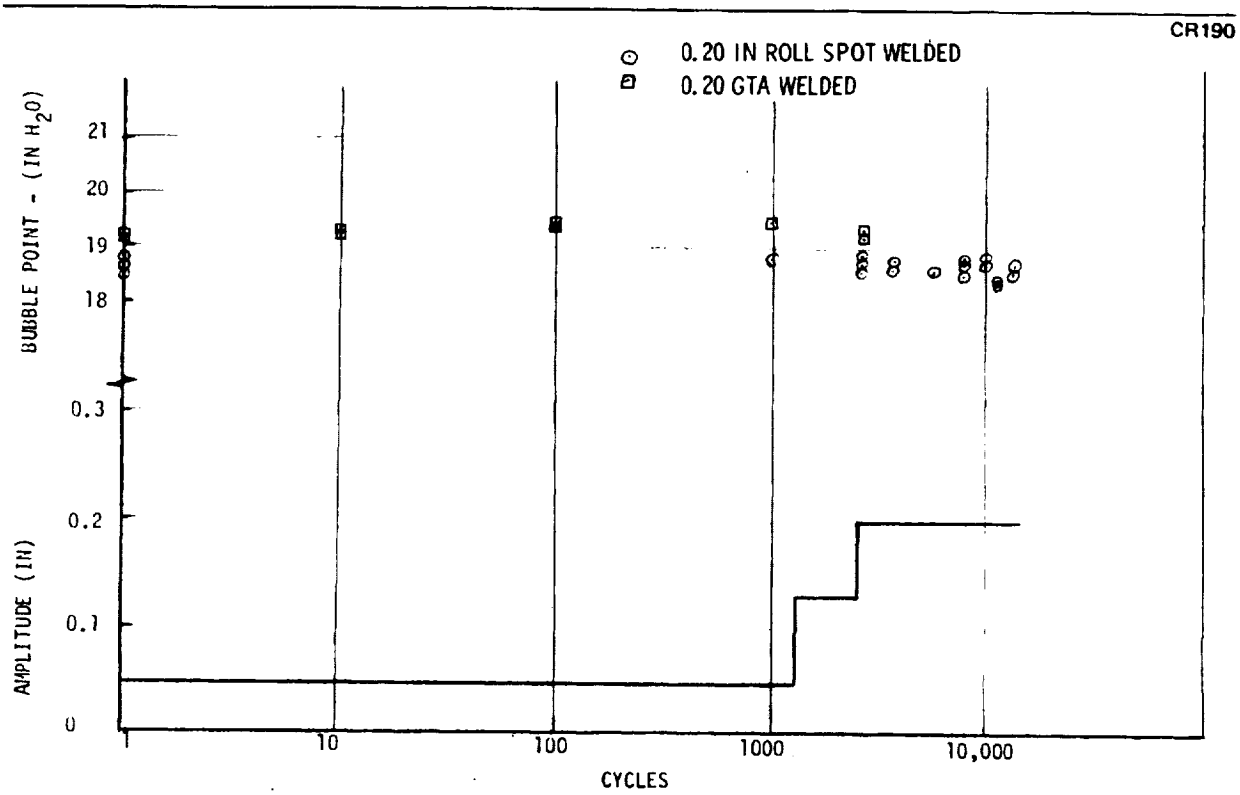

Figure 20. Influence of Deflection Cycles on Screen Element Bubble Point

Welding is preferred over various mechanical techniques because it is inherently more permanent and eliminates the need for a seal common to mechanical attachment. The problems to be overcome in the welding process are primarily concerned with controlling heat addition to prevent burning of fine wires within the screen and to prevent excessive distortion.

In some designs, it has been proposed that the screen be used in a flat state. In addition, it has been recommended that it be joined to a flat stainless-steel sheet (the screen will most probably be stainless steel to minimize difficulties brought about by differential thermal contraction which potentially can degrade the screen bubble point). This sheet in turn is mechanically attached to the channel or support structure itself after the channels have been positioned within the propellant tank.

Two gauges of stainless steel sheet were selected for use during the welding tests: 0.05 and 0.08 cm (0.020 and 0.032 inches). Preliminary tests were run with 200 x 1,400 stainless steel screen. The screen was sandwiched between two pieces of the same gauge sheet, and the three layers were fused together. The weld bead area is as sketched in Figure 21.

The roll spot-welding process involves a series of overlapping spot welds created at the interface or interfaces of lap surfaces. The weld is created by the resistance to welding current across the interface and the simultaneous application of pressure by means of slowly rotating copper wheels. The primary welding variables include welding current (high amperage, short duration) contact pressure, and travel speed. Figure 22 shows several of

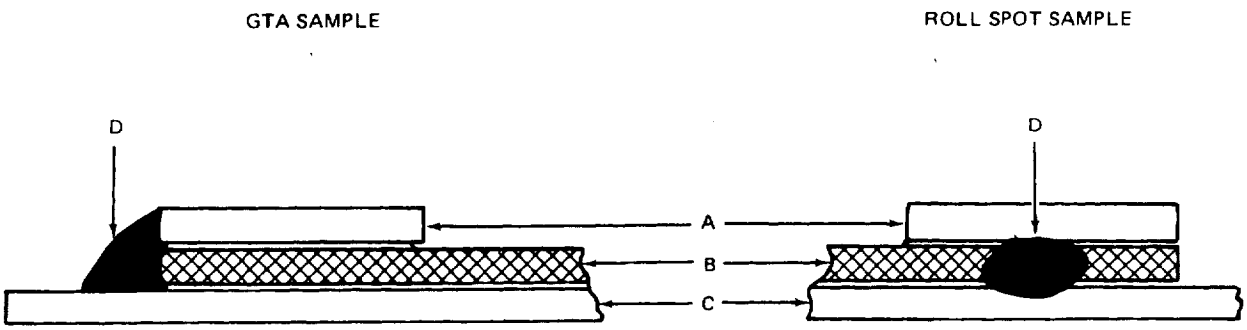

A – RETAINING FRAME
B – SCREEN ELEMENT
C – PERFORATED PLATE
D – WELD BEAD

Figure 21. Selected Screen Attachment Weld Samples

the preliminary roll spot-welded specimens. Peel tests and section cuts made perpendicular to the weld indicated that the fusion was satisfactory. To avoid skewing and misalignment, several spot welds were used to secure the two layers of stainless steel sheet and screen prior to edge welding.

Preliminary GTA welding tests also used both gauges of stainless steel sheet in a lap-joint configuration. The welds were made by clamping the small assemblies in a vice between two pieces of 1.27 cm thick copper plates to serve as chill balls and control distortion. Figure 22 shows several of the weld specimens. Distortion is significantly less in the GTA specimens than in the roll-spot specimens. Sections made through the weld indicate good fusion in both gauges of material. Attempts to form a lap joint between a screen and single piece of sheet were unsuccessful. The latter configuration resulted in several holes burned in the screen. Preliminary tests with configurations in which the screen edge is welded directly to the base plate and in which sandwiches of two sheets of stainless steel and screen were used indicated that this technique could be employed if necessary.

As a result of these preliminary findings, representative screen elements were fabricated for ultimate bubble point evaluation. These screen elements consisted of a perforated steel backup plate, the fine mesh steel screen, and a thin steel "picture" frame. These were welded together by both fusion- and roll-spot-welding techniques. Material thicknesses of 0.051 cm and 0.081 cm were successfully fabricated. Although distortion was more of a problem with roll-spot welding, both techniques appeared adequate. The completed 12.7 cm square screen elements are pictured in Figures 23 and 24. All speci-

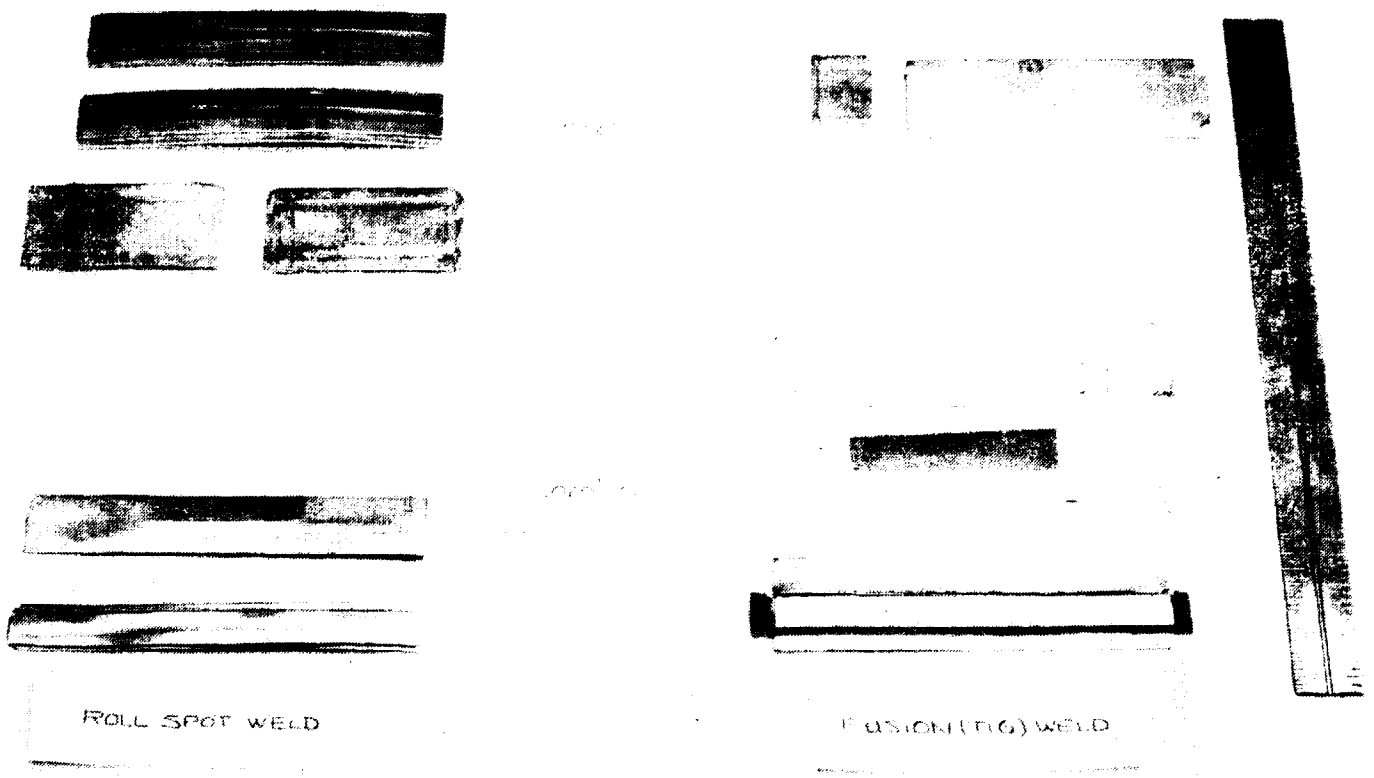

Figure 22. Preliminary Weld Samples

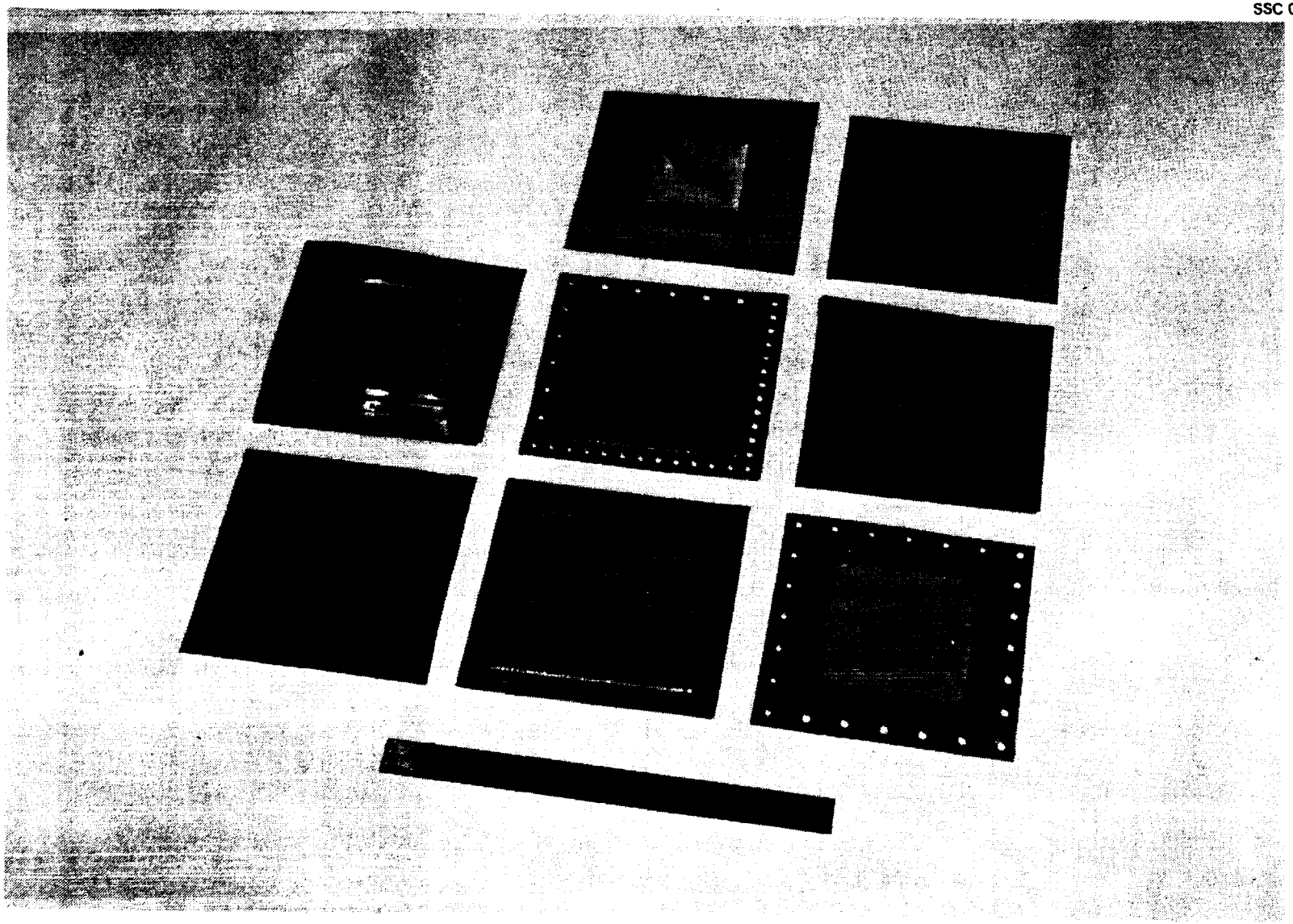

Figure 23. Fabricated Screen Elements

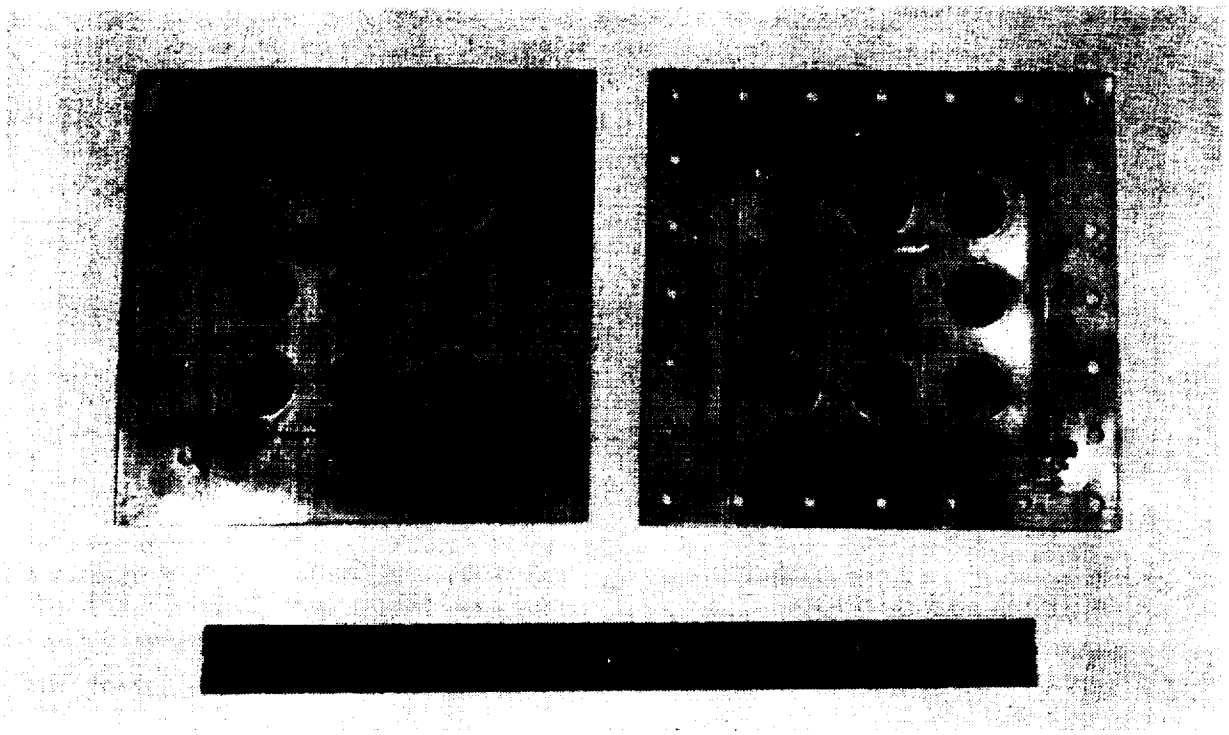

Figure 24. Screen Elements – Rear View

mens were bubble-point tested using the apparatus shown in Figure 25. In all cases, the screen elements exhibited the bubble point of the basic screen material. Thus, the fabrication process did not degrade the retention capability of the basic screen mesh.

In consultations with filter fabricators, it was determined that these same welding techniques could be successfully applied to building cylindrical screen units with solid circular end flanges such as used in the final recommended device designs. The filter fabricators also indicated that their experience had taught them that a carefully controlled roll-spot weld could be created without sandwiching the screen between two layers of sheet metal. They demonstrated that it was possible to roll-spot weld the fine mesh screen directly onto a single piece of stainless steel support material. This approach results in a small weight savings and exposes the weld to patch repairs if required. The sandwich configuration is very difficult to seal if a leak path occurs within the sandwich.

2. Duct Fabrication and Element Joining Tests. During the initial phases of the design study, solid wall ducts were strong candidates for the acquisition device design. The ducts were attractive because it was felt that very light weight and simple joints could be made between subassemblies by nesting the units together and securing them with rivets. Thus, a typical full-scale duct was built to assess its structural integrity. The duct, about 1.1 meter long, was fabricated from 0.051 cm (0.02 inch) sheet 6061-T4 aluminum. (A solid aluminum blank was used in place of a screen in this assembly.) A prime

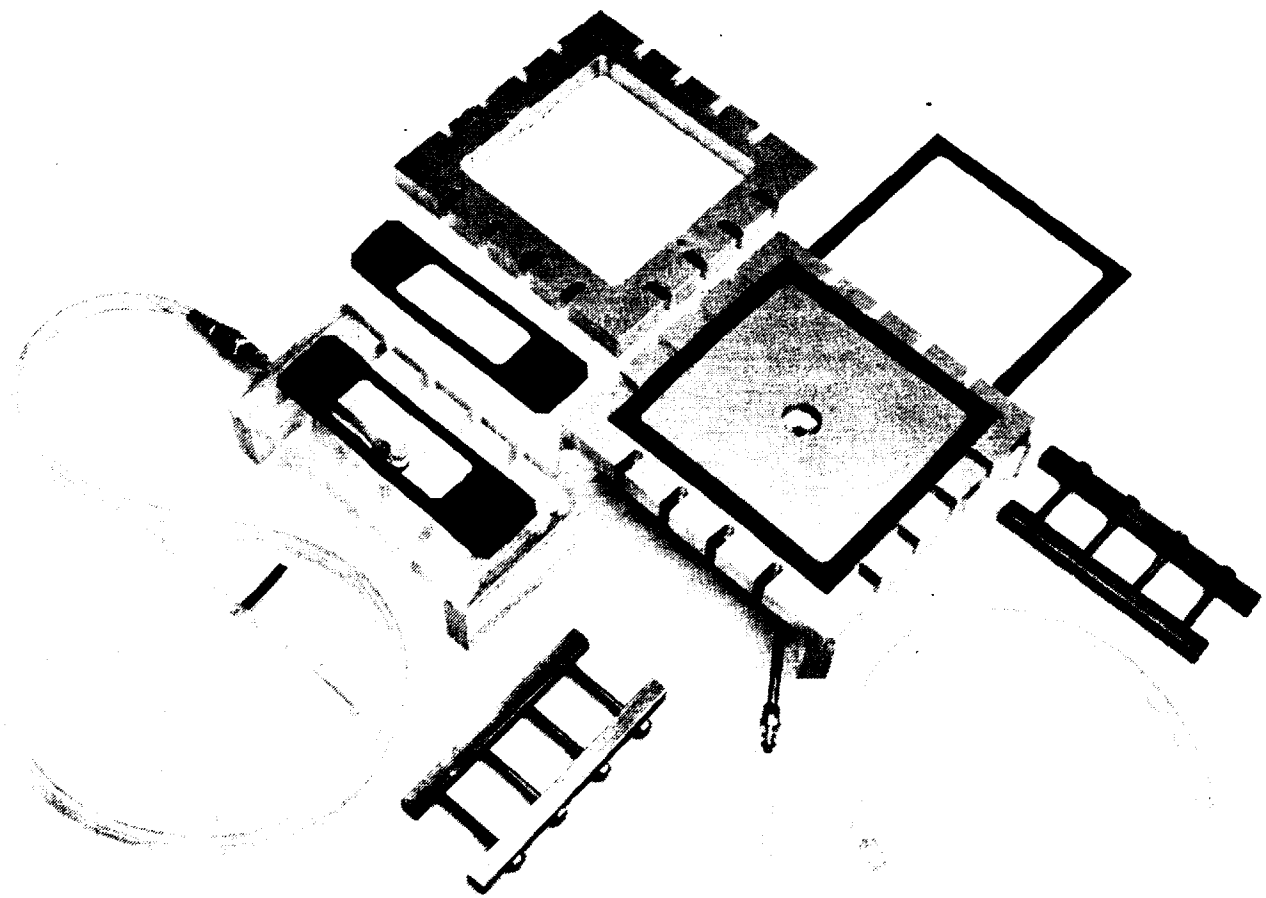

Figure 25. Screen Sample Bubble-Point Test Apparatus

candidate fabrication technique for building up the channels within the tank was conventional riveting, and this was used in fabricating the duct section.

In cross-section, the assembly unit was of the following dimensions:

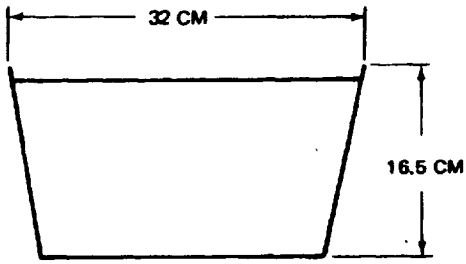

The top of the channel was left solid in the region where customarily it would be cut out beneath the screen. Both ends of the segment were capped so that leak tests could be conducted. No. 40 soft aluminum (Type A) rivets were used throughout the unit. These rivets could be set with a hand squeezer where the location permitted; otherwise, a small hammer and backup block were used.

The segment consisted of three subsegments joined at two nested joints. Both joints (2.5 cm overlap) utilized a rivet pattern of two rows with 1.27 cm spacing, each row having a rivet spacing of 1 cm. The rivets were staggered in the two rows. In one joint, a 1/16 inch diameter indium-tin wire was routed between the two rows of rivets as a gasket. The top cover of the channel was riveted to the sides with a single row of rivets having 1.27 cm spacing; no sealing material was used. The completed duct is shown in Figure 26.

Prior to attaching the end caps on the segment as the final phase of assembly, a visual check was made of the two channel joints. Light leaks could be seen at both joints in four locations.

Following the completion of assembly, the joints between the top and sides of the channel were leak-checked by pressurizing the assembly while it was submerged in isopropyl alcohol. Leak tightness to a ΔP of 51 cm water column (W.C.) is required to match the retention property of 250 x 1370 mesh on the channel. Leaks at several locations were evident at 10 cm W.C. Although sealants could have been used in the joint, their use would raise compatibility problems, particularly with the LO_2.

In conclusion, it is apparent that the riveted, trapezoidal channel segment has inherent weaknesses that cannot be corrected simply. The corners in the bottom of the channel could be more gently rounded to eliminate leakage there, but on top this is not possible. A greater bend radius on top would preclude access required for close rivet spacing. Thus, riveting to achieve a leak-tight joint against bubble-point pressures does not appear feasible. The unit does exhibit a surprising degree of overall rigidity, even though assembled from light gage material, and the use of 0.051 cm (0.020 in.) sheet material seems justified.

a. Screen Element Mechanical Attachment. The combination of screws and nutplates has been proposed for mechanically attaching the screen

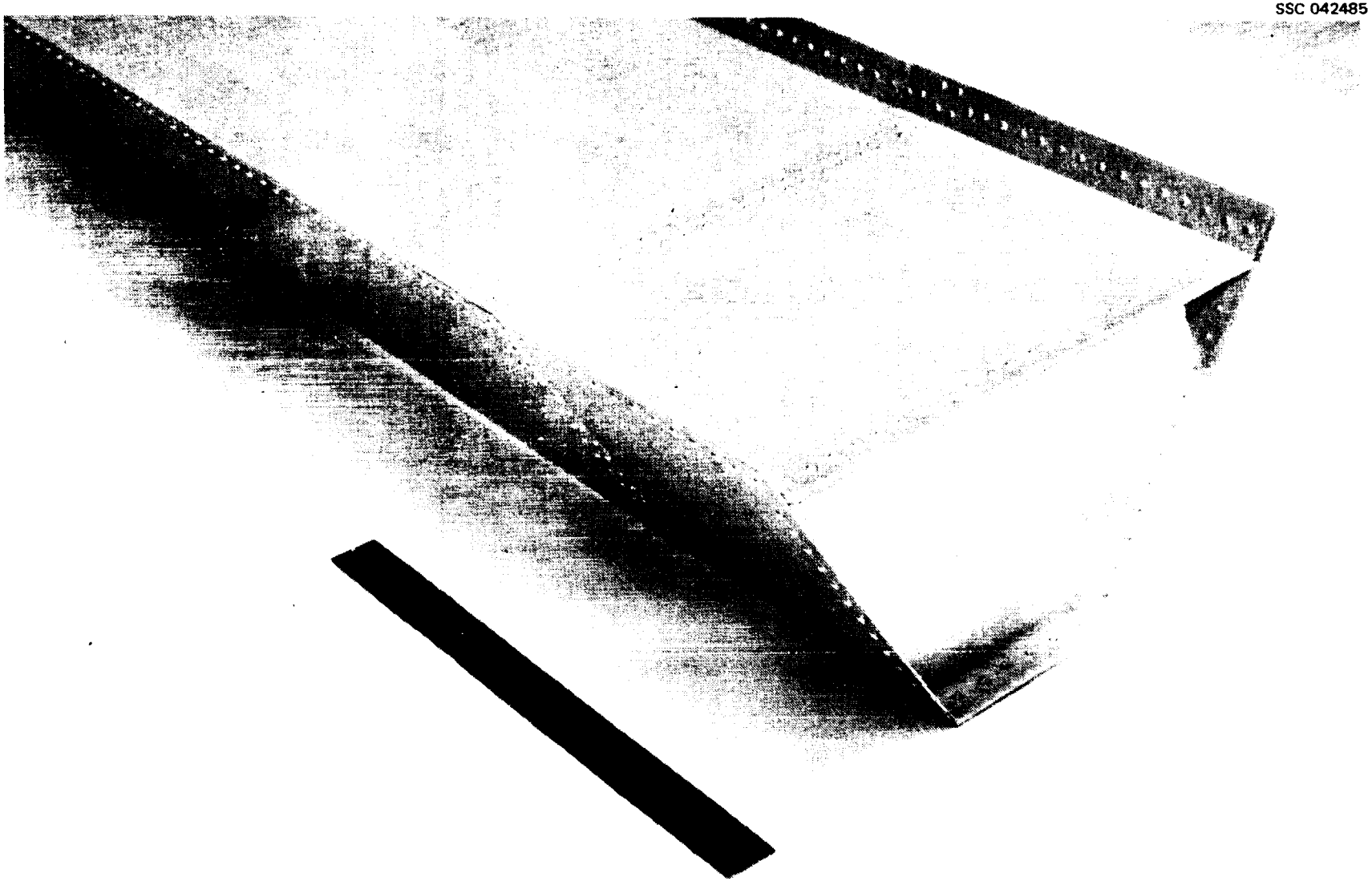

Figure 26. Fabricated Solid Duct

elements (screen/backup plate combination) to the aluminum frame that constitutes the top of the acquisition channel. A bench test was conducted to determine the effectiveness of this type of attachment. The objectives were to determine the necessary screw spacing and to determine if a gasket material was necessary to effect a leak-tight joint. The joint must be leak-tight when submerged in isopropyl alcohol and subjected to a ΔP of 51 cm W. C. This ΔP corresponds to the bubble point of a 250 x 1370 dutch twill screen mesh in isopropyl alcohol.

The two screen elements used were the stainless steel specimens fabricated as part of the welding bench test (see Figure 23). One specimen had seven holes with a spacing of 2.65 cm along each of the four edges. The second specimen had this same pattern on two adjacent edges and 13 holes with 1.32 cm spacing along the remaining two edges. The acquisition channel frame/nutplate combination was simulated by an aluminum baseplate with a sufficient number of tapped holes to match those in the screen/backup specimens. The various test components are illustrated in Figure 27. Neither specimen which was attached directly to the baseplate proved to be leak tight. Both 10-32 and 6-32 screws were used. When leak tested, there were numerous small leaks. This occurred between screws on all four edges of both specimens.

Next, a 1.6 mm diameter indium-tin wire (Cerroseal 35) was used as a gasket with both specimens. The ends of the wire were overlapped as near as possible to one of the screws. The first specimen was leak-tight at the required ΔP of 51 cm W. C. The second specimen had a single leak at the point of overlap on the indium-tin wire. The indium-tin wire thus appears to be a viable solution to sealing the screen to the channel in a nonpermanent fashion. This material would have to be controlled closely to assure compatibility with liquid oxygen. Also, the frame on the acquisition channel must be sufficiently rigid to prevent deflection between screws, as was the case with the baseplate used in the bench test. If the channel frame distorts significantly under the loading caused by the attachment screws, then the positive results of the bench test would be invalidated.

3. Screen Repair Study Investigation. It is anticipated that imperfections will be present in large pieces of screen material to be used in acquisition device production. Even the most closely controlled weaving on the best of looms cannot eliminate possible defects. The screen bubble point can be seriously reduced by broken or missing wires. Therefore, it is necessary that patching techniques be available to make local repairs. Prior to fabrication, a light table can be used to disclose such defects. A bubble point test of the screen material as taken off the roll may also be desirable and feasible at this point. In any case, defects which were caused by the fabrication processes and handling will also be disclosed in the final bubble point acceptance test of the device.

Techniques that were considered as potential repair candidates were sheet metal patches, solder, and adhesives. Small sheet metal patches spot-welded over inperfections have been used successfully on an MDAC IRAD screen acquisition device for LH_2 service. It is expected that this approach would be applicable to a LOX system as well. A survey of different types of solder did not disclose a compound that would not be expected to become brittle at cryogenic temperatures. This embrittlement may lead to cracking, and thereby, destroy the effectiveness of the patch. However, possibilities in the area of soldering were not exhausted in our limited investigation.

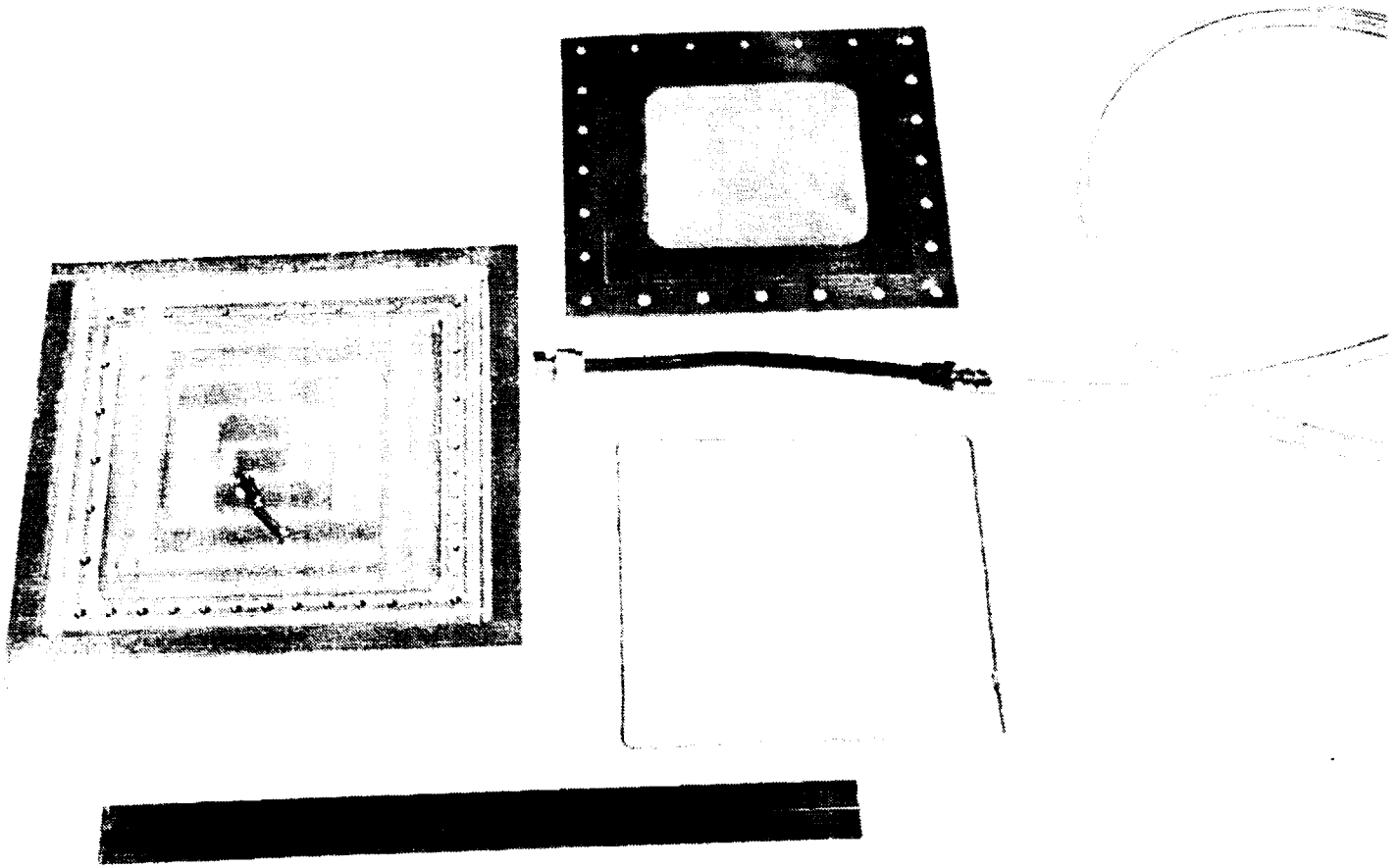

Figure 27. Attachment Evaluation Test Apparatus

Polyurethane adhesive was investigated as a useful repair material in LH_2 since MDAC has found this to be one of the few materials that retain flexibility at LH_2 temperatures. The adhesive was placed on small swatches of fine-mesh stainless steel screen and submerged repeatedly in LH_2. No degradation of the bond was observed. Small pieces of screen were also bonded to fittings with this adhesive for the bubble point tests in LH_2. No difficulties were encountered. Polyurethane is not generally compatible with an oxidizer environment and an extensive series of coatings is required for protection in LOX.

4. Coupling Seal Evaluation. Marman-type flanges have been proposed as a leak-tight means of joining segments of an acquisition device. The Marman flanges can be brought together simply and secured with a V-band. This type of joint has been used many times in the cryogenic environment and is readily available in a range of sizes. The seal is effected by an O-ring located in a gland on one of the mating flanges.

Four O-ring candidates were selected as potential sealing agents on a seven inch diameter Marman flange. These candidates were tested in LH_2 (See Figure 28.) A Marman joint containing the O-ring was pressurized (ΔP = 5 psia) while submerged in LH_2. Leakage was detected by the observation of bubbling anywhere on the perimeter of the joint. In actual use, the flange joint is under compression due to pressure forces ($\leq$screen bubble point). However, the pressurized flange test was much more straightforward and should yield a conservative result. A Creavey seal (teflon-coated stainless steel spring) was selected as the sealing O-ring. Three test units showed no detectable leakage. The particular coupling tested was a type 4570-700N 7-in diameter unit with an AS 300-7.360 Creavey seal. This is one of the more rugged Marman units and it is recommended that lighter flanges be leak-tested as part of a weight reduction program.

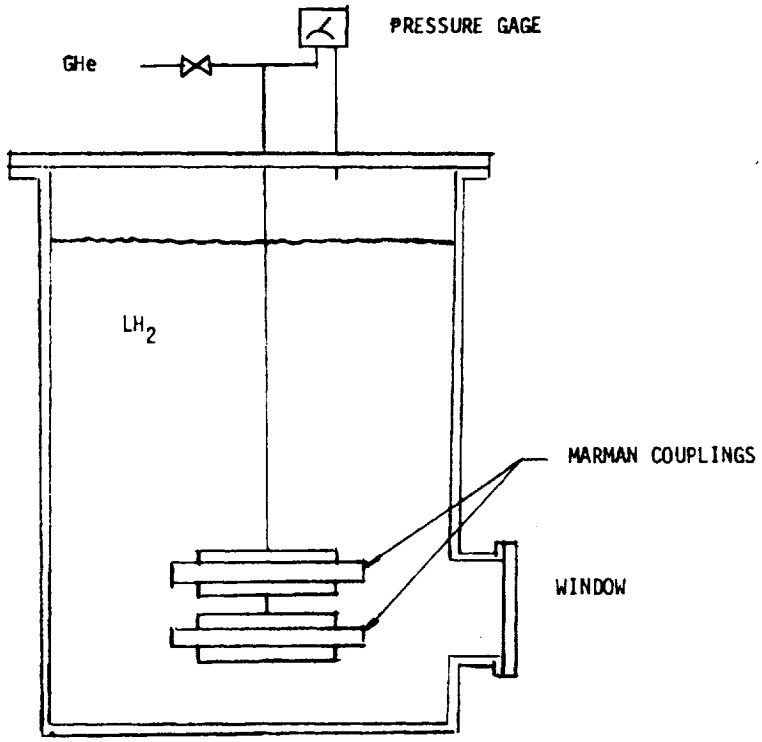

Figure 28. Coupling Leak Test Setup

C. Operational Problems Investigation

As the design study progressed, a number of operational problems became defined that could lead to acquisition device liquid retention failures. Limited experimental investigations were initiated in these areas to establish appropriate design criteria and operational limits, or at least further define the problem and set up the requirements for further research. Four areas were pursued: (1) screen heat transfer problems that could lead to device retention breakdown; (2) device vibration and its influence on retention breakdown; (3) gas ingestion problems in the practical utilization of multi-layer screens; and (4) the feasibility of film bubble-point test for in-place device checkout. These are discussed below.

1. Screen Heat Transfer Experiments. The potential screen heat transfer problem represents one of the major problems for a cryogenic acquisition/expulsion device. It was found in the design study that it strongly influenced the overall feed system design. Therefore, considerable effort was expended on this problem, and several experimental programs were conducted to define and explore the problem.

a. Heat Transfer Effects on LH_2 Bubble Point Tests. The presence of a warm ullage within the propellant tank may adversely affect the retention capability of a fine-mesh screen. If evaporation from the screen exceeds the rate at which liquid can be resupplied from that contained by the screen system, drying will result, with a serious loss in retention.

The apparatus sketched in Figure 29 was available to conduct bubble-point tests in LH_2 with a controlled rate of heat addition to the liquid from a warm pressurizing gas (GH_2) at atmospheric pressure. This equipment had been used to conduct identical tests in LN_2 as part of an MDAC IRAD program. The results of LN_2 tests are reported in Reference 4. No change in bubble point was observed during these tests using six different fine-mesh screen samples with heat transfer rates up to 9.5×10^3 watt/m^2 (3,000 Btu/hr-ft^2).

The test apparatus includes a resistance heater and electric fan positioned directly above the screen (Figure 30). The evaporating liquid is heated and directed down against the screen to further the evaporation process at the screen. Gas is bled from the foam-insulated cylinder at a sufficient rate to hold the ΔP across the screen at the desired level. Net heat transfer to the screen is computed, by multiplying the net mass flow from the cylinder and the latent heat of vaporization. Pressure across the screen is gradually increased until failure occurs. Failure was detected visually by observing the screen through windows located around the bottom of the dewar.

Two screen specimens (250 x 1.370 and 200 x 1,400, see Figure 31) were prepared by attaching the screen to sample plates which in turn were attached to the lower end of the foam insulation cylinder. Figure 32 shows the details of the screen sample installation in the test apparatus.

Based on a preliminary bubble-point test in isopropyl alcohol (σ = 21.4 dyne/cm at 294 °K), the expected bubble point in LH_2 (σ = 1.95 dyne/cm at 20.3 °K) would be 36.9 mm of water column (W.C.) for the 200 x 1400

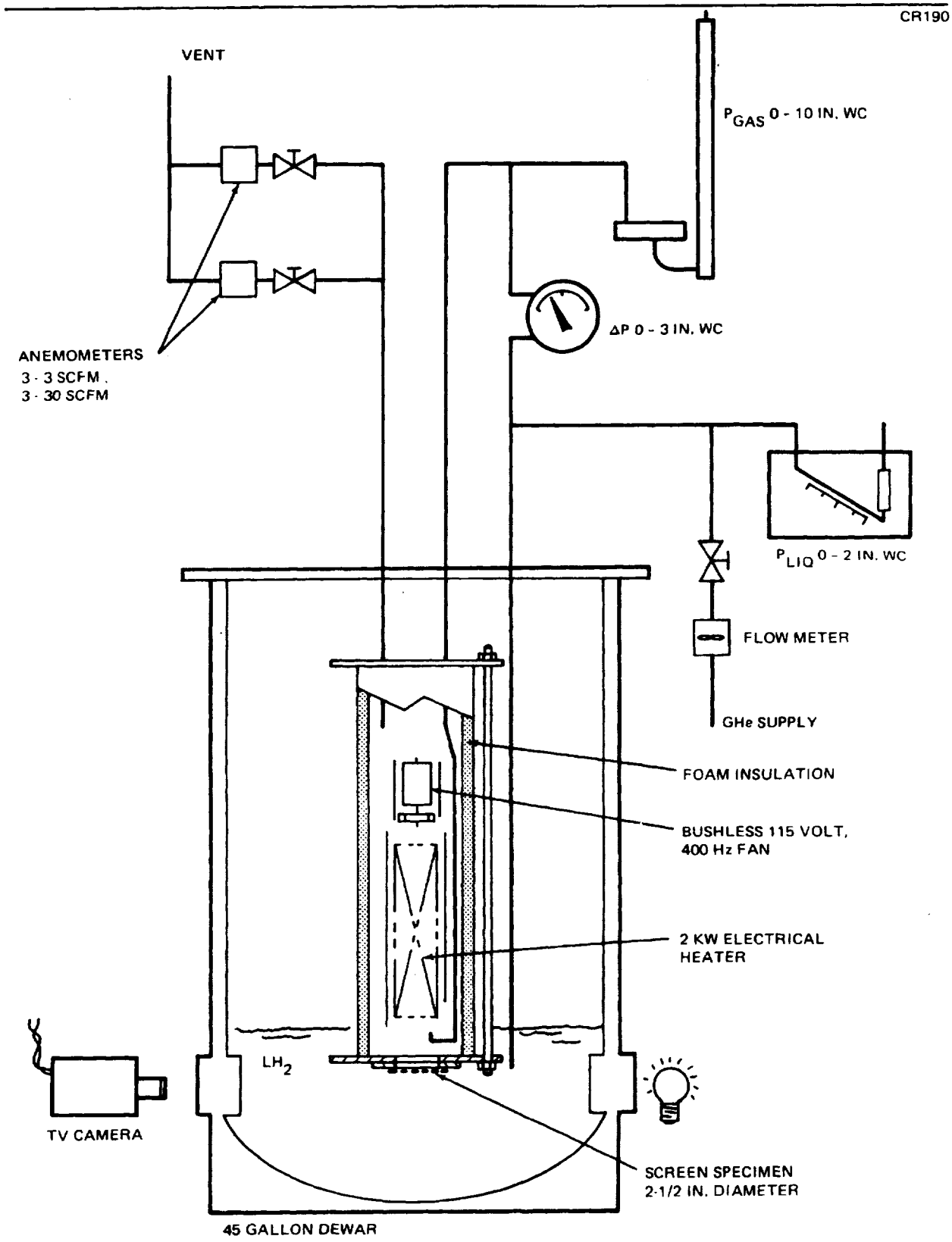

Figure 29. Screen Heating Apparatus

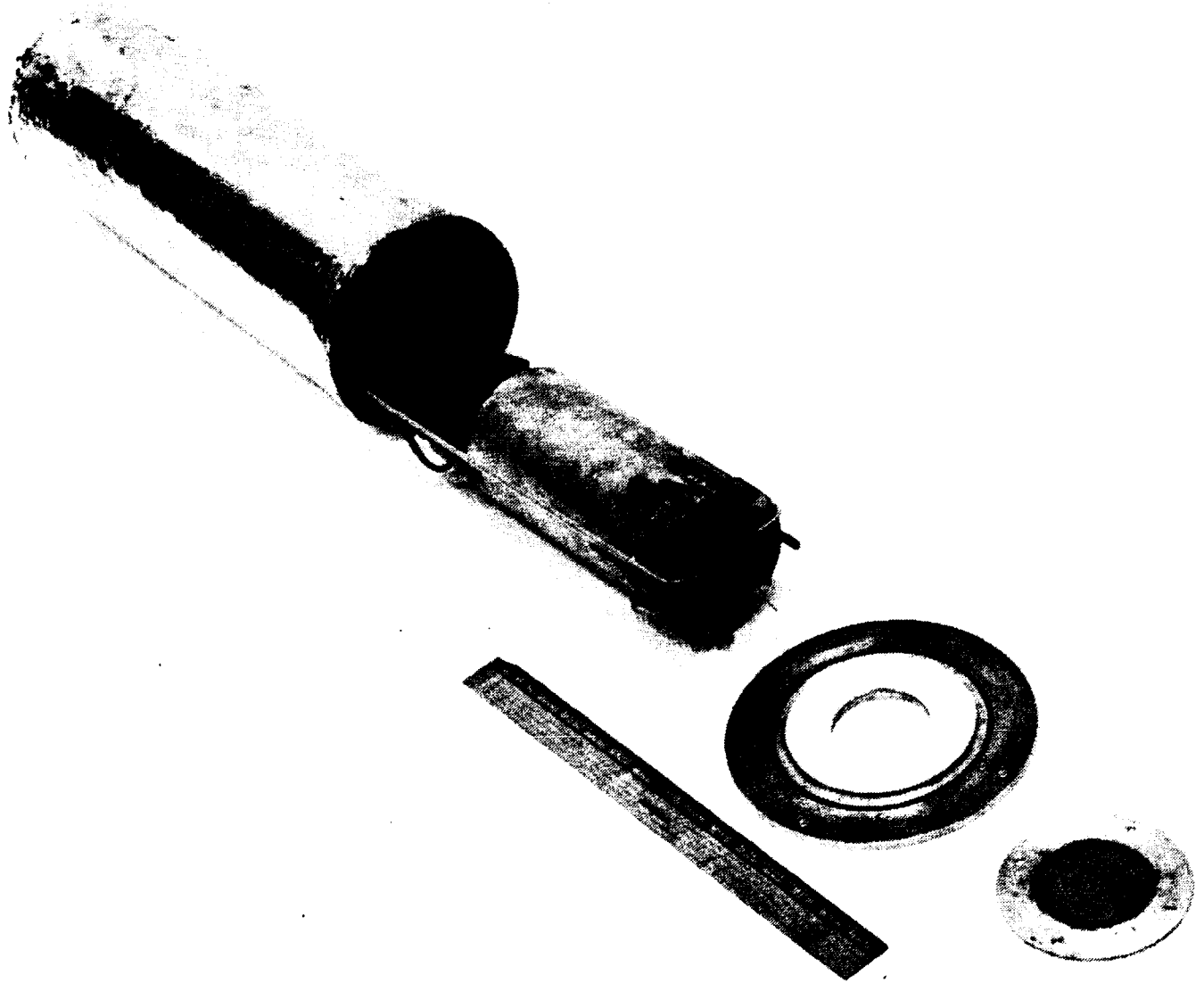

Figure 30. Heat Transfer Test Apparatus

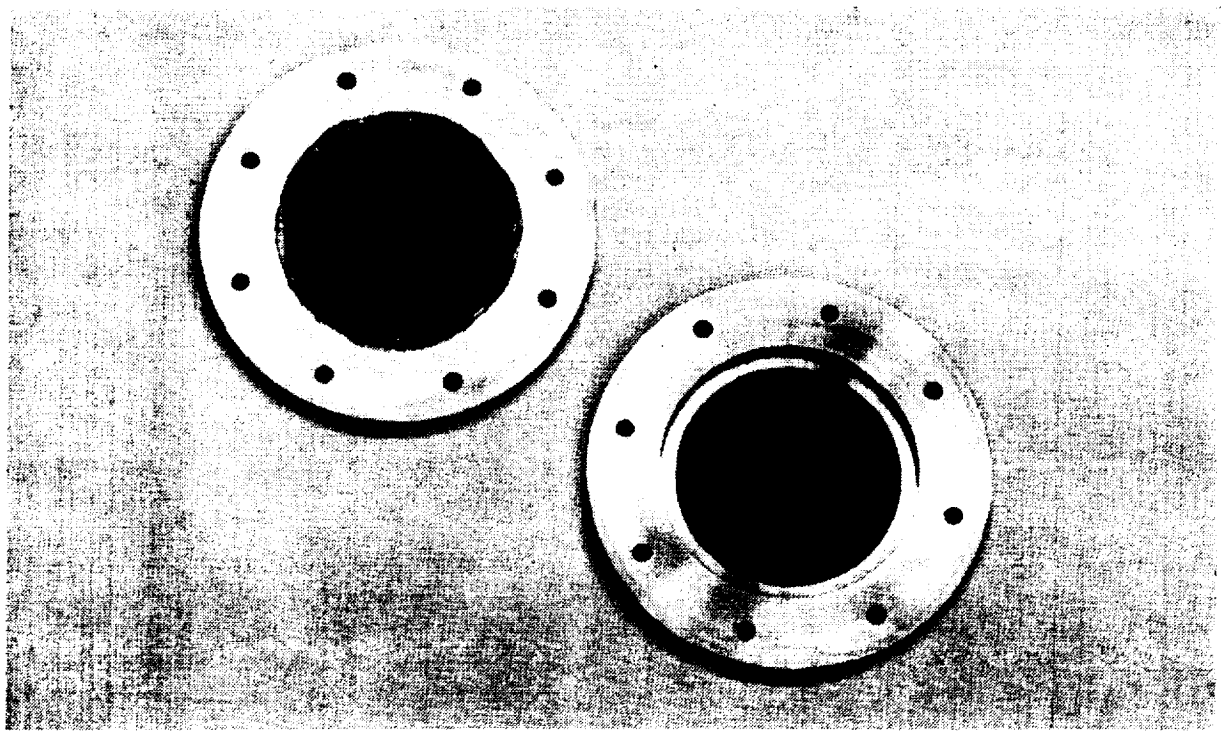

Figure 31. Heat Transfer Test Screen Samples and Holders

mesh. None of the test data used to compute the net heat transfer to this screen is reported here since leaks in the electrical feedthrough and a cracked O-ring seal were discovered during disassembly, which invalidated the data. The vent rate, though suspect, showed a net heat transfer coefficient of approximately 25 joules/m^2 sec °K. The data for the 200 x 1400 screen indicated a serious reduction in bubble point with an increasing rate of heat transfer to the screen. Reductions of up to 50 percent in bubble-point were observed. Prior to installing the 250 x 1370 mesh sample, all leaks in the system were repaired. The test data for the 250 x 1370 mesh screen are shown in Figures 33 and 34. An increased vent rate was observed with this screen as the heat transfer coefficient approached the range of 40 to 60 joules/m^2 sec °K as shown in Figure 33. As with the 200 x 1400 specimen, the foam insulated cylinder would not pressurize itself when the vent line was closed off. An acceptable explanation for this occurrence was not discovered (during disassembly, no potential leak paths were uncovered). The heat transfer coefficients were computed based on data taken with the vent line open and a small ΔP (2.5 mm W.C.) across the screen. This heat transfer coefficient does not change as the ΔP across the screen increases (this was demonstrated in the LN_2 tests reported in Reference 4). Figure 34 presents the measured bubble point as a function of temperature differential at the screen. This shows a rapid dropoff in bubble point pressure with increasing gas temperature.

The test data of Figure 34 were generated in the following manner. At the fixed values of T_1, the heater was turned up to rapidly increase the pressure above the screen to the breakdown point. The temperature T_1 did

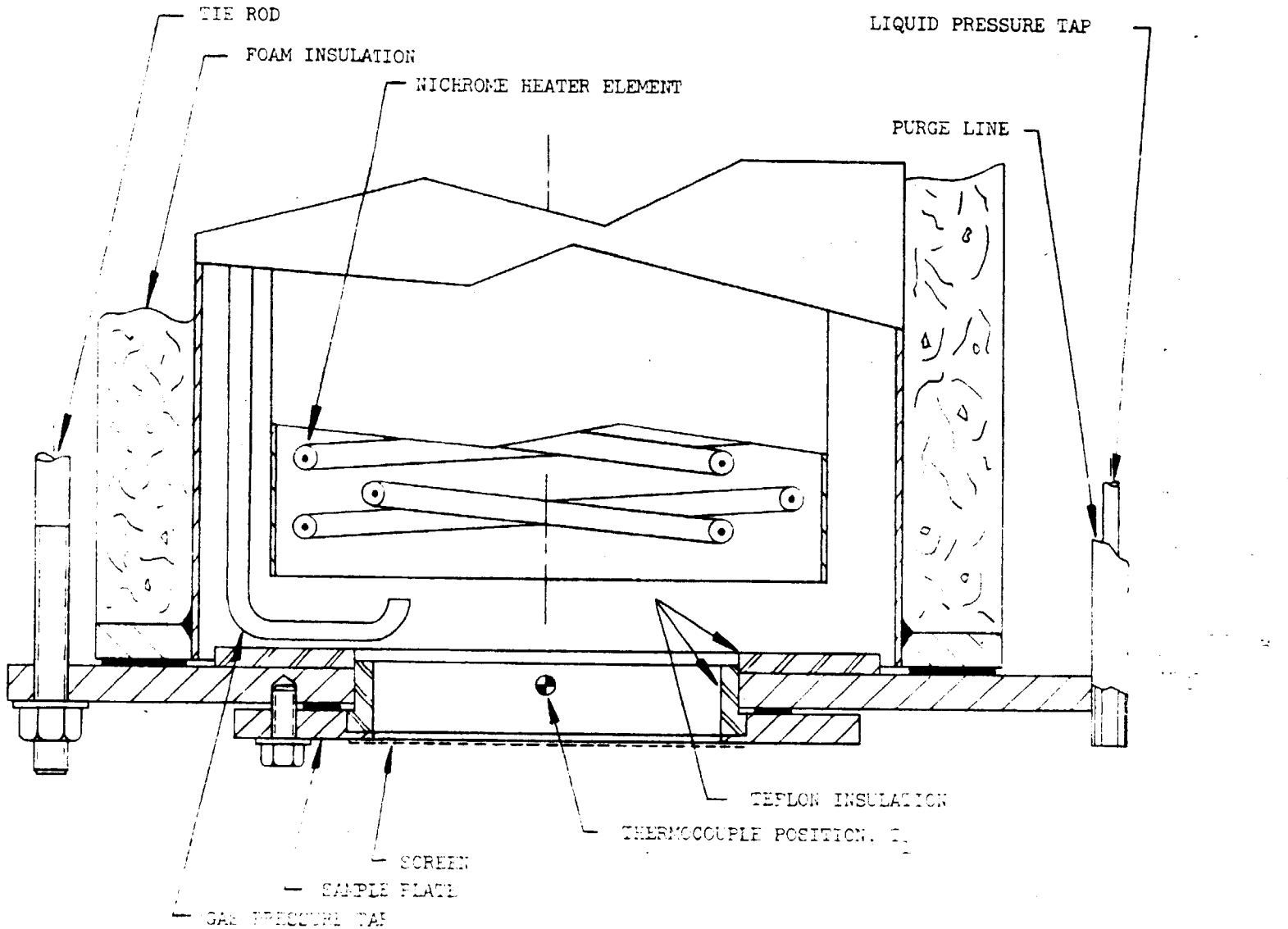

Figure 32. Section View of Screen Sample Plate (Full Scale)

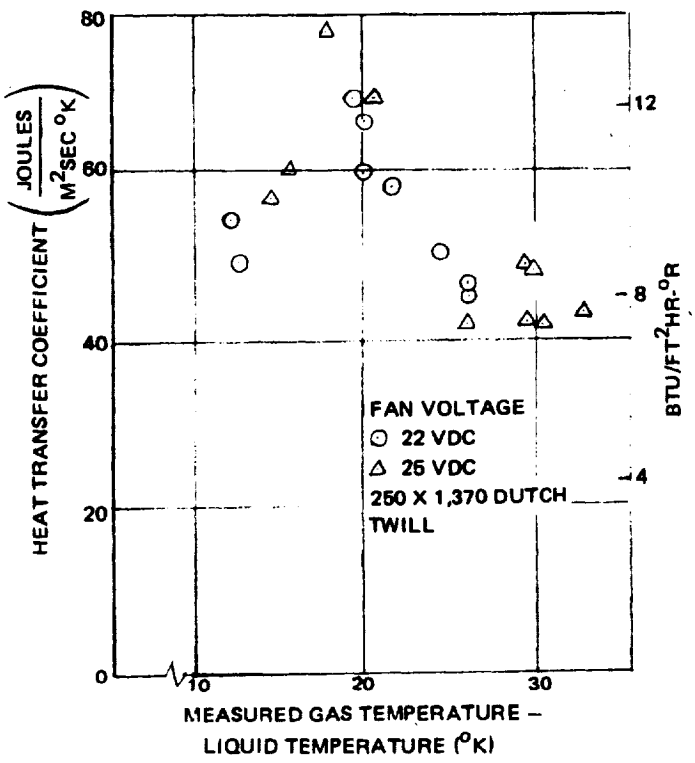

Figure 33. Forced Heat Transfer Coefficient at Screen

not change during this operation. This procedure was used to replace the planned technique of throttling the vent to raise the pressure. The disadvantage in using the heater to raise the pressure is that there is a tendency to lose control of the pressure increase rate. The heater caused the pressure to rise in a rapid fashion which may have exceeded the response rate of the fluid-filled inclined manometer recording the ΔP across the screen. Increased T_1 resulted in a small, continuous failure of the screen. The steady-state pressures observed at those points should be very close to the bubble point pressure. Based on the alcohol tests, the LH_2 bubble point for the 250 x 1370 mesh should be 43.2 mm (1.7 in.) W.C.. The test data for gas temperatures below 27.6 °K is within 10 percent of this value. At higher temperatures a continuous failure was observed in some instances, as noted in Figure 34.

The data in Figure 34 was replotted in Figure 35 as a ratio of the measured retained head to the head with no heat transfer. (Minimum gas temperature.) This shows the dramatic reduction in retention performance with local ullage gas temperature.

From these tests, it was shown that the presence of a warm gas pressurant can seriously reduce the bubble point performance of a screen. This result is in direct contradiction to that observed during testing with LN_2 in which there was no significant bubble point change.

Although the previous LN_2 tests indicated that a screen might be capable of sustaining high heating rates without head retention loss, these LH_2 results cast strong doubt on the practical feasibility of using screen acquisition

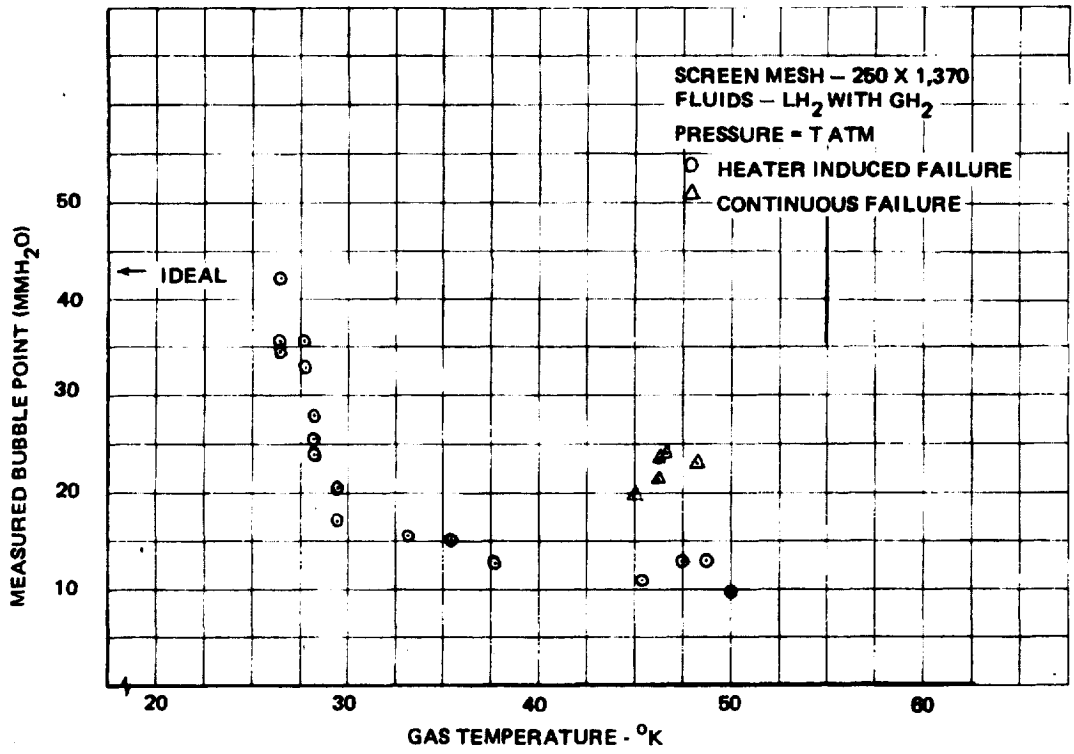

Figure 34. Bubble Point Data for 250 X 1370 Mesh in LH_2

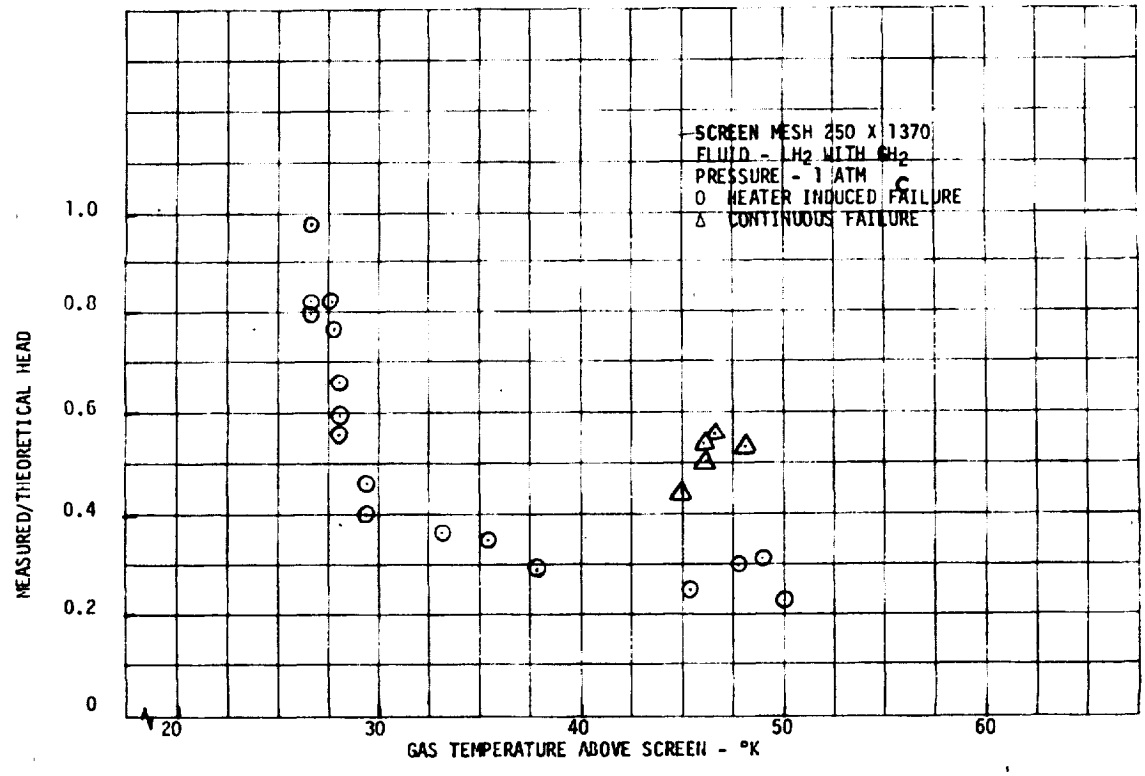

Figure 35. Influence of Warm GH_2 Above Screen Retaining LH_2

devices where direct contact occurs between the screen and a warm pressurant gas. Extensive experimental research would be required to firmly establish design criteria and operational limits before warm gas pressurization could be confidently applied to any specific screen system for an LH_2 tank.

b. Pressure-Decay-Induced Screen Breakdown Experiment. Autogenous pressurization of exposed screen acquisition devices involves complicated heat and mass transfer phenomena, especially in a low-g environment. As discussed in the design study, Volume I, boiling can occur within a screen device as a result of tank pressure decay. This phenomenon could cause the screen acquisition system to fail, either due to the ingestion of vapor bubbles or to the drying of the screen. Since virtually no work has been done on the problem of pressure-decay-induced screen boiling, a test was conducted to demonstrate the severity of the problem.

It was first necessary to fabricate a screen device which had a minimum of internal solid supports, since boiling on these areas would obscure the boiling-off of the screen itself. The device shown in Figure 36 minimized all boiling except for that on the screen. The liquid hydrogen contained within the screen is not in direct contact with any weldment or solid supports. As shown in the Figure, the welded strips join the screens so as to provide a cooling flow path. The configuration selected is similar to that of a milk carton to facilitate fabrication. The device is formed by bending the screen and joining with two weld strips, rather than cutting and joining the screen, which would involve more complicated fabrication. Two thin weld rods (approximately 1/16-inch diameter) were bent and placed inside the screen device at the edges to support the walls.

The pressure decay test was conducted within the 130-liter LH_2 dewar that has been used in the previous screen element heat transfer tests. This dewar is particularly useful because it contains five small circular windows that permit observation of the LH_2 test region. Figure 37 shows the placement and operation of the significant test components.

Prior to LH_2 testing, the screen carton was bubble-point tested by submerging it upright in isopropyl alcohol and bubbling gas into the open lower end. The maximum column height of gas that could be trapped within the carton was 18 cm. Several regions along screen folds were sealed with polyurethane adhesive to obtain this bubble point. The corresponding bubble point in LH_2 (σ = 1.95 dyne/cm at 20.2°K) is equal to a liquid head of 19 cm.

A cold ullage region was created around the screen carton by extending it upward into an inverted rectangular box that was foam-insulated and submerged completely in LH_2 (dimensions: 20 x 20 x 25 cm). Gaseous hydrogen could be delivered to this ullage region by either an overhead line (prechilled by LN_2) or a submerged pressurization line. It was possible to move the screen carton in and out of the rectangular box by means of a mechanical linkage extending through the dewar lid. Rotating the screen downward and to the side as shown in Figure 37 allowed the ullage to be prepressurized before introducing the screen and also refilled the screen carton with liquid. The screen carton extended 13 cm into the ullage region. Therefore, the safety factor on surface tension retention at 20.2 °K is 1.5 (= 19/13). This safety factor diminishes as the liquid temperature increases (causing a reduction in surface tension). The screen device is shown in Figure 38.

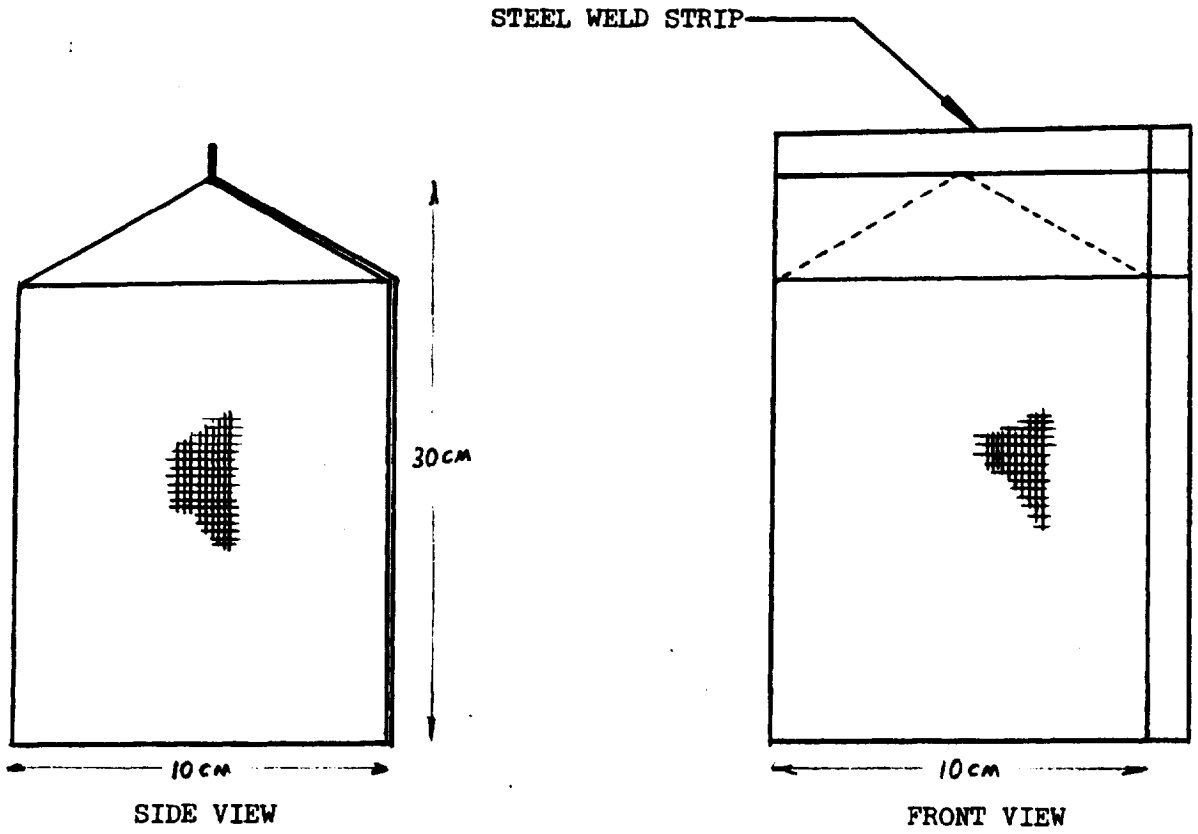

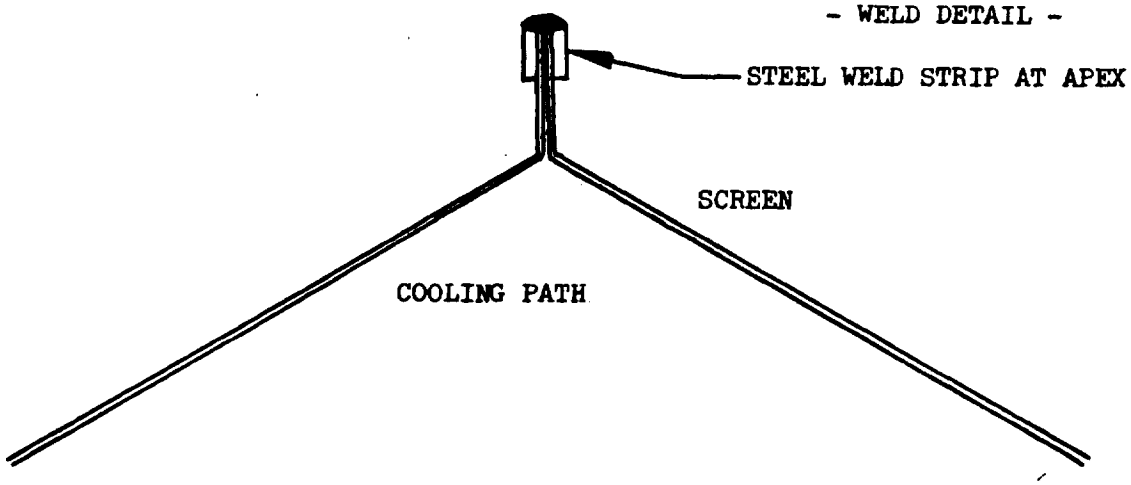

Figure 36. Milk Carton Configuraton Screen Device for Pressure Decay Induced Boiling Test

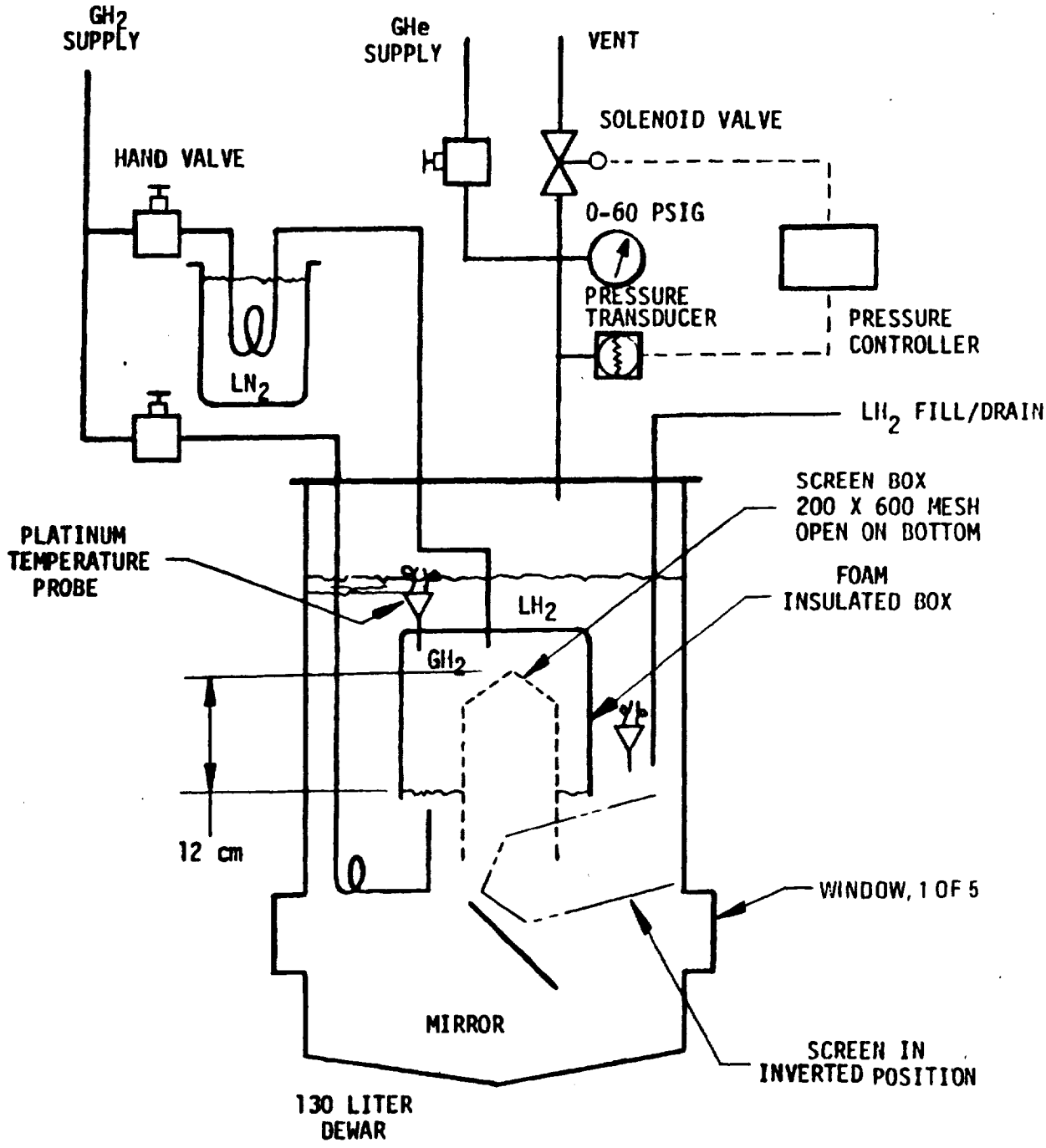

Figure 37. LH_2 Pressure Decay Apparatus

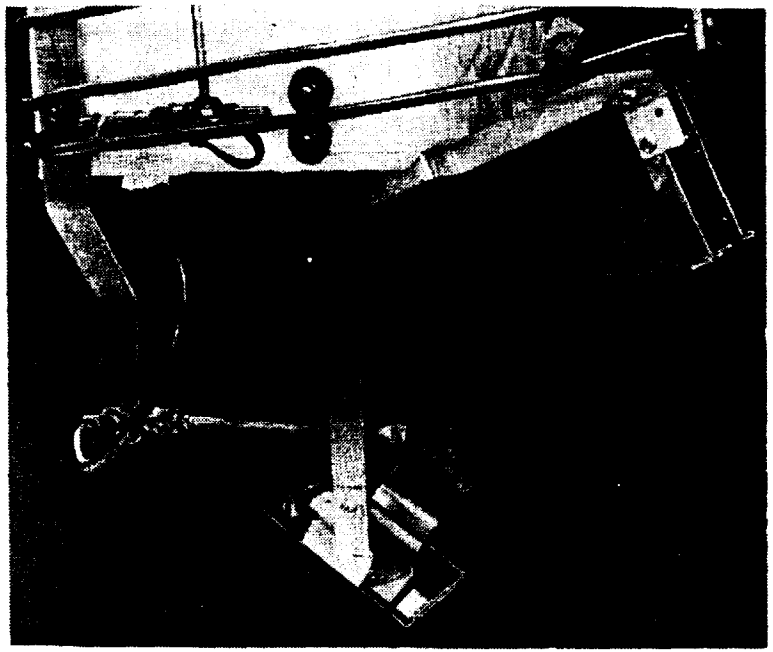

(A) RETRACTED POSITION

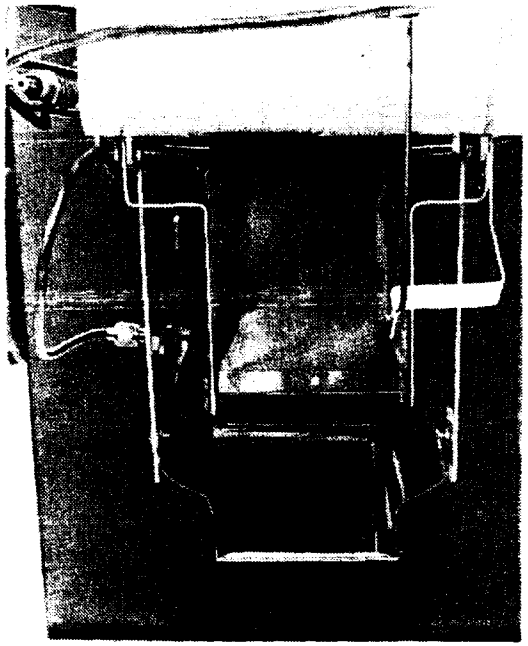

(B) MIRROR VIEW- VERTICAL POSITION

Figure 38. Milk Carton Test Apparatus

The combination of a dewar pressure transducer, vent solenoid valve, and pressure controller was used to fix the hold and decay pressure profiles within the ullage region around the screen carton. A typical test consisted of holding the ullage pressure constant for several minutes and then venting to 0 psig in a linear fashion in several additional minutes. The controller was adaptable to varying hold pressures and decay rates.

Observation of the inside of the screen carton was facilitated by a mirror located in the bottom of the dewar. When viewing through one of the window ports, the complete interior of the carton could be seen as an image in this mirror (see Figure 38). A portion of the inside of the insulated box could also be viewed through a window port. Lighting was provided by a high-intensity lamp positioned above a window on the top of the dewar. During some of the tests, boiling of the highly stratified layer in the dewar produced a dense hydrogen fog which decreased the light level so that the interior of the screen could not be observed.

A series of 23 test sequences was conducted in which the screen carton was exposed to a GH_2 ullage of varying temperature and pressure. Five of these tests were recorded on film using an Arriflex movie camera running at a nominal speed of 12 frames per second. Difficulties encountered in maintaining proper lighting conditions compromised film quality, but with detailed study general results could be obtained.

The standard test procedure consisted first of forming a cold ullage region in the foam insulated box with the screen carton lowered beneath the box. The submerged gas pressurization line (see Figure 34), could not be used for pressurizing the foam box because of excessive LH_2 heating and boil-off in the bulk region and GH_2 condensation in the line. Therefore, the overhead pressurization line introduced the gas which was permitted to chilldown with additional GH_2 added as required to displace LH_2 from the box. The screen carton was raised into the ullage once the desired gas temperature and pressure were achieved. A hold period at constant pressure followed with a duration of 0 to 15 minutes. The last phase of the test consisted of reducing the ullage pressure in an approximately linear fashion to 0 psig. A compilation of test data is given in Appendix B.

Three tests resulted in screen stability failures within several seconds of raising the screen into the ullage. These tests were those with the warmest ullage conditions, and the failure is attributed to the presence of the warm gas. The ullage temperature was approximately 39 °K (70 °R) in two instances and 44.5 °K (80 °R) in the third. A test discussed in the previous section had shown that this gas temperature was sufficient to cause breakdown of the screen.

A difficulty encountered when the screen device entered the ullage was that additional chilldown of the ullage caused the liquid level to rise in the foam insulated box. The rising level reduced the hydrostatic pressure on the screen and reduced the area of screen on which condensation could take place. In seven tests, attempts were made to add GH_2 at varying rates to the ullage during the hold period to maintain the liquid level at the bottom of the foam box. In each of the seven cases, the screen stability failed shortly after exposure to the gas stream. These failures are attributed to the direct gas impingement from the overhead pressurization line onto the screen surface. Tests at the same gas temperature in the absence of gas impingement showed no failure.

In two cases among the remaining eight tests, there were no screen failures during either the hold or decay period. The hold periods at 3 atm were 2 and 15 minutes, respectively. The absence of failure might best be explained by the rising liquid level around the screen carton. This would reduce or eliminate the ΔP acting across the screen surfaces. The other six tests also took place at 3 atm and screen failure occurred in each case. The maximum gas temperature during hold was approximately 30.7 °K (55 °R). The failures coincided with the ullage pressure dropping below the vapor pressure within the bulk liquid. It was not possible in these tests to generate the largest portion of the liquid heating within the screen via the warm ullage gas. Heating of the liquid originated primarily at the boundaries of the liquid at the bottom, sides, and top of the dewar.

The series of tests just described emphasized several considerations important to the operation of a LH_2 surface tension acquisition device. First, the use of warm gas (which can be aggravated by direct impingement on the screen) is to be avoided. Gas temperatures of 39 °K (70 °R) destablized the screen in these tests. Secondly, dropping the ullage pressure below the saturation pressure caused the formation of vapor within the screen and, in these tests, caused gas to break through the screen from the ullage region. These results again point up the potential difficulty in using warm gas pressurization with screen surface tension acquisition devices.

c. Quantitative Screen Heat Transfer Experiment. The tests described above served to identify a potential thermal problem with basic screen devices. To adequately design and evaluate surface tension acquisition systems, the quantitative relationships between screen heat flux and head retention capability and the influence of design or operational characteristics on this relationship is needed. Therefore, a program was initiated in an attempt to generate such information under a limited range of conditions.

This problem has been investigated under the MDAC-IRAD program, and a special screen device and surrounding cryostat had been designed to permit a test screen to simultaneously retain a column of LH_2 while being heated by a combination heater and heat flux meter. The device was observed visually to monitor liquid behavior, and the heat flux to the screen was directly read by a heater/heat flux meter. Critical temperatures and liquid levels in the system were measured as required. In the experiment, a pressure can be imposed across the screen equal to a retained head or the screen can physically retain a full liquid column as in the previously-described "milk carton" experiment.

Figure 39 shows the test schematic. The screen element is bonded into the rectangular box and a heater/heat flux meter is fitted into the top above the screen. The heater is placed about 0.6 cm, or boundary layer thickness, above the screen element. Evaporation can escape only from the slot on one side of the box, and temperature probes are placed at this location in order to compute the sensible energy increase of the gas. Two screen test devices were installed side-by-side within the available dewar, used previously under this contract. One device contained a plain 200 x 600 screen sample and the other contained a dual 200 x 600 screen sample. This arrangement permits examination of both samples simultaneously with one test setup and direct

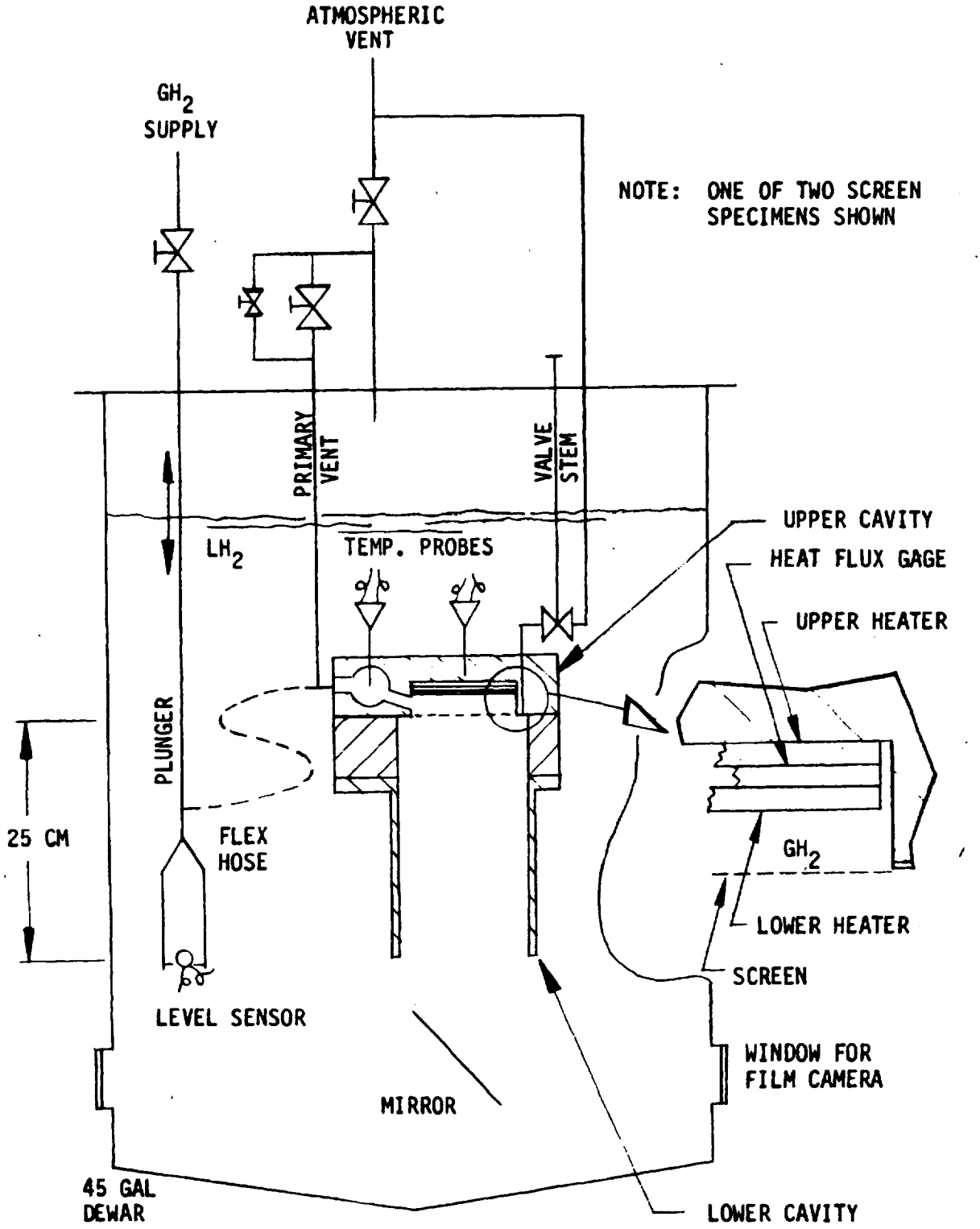

Figure 39. Heat Flux Test Apparatus

comparison of a single- and dual-layer screen as to their influence on thermal-induced retention breakdown. The 200 x 600 was selected because it is representative of the mesh size used in the recommended system designs and because it is the finest mesh that could be tested within the constraints of our available dewar.

The screen is installed at a slight angle, and a vent port is provided at the back of the unit just below the screen level in order to assist in bubble-free filling of the screen device. (These screen devices are too large to permit physical rotation to assist filling, as was done in the "Milk carton" tests.)

Instrumentation consists of photographic coverage to observe retention breakdown and retained head level, liquid gas temperature profile, dewar pressure, gas temperature leaving the screen element, and a direct reading of the heat flux being supplied to the screen. The device to provide this last reading is a null meter, which is essentially a guarded heater designed so that a specific electrical energy input can be interpreted as one-dimensional output hear flux to the screen. A carbon-resistant liquid level sensor was also installed to detect breakdown within the unit to back up visual observaion.

The test procedure was as follows:

1. Prior to filling the test dewar with LH_2, the plunge was raised to align its lower end with the plane of the screen, using a external positioning indicator. A flexible hose between the plunger and the upper cavity permitted this movement. This action precluded failure of the screen during filling.

2. The test dewar was filled with LH_2 to a level above the internal test apparatus. The ullage was normally vented to the atmosphere.

3. The lower cavity beneath the screen (screen size about 10 x 10 cm) was purged of gas by means of a vent port alongside one corner of the screen. A slight tilt (~5°) to the apparatus assured that the gas removal was complete. Flow in this vent line was controlled by a close-coupled, submerged needle valve. This valve position eliminated backflow of vapor in the vent line due to vaporization and warming of the line in the ullage, which would occur if the shutoff valve were outside the dewar. Visual observations assured that liquid filled the lower cavity and covered the lower surface of the screen.

4. The plunger was lowered to such a position that the desired ΔP was applied to the screen. This ΔP corresponded to the LH_2 head established by the vertical distance between the end of the plunger and the screen. This distance was limited to 20 to 30 cm with 200 x 600 mesh. Individual tests were run at discrete positions such as 20-, 25-, and 30-cm vertical displacement.

5. The plunger was slowly purged with GH_2 to remove all the LH_2 between the lower end of the plunger and the upper cavity. This step imposed the desired ΔP on the screen. Precautions were taken so that liquid was not trapped in low points along the line. The flexible line was also routed so that condensation in the line did not run into the upper cavity. Bubbling out of the lower end of the plunger indicated that the plunger was full of GH_2. This was also indicated by the carbon resistor/level sensor.

6. The lower heater (immediately above the screen was activated, and the input was slowly increased until the screen failed. Failure was evidenced by the liquid dropping out of the lower cavity and rushing into the plunger to cover the level sensor. Prior to failure the evaporating liquid was routed out of the upper cavity and through the primary vent line, with a small portion directed into the plunger to maintain the proper ΔP across the screen. The temperature of the gas leaving the screen was sensed at the exit from the upper cavity by a platinum probe. The primary vent line was insulated to prevent condensation.

7. The upper heater was continuously controlled so that the output of the heat flux meter between the two heaters had a zero output. When this was the case, the power input to the lower heater was flowing into the evaporating liquid and the following equation was satisfed.

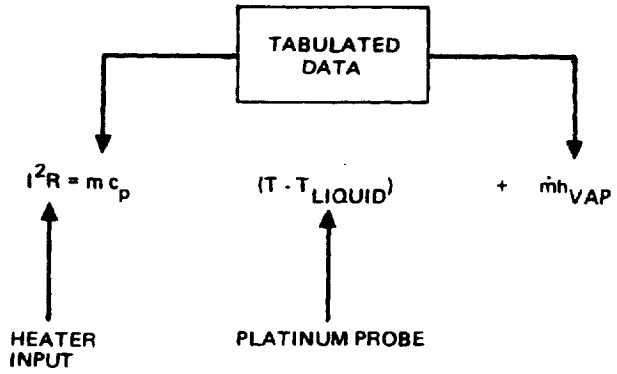

with $\dot{m}$ being the mass evolution rate from the screen surface and

$$Q_{SCREEN} = \dot{m}h_{VAP}$$

This equation neglects conduction into the liquid.

A thermocouple in the upper cavity block was monitored to assure that physical damage to the apparatus did not occur.

The procedure was repeated for additional discrete positions of the plunger. In the original design, the heater holder and extension blocks were made of plexiglass. The completed holder is shown in Figure 40, and the complete test apparatus as installed on the dewar lid is shown in Figure 41. However, during initial testing, the plexiglass heater holder plate developed cracks and leakage which negated initial test results. These cracks were caused by stress concentrations as a result of bolt placements and the device had to be redesigned. This redesign consisted of replacing the plexiglass heater block with a similar design using aluminum which contained a small plexiglass block around the heater for insulation. The thick square plexiglass

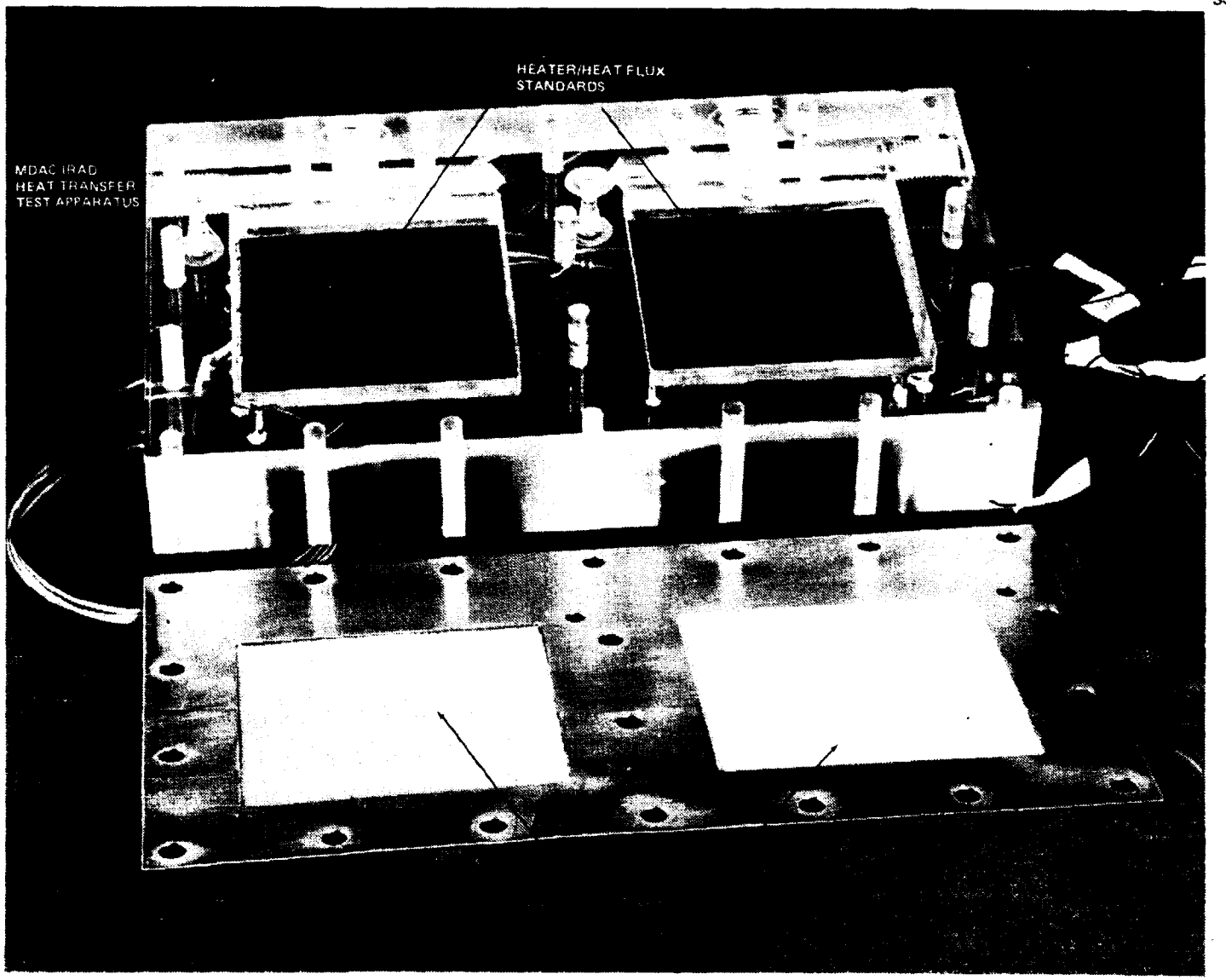

Figure 40. Screen Holder Test Component

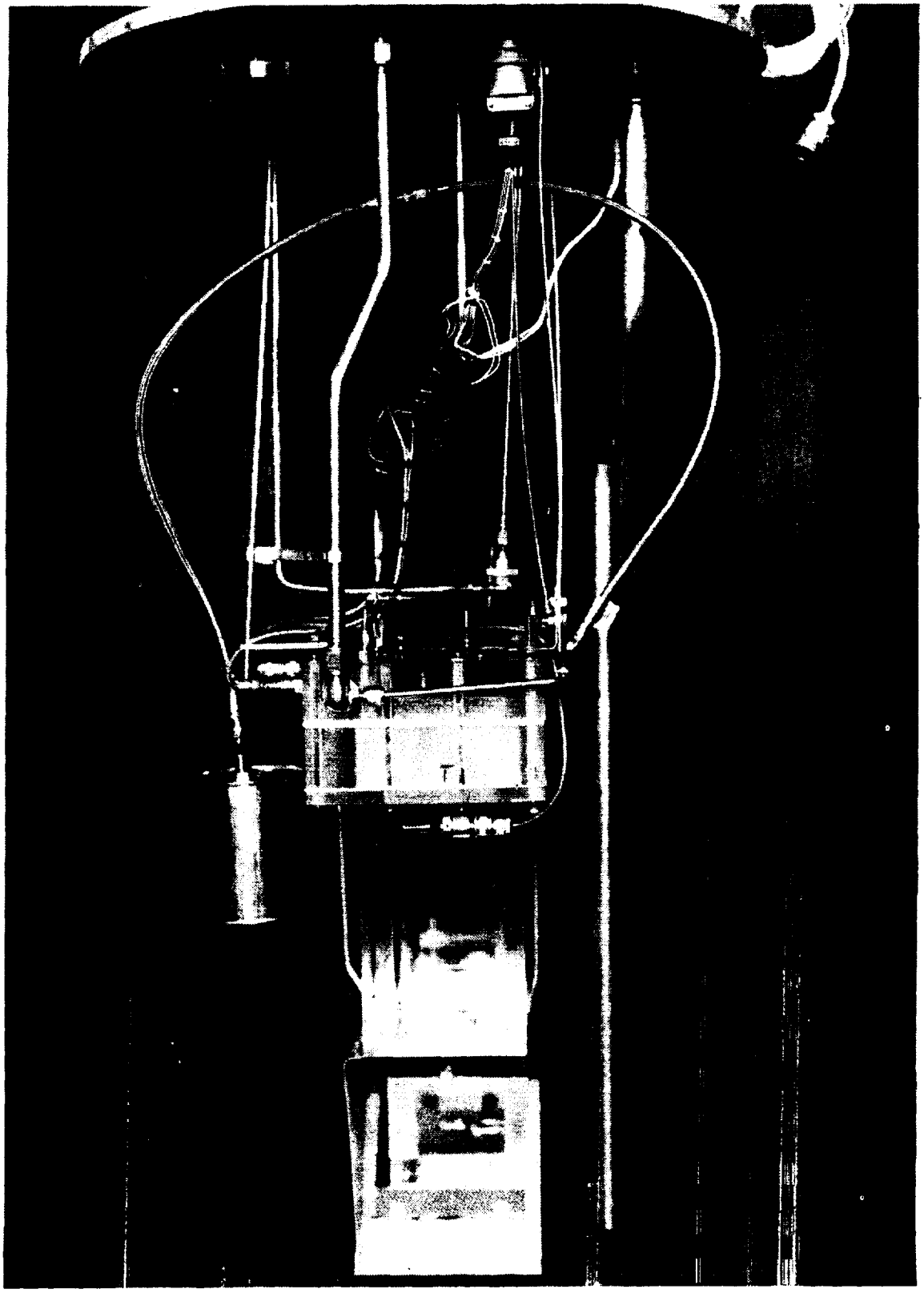

Figure 41. Screen Heat Transfer Test Apparatus

lower extensions were also replaced with thinner plexiglas cylindrical units. The plexiglas parts were also held together between metal strips rather than having the bolts tighten directly against the plastic faces. This structure did not sustain cracking during the subsequent LH_2 tests.

During the tests, all elements of the system behaved in a nominal manner. The International Thermal Instrument Company 10 cm square heater/heat flux standard meters performed as expected, although a little practice was required to refine the heater balancing procedure. The level sensor also gave good indication of breakdown. Visual observation was much poorer than expected because of light reflections and scattering within the dewar. However, this did not represent a problem since reduced retention capability did not occur under any heat transfer condition tested.

In the procedure, each screen unit was tested separately, first with the dewar liquid level at about 12.7 cm (5 inch) above the screen level, and then with the liquid level at about 5 cm (2 inch) below the level of the screen. With the single layer screen, head across the screen was set at just below its retention limit, which was experimentally determined to be equivalent to 34.4 cm (13.5 inch) of LH_2 (with no heat flux). The heater was energized, and the heat flux was gradually increased up to the maximum capability of the test apparatus. This level was 112.5 watts (384 Btu/Hr). Based on the area of the screen, this is 10910 watt/M^2 (3460 Btu/Ft^2/Hr) which is well above that anticipated within a cryogenic tank. At this point, the head across the screen was increased to 34.4 cm (13.5 inch) of LH_2, where breakdown occurred at the same head as with no heat flux. The results with the dual screen element were much the same. In this case, the breakdown head was determined to be 33.7 cm (13.25 inch) of LH_2 and a maximum heat load of 133 watt (454 Btu/Hr) equivalent to a heat flux of 12894 watt/M^2 (4090 Btu/Ft^2/Hr) was achieved without a reduction in the breakdown head retained by the screen. This is shown in Figure 42 which shows actual data from the tests. In the tests, screen breakdown was evidenced by liquid rushing into the plunger and submerging the level sensor therein. As shown in Figure 42-b, with no heat flux imposed on the double screen, when the head on the screen was increased to 33.7 cm (13.25 inch) the level sensor went to liquid, i.e., breakdown occurred. In Figure 42-a, the head (plunger position) was set at 31.1 cm (12.25 inch) and heat flux was applied to the screen to the maximum level obtainable (130 watts) without screen breakdown. The plunger was then lowered to apply head of 33.7 cm (13.25 inch) before breakdown occurred, as shown in Figure 42-a. At this point, the temperature of the gas above the screen was at least 41.6 °K (75 °R).

Based on the conflicting results of the three heat transfer experiments, a conclusive statement cannot be made as to the ability of a screen device to retain LH_2 in the presence of a warm pressurant gas, and additional research is warranted in this area. Analysis has shown, however, that there may be a subtle difference in the imposed conditions in the "milk carton" experiment and in the test described above. In principle, there was a difference in the temperature distributions in the two test modes such that in the tests above, the liquid beneath the screen was subcooled with respect to the surface temperature, while in the "milk carton" test, the liquid beneath the screen was slightly superheated with respect to the saturation temperature beneath the surface. This fundamental difference between a supported column of liquid and a submerged screen with an applied pressure difference may possibly

FOLDOUT FRAME

FOLDOUT FRAME 2

CR190

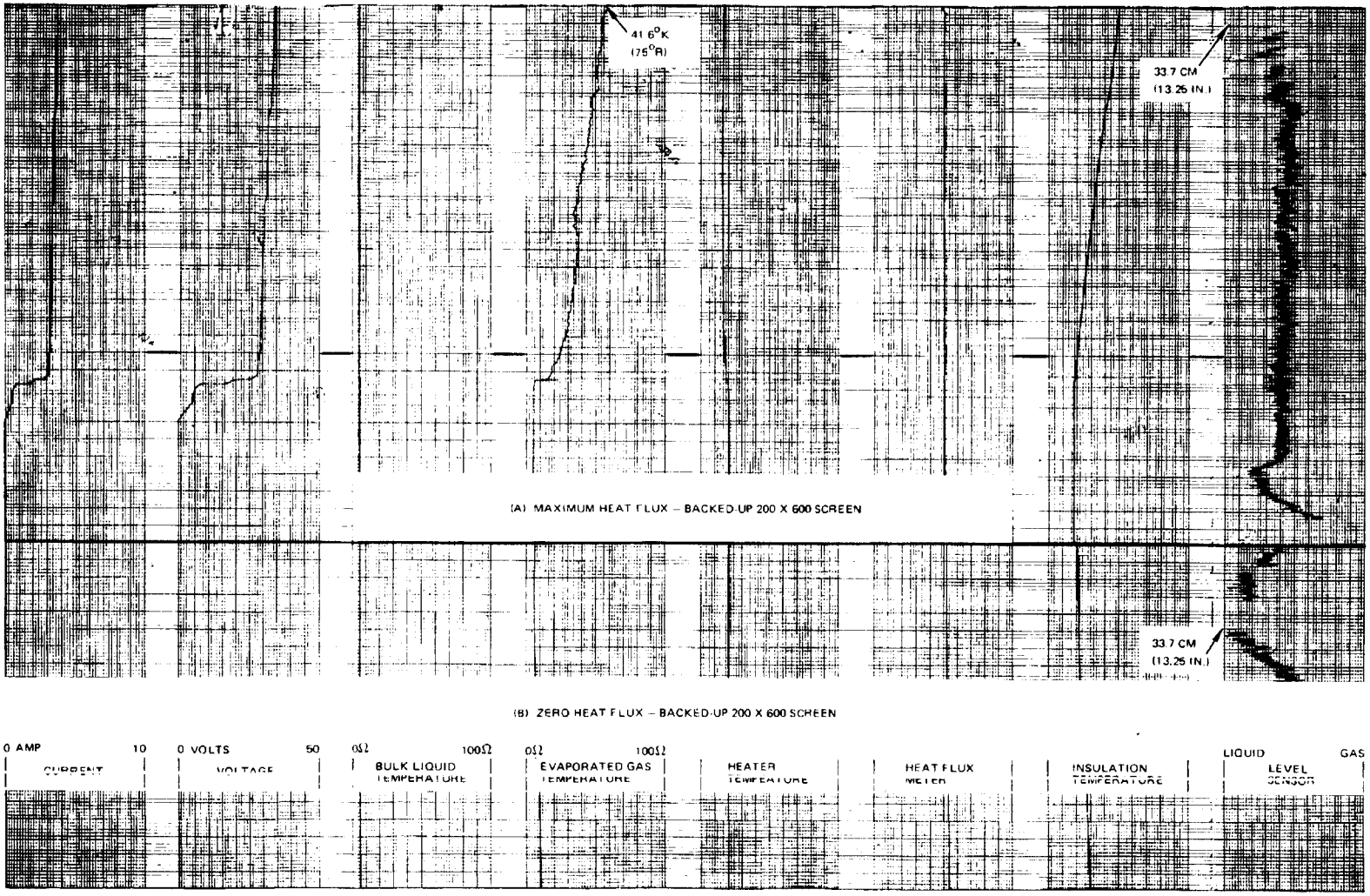

Figure 42. Screen Heat Transfer Test Data

account for the observed differences. For the screen submerged in liquid hydrogen, which can be assumed to be initially saturated at atmospheric pressure, the bulk temperature is 20.55 °K (37 °R). Immediately prior to the test, GH_2 is used to expel liquid in the upper cavity, above the screen, and establish a liquid interface. Since the plunger is set at a given level, the pressure above the screen, P_A is:

$$P_A = P_D + \rho gH + \rho gh$$

where P_D is Dewar ullage pressure, H is the height of the liquid in the dewar above the level of the screen and h is the depth of the bottom of the plunger and cup below the level of the screen.

Equilibrium conditions with respect to the saturation temperature and pressure relation are valid at the interface even with heat transfer. Therefore, the temperature of the liquid vapor interface is known precisely, since the pressure above the screen P_A, is known. The ratio of saturation pressure changes is known for a range of LH_2 temperatures. For small temperature differences, the saturation temperature, T_s at the interface is

$$T_I = T_S = T_{s_{initial}} + \frac{\Delta T}{\Delta P} (\Delta P)$$

where

$$\Delta P = P_a - P_{\text{initial saturation}}$$

or,

$$\Delta P = P_d - P_{\substack{\text{initial} \\ \text{saturation}}} + \rho g (h + H)$$

If the pressure in the dewar ullage is not increased after the bulk liquid is saturated at $P_{initial}$ (for example, to minimize boiling), then we have

$$P_D = P_{\text{initial saturation}}$$

and

$$\Delta P = \rho g (h + H)$$

Since the total height in this case will be of the order of 0.61 meters (2 ft), the pressure increase from the ullage region to the inside of the screen device at the top will be

$$\Delta P = \rho g (h + H) = 0.04 \text{ N/cm}^2 \text{ (0.06 psi)}$$

The pressure change versus temperature change to LH_2 is

$$\left.\frac{\Delta P}{\Delta T}\right|_{20.55\ K\ (37°R)} = 3.1\ N/cm^2/°K\ (2.5\ psi/°R)$$

and therefore, the saturation temperature at the interface is 20.563°K (37.024°R) or 0.013°K (0.024°R) higher than the bulk liquid temperature. In effect, the LH_2 bulk liquid beneath the screen is subcooled with respect to the heated screen surface by at least 0.013°K (0.024°R). If transient boiling beneath the screen is the mechanism by which loss of retention due to screen dry out occurs, then it would be expected that the temperature increase above that of the bulk liquid must be equal to or greater than the measured superheat temperatures for the initiation of subcooled boiling as reported, for example, in Reference 5. The lowest observed superheat temperature difference for liquid hydrogen was found to be 0.033°K (0.06°R). Therefore, if boiling were to occur, the temperature of the portion of the screen wires in contact with the liquid would have to be raised to at least 20.583 K (37.06 R); the heat flux in this case would be expected to be very large. Based on this model for screen failure, it is anticipated that screen breakdown would not occur even at the very high flux rates. However, conditions are changed when the liquid column is supported by a screen, as in vehicle, or as in the "milk carton" tests. The pressure above the screen, P_A, is equal to the dewar pressure, P_D. The liquid can be assumed to have been initially saturated at a given pressure such that $T_{liquid} = 20.55°K\ (37°R)$. This temperature would be constant throughout the liquid column. However, since the hydrostatic pressure in the column decreases linearly up to the screen, the saturation temperature of the liquid also decreases. Assuming a liquid column height of 0.3m (1 ft), the pressure in the liquid immediately beneath the screen is

$$P_d - \rho gh = P_d - 0.02\ N/cm^2\ (0.03\ psia)$$

The saturation temperature of the liquid beneath the screen is therefore,

$$T_s = T_{\substack{\text{initial}\\\text{saturation}}} - \frac{\Delta T}{\Delta P}\ (\Delta P)$$

which gives

$$T_s = 20.55 - \frac{0.02}{3.1} = 20.543°K\ (36.988°R)$$

whereas the actual bulk temperature of the liquid is 20.55 °K (37 °R). The liquid is superheated with respect to its saturation temperature, and, therefore, boiling may occur at lower superheat temperature differences, and, correspondingly, lower heat fluxes, than for the previous case in which the bulk liquid is subcooled. In addition, the liquid-vapor interface formed at each pore in the screen is a potential point at which bubble growth can occur in the superheated liquid. The temperature distribution described above corresponds to the condition under which the "milk carton" screen configuration was tested.

An attempt was made to test the above thesis in the heat flux tests by lowering the LH_2 level in the Dewar below the screen level. With the LH_2 level 5 cm (2 inch) below the screen, no effect of heat transfer on screen retention was noted, and the screen failed again at 33.7 cm (13.25 inch) with applied power of both 0 watts and over 100 watts. It is believed that no effect of superheating was noted because the way the apparatus screen column was filled precluded obtaining superheated liquid below the screen; rather, the LH_2 was saturated. A revised series of tests to explore this phenomenon in more detail has been proposed to NASA-MSFC.

2. Screen Vibration Tests. The operational environment of a surface-tension acquisition device includes oscillatory inputs having their origin in rotating machinery, acoustics, flow instabilities, etc. Figure 43 indicates the possible range in vibration parameters that may be expected on the Space Shuttle Vehicle (Reference 6). The nature of the response of the liquid/gas interface within a screen to a vibration input has not been clearly defined.

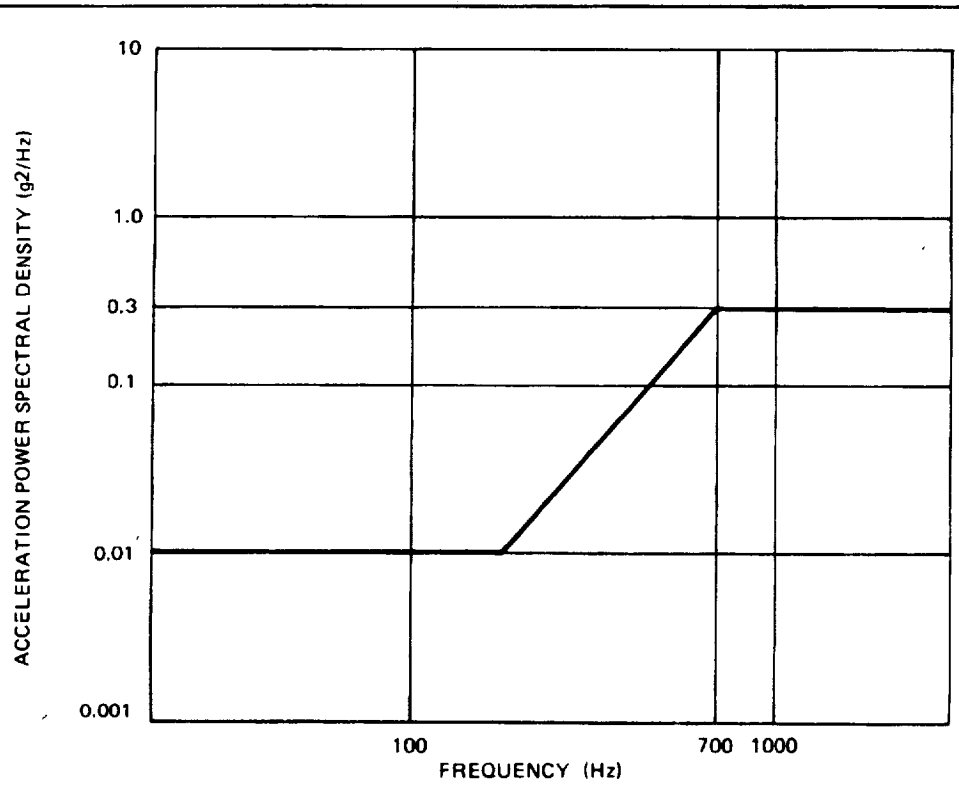

Figure 43. Orbiter Engine-Induced Vibration Spectra

Reference 7 summarizes test results related to the change in expulsion capability for a complete pleated-screen tank liner when subjected to sine and random vibration. One effect clearly demonstrated was that for low frequency sine vibration ($\omega < 85$ Rad/sec) the oscillations acted to modify the hydrostatic head within the propellant simulant as indicated by $a_v = \omega^2 A$, where a_v is the induced peak acceleration and A the vibration amplitude. These tests were, however, unnecessarily obscured by the complex geometry employed. Overall system behavior was demonstrated, but the underlying behavior at the various points on the screen could not be deduced.

Tests to gain additional insight into vibration related phenomenon with wetted screens were conducted using the simple apparatus sketched in Figure 44. Four pieces of screen are sandwiched between a metal base plate containing eight pressurization ports (two per screen) and a plexiglas block containing eight cylindrical holes; two above each piece of screen (diameters 1 and 2.54 cm). The base plate is mounted directly on a shaker platform. The cavities in the plexiglas block allow a small amount of alcohol to be placed over each screen so that the bubble point can be measured when pressurization with GN_2 takes place through the appropriate port in the base plate. The transparent block permits screen breakdown to be observed directly.

The objective of the test series was to subject small, wetted-screen elements to a controlled pressure differential while providing a sinusoidal displacement input to the screen and fluid column supported by the screen. The independent variables were:

A. Axis of Vibration
   1. Parallel to screen surface
   2. Perpendicular to screen surface

B. Vibration Frequency – 5 to 1000 Hz

C. Vibration Acceleration – 1/4 to 4 g's as measured by an accelerometer on the shaker platform

D. Liquid depth above screen (isopropyl alcohol) – 0.6 to 38 cm

Photos of the completed apparatus are shown in Figures 45 and 46. The extension piece consisted of a series of 50-cm vertical metal tubes which were positioned directly over the holes in the block.

The first test sequence has vertical sinusoidal vibration perpendicular to the surface of four screen specimens (325 x 325, 850 x 155, 200 x 600, 250 x 1370). Figure 47 shows our test setup with the test device installed on the shaker. The isopropyl alcohol liquid depth above each screen was 2 cm, or less, in all cases. As an initial step, the static bubble point of each screen was measured. Next, a ΔP somewhat less (10 to 20 percent) than the static bubble point was placed across each screen, and the frequency range 5 to 100 Hz was swept at 2 octaves/minute at a fixed g-level. The frequencies at which gas breakthrough occurred were recorded. Customarily, once failure took place, it continued as the frequency increased to 1 kHz. The results of these shallow depth tests are shown in Figures 48 and 49. The vertical separation of the two lines associated with any particular g-level is a qualitative measure of the amount of gas breakthrough; a single line denotes no failure.

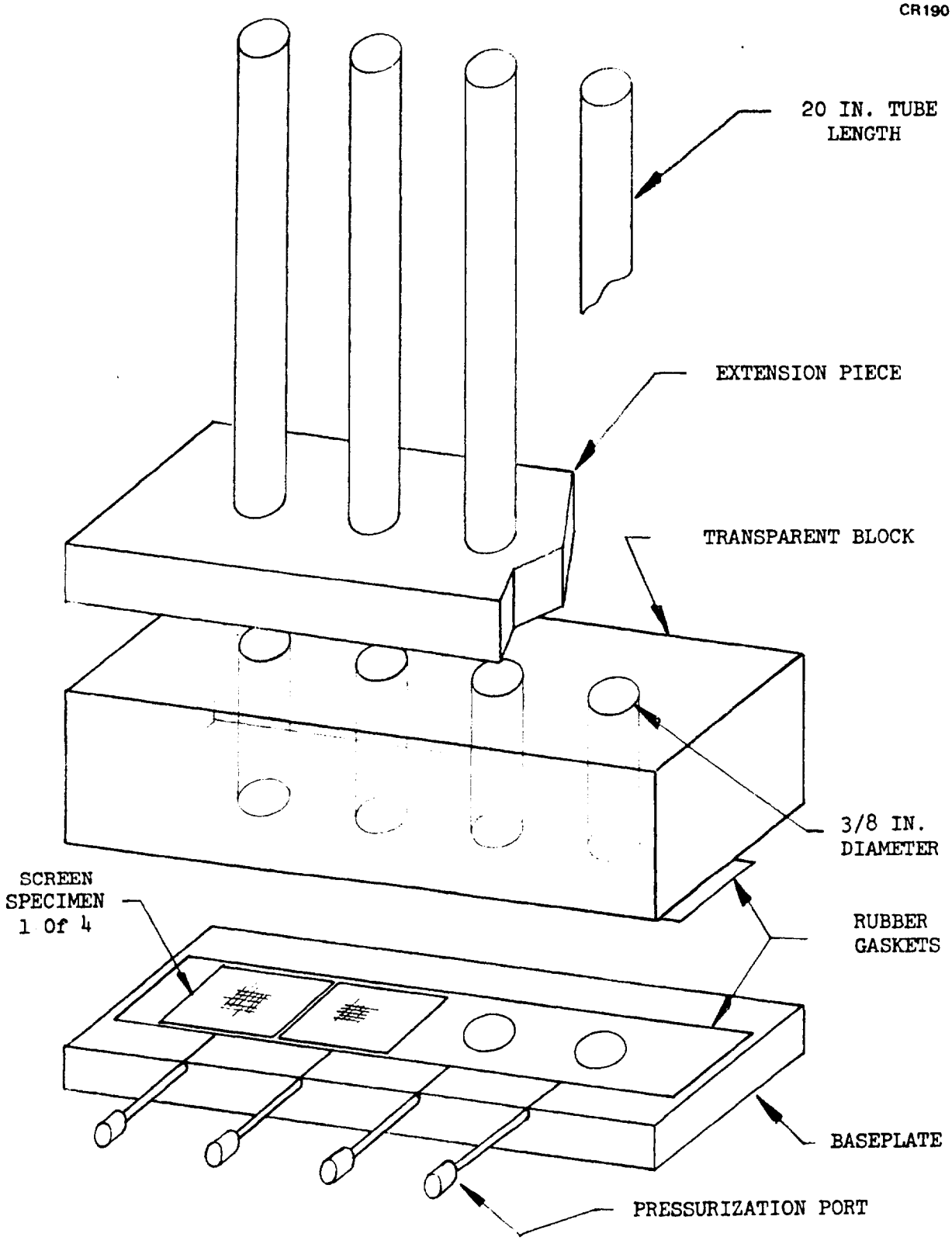

Figure 44. Diagram of Vibration Test Apparatus

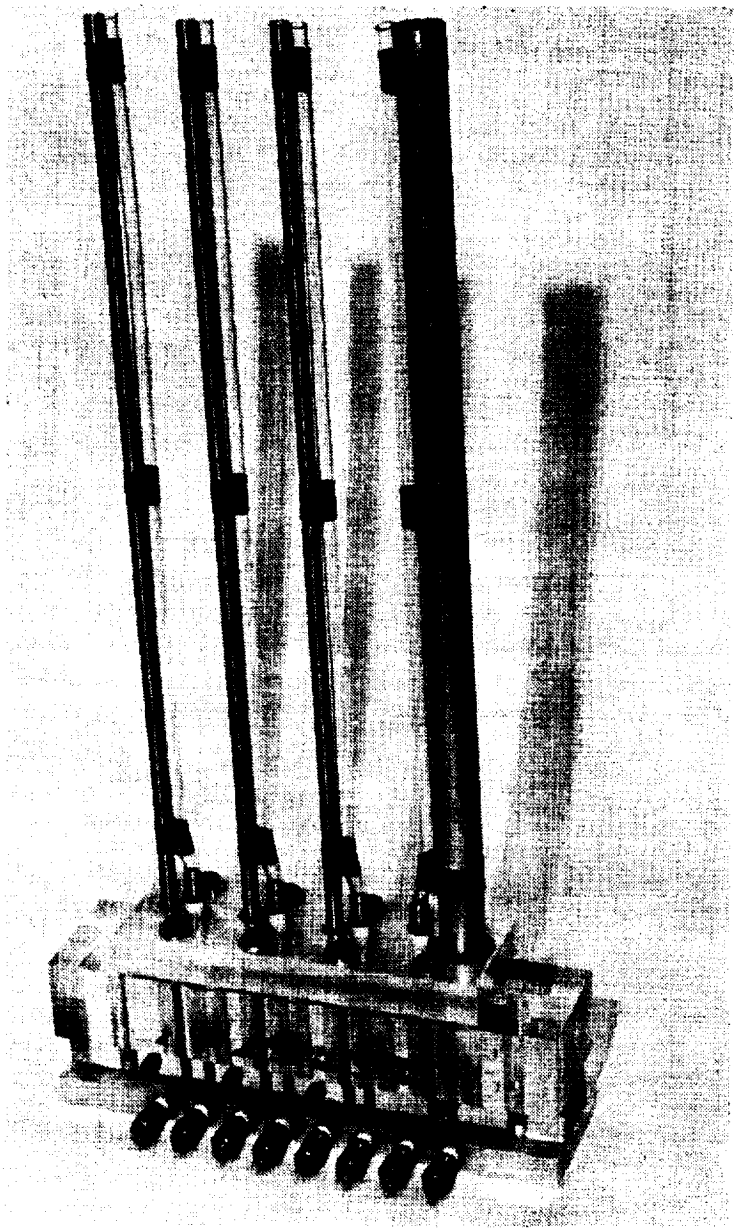

Figure 45. Photograph of Vibration Test Apparatus

The data indicate that vibration results in premature gas breakthrough in all four specimens. Also, increasing g-level results in increased bubble point reduction. The extent of the bubble point reduction will be discussed more thoroughly in combination with the large liquid depth tests.

The second test sequence was conducted with sinusoidal vibration acting parallel to the screen surface with a small liquid depth (<2 cm). The procedure was changed such that the ΔP across the screen was slowly increased to failure at fixed values of frequency and g-level. The test data is shown in Figures 50 and 51. Vibration in this axis has a very slight effect on the

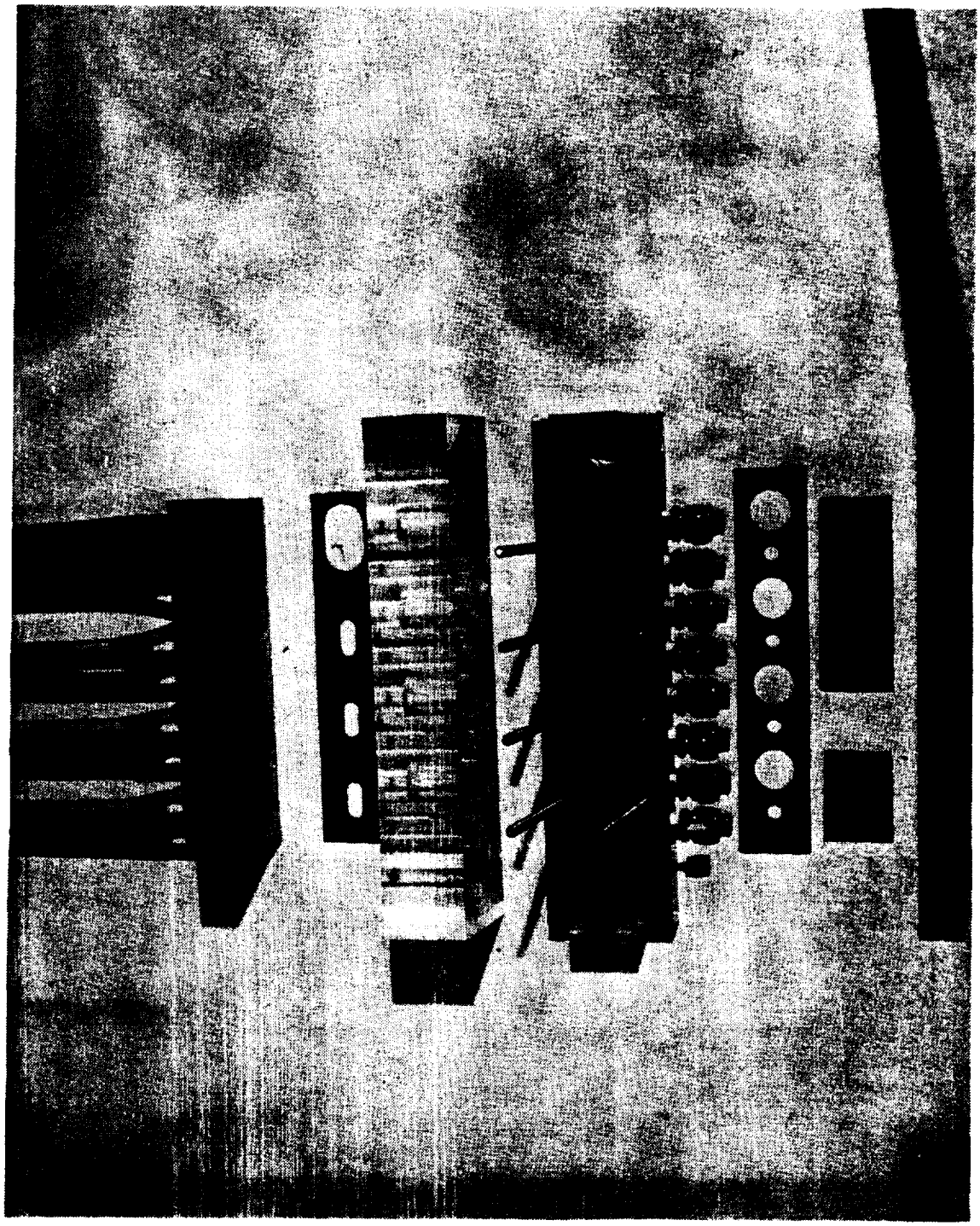

Figure 46. Vibration Test Apparatus Disassembler

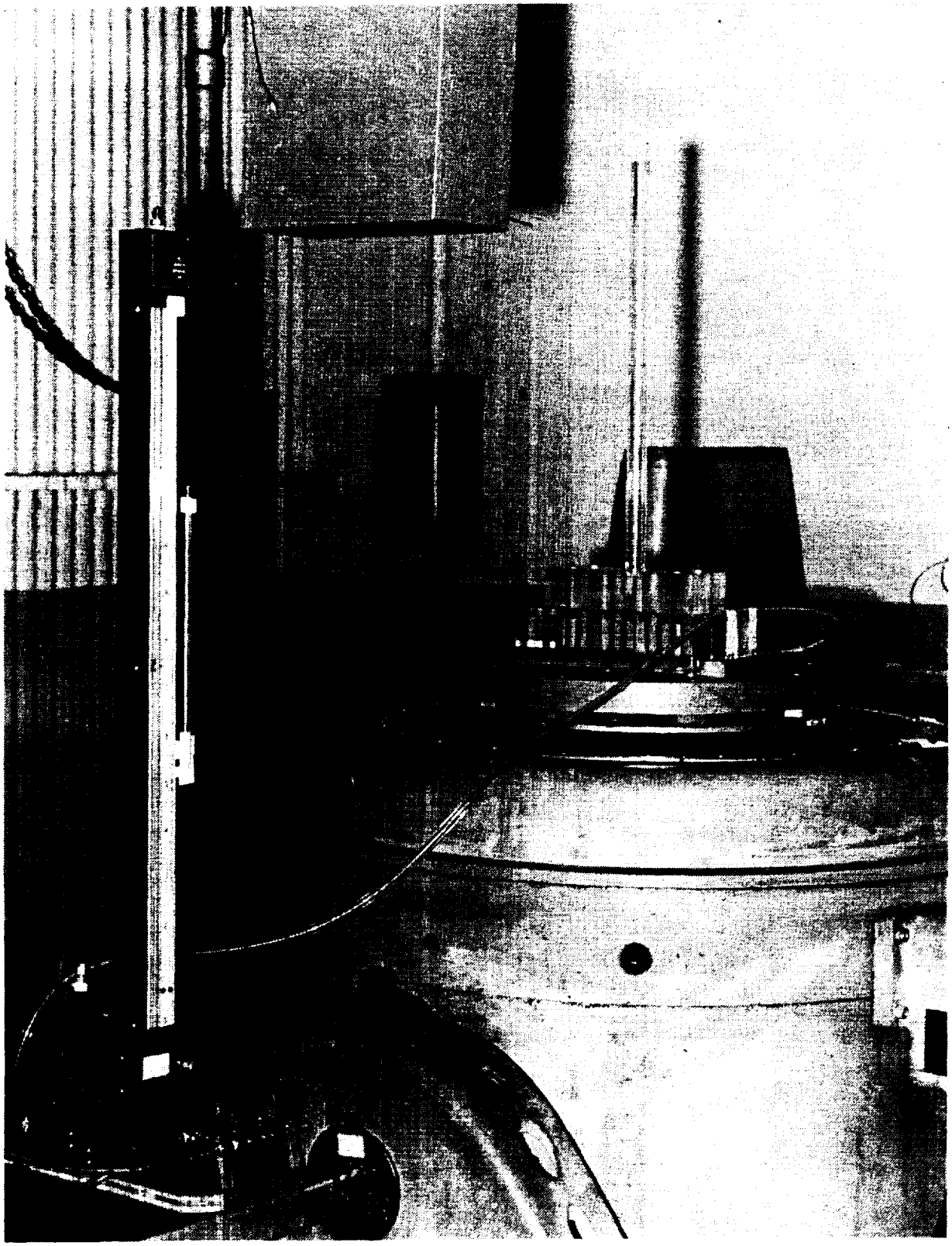

Figure 47. Vibration Test Setup

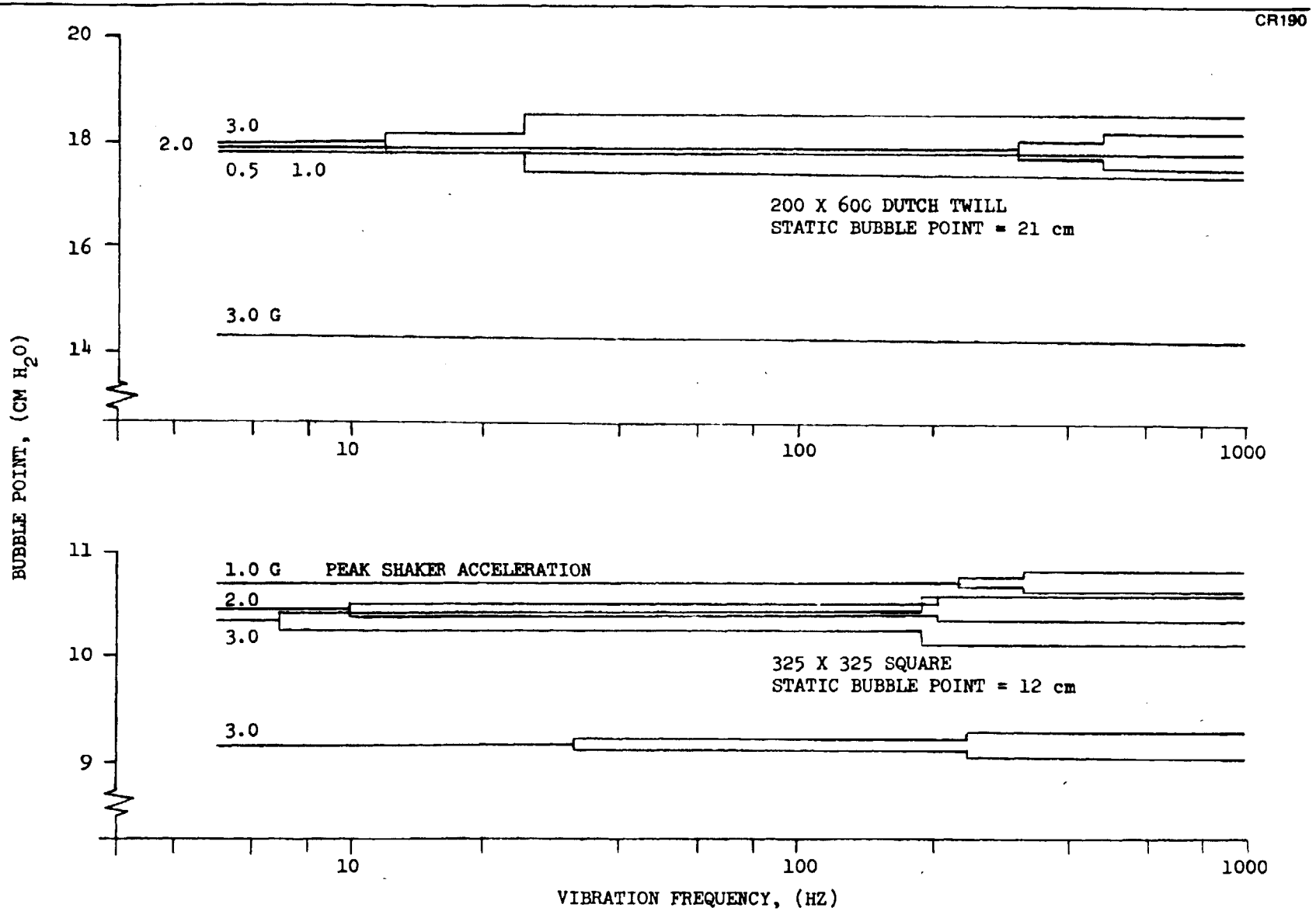

Figure 48. Vertical Sinusoidal Vibration – Shallow

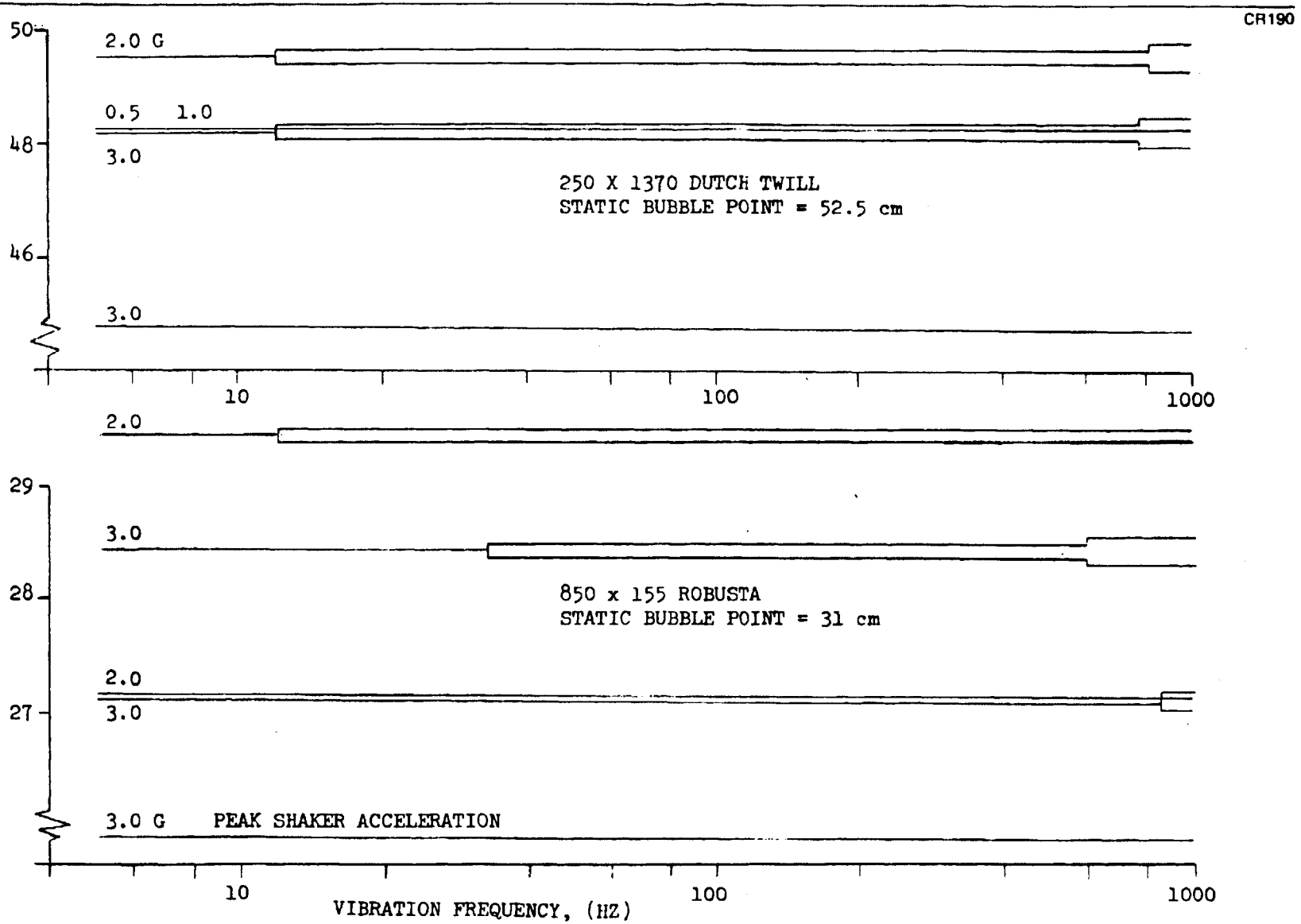

Figure 49. Vertical Sinusoidal Vibration – Shallow

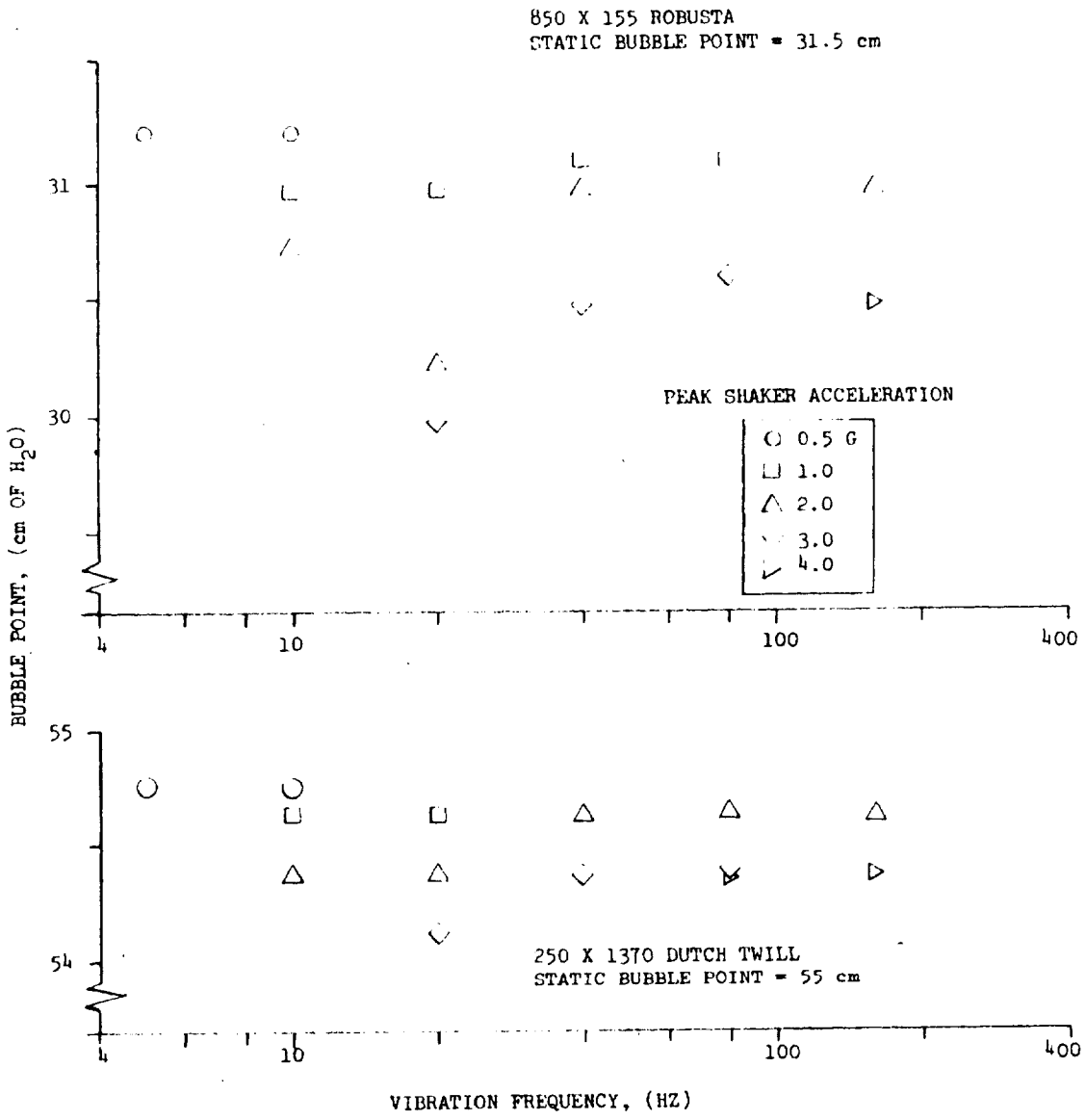

Figure 50. Horizontal Sinusoidal Vibraton

bubble point pressure. This indicates that the vibration does not alter the nature of the numerous interfaces within the pores of the screen. It is proposed, then, that the primary effect of the oscillations is to alter the pressure field within the liquid. The evidence supporting this hypothesis will become more apparent in the last test series, wherein a large liquid depth was combined with vertical excitation.

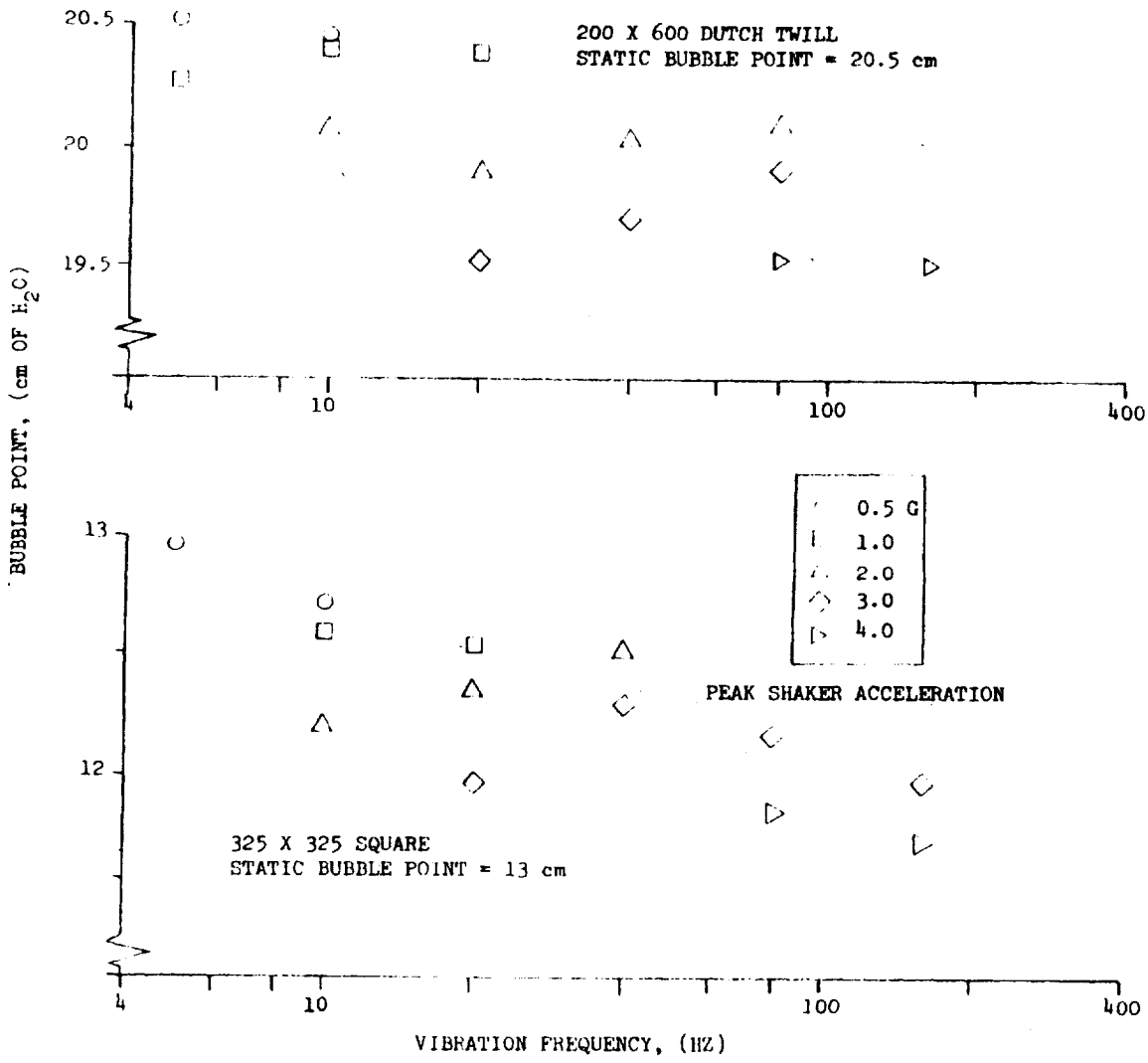

Figure 51. Horizontal Sinusoidal Vibration

In the first test series, the combination of experimental technique and shallow liquid depth failed to emphasize the importance of the reduction in liquid pressure above the screen. When this occurs, the head acting in opposition to the gas pressure below the screen is reduced, allowing more ready passage of the gas.

The third and last test sequence was conducted with a large (23 to 39 cm) liquid column above three screens with the axis of vibration perpendicular to

the screen. Again, the procedure consisted of slowly increasing the gas pressure to breakdown at fixed values of g level and frequency. The test data are shown in Figures 52 through 54. The data are shown as an effective g-level (g_{eff}) which is defined by:

$$\Delta P_{BP} = P - \frac{\rho_{ALCOHOL}}{\rho_{H_2O}} H (1 - g_{eff})$$

where:

ΔP_{BP} = Static bubble point (cm W. C.)

H = Alcohol depth (cm)

P = Manometer pressure at breakdown (cm W. C.)

ρ = Liquid density

This mathematical model assumes that the vibration reduces the head above the screen. The quantity g_{eff} can be thought of as a gravitational level (in g's) acting in opposition to normal gravity. When g_{eff} equals 1.0, the vibration-induced and gravitational forces cancel, and the bubble point corresponds to that set by surface tension forces alone. For g_{eff} larger than 1.0, a negative pressure situation appears with the effective hydrostatic pressure above the screen less than atmospheric. The pressure field is similar to that responsible for the phenomenon of sinking bubbles. In this latter case, the treatment of the pressure oscillations as a one-dimensional acoustic wave has yielded satisfactory results.

Figures 52 through 54 indicate that the vibration environment can have a dramatic effect on the bubble point pressure at all of the frequencies tested. Values for the effective acceleration greater than 1.0 indicate that the sinusoidal vibration reduces the pressure above the screen to less than atmospheric pressure. The data also shows that g_{eff} can be considerably larger or smaller than the peak vibration on the shaker platform. It is anticipated that the nature of the pressure waves within the liquid will be dependent upon the shape of the supported liquid column. The experimental apparatus was designed to minimize this effect by using straight, vertical liquid columns.

To further analyze the test results, the test data was correlated in terms of a dimensionless bubble point. To first order, the pressure in a vibrating column of liquid is obtained as the sum of the atmospheric pressure, hydrostatic pressure, and the time-varying pressure resulting from the vibrational acceleration, a, immediately above the screen. The pressure is approximated as

$$P_{screen} = P_{atmos} + gh + ah\cos\omega t$$

Additional terms would result if effects were included such as the radial variation in pressure, the effect of wall viscosity, compliance of the tube, screen, or liquid, and free surface slosh.

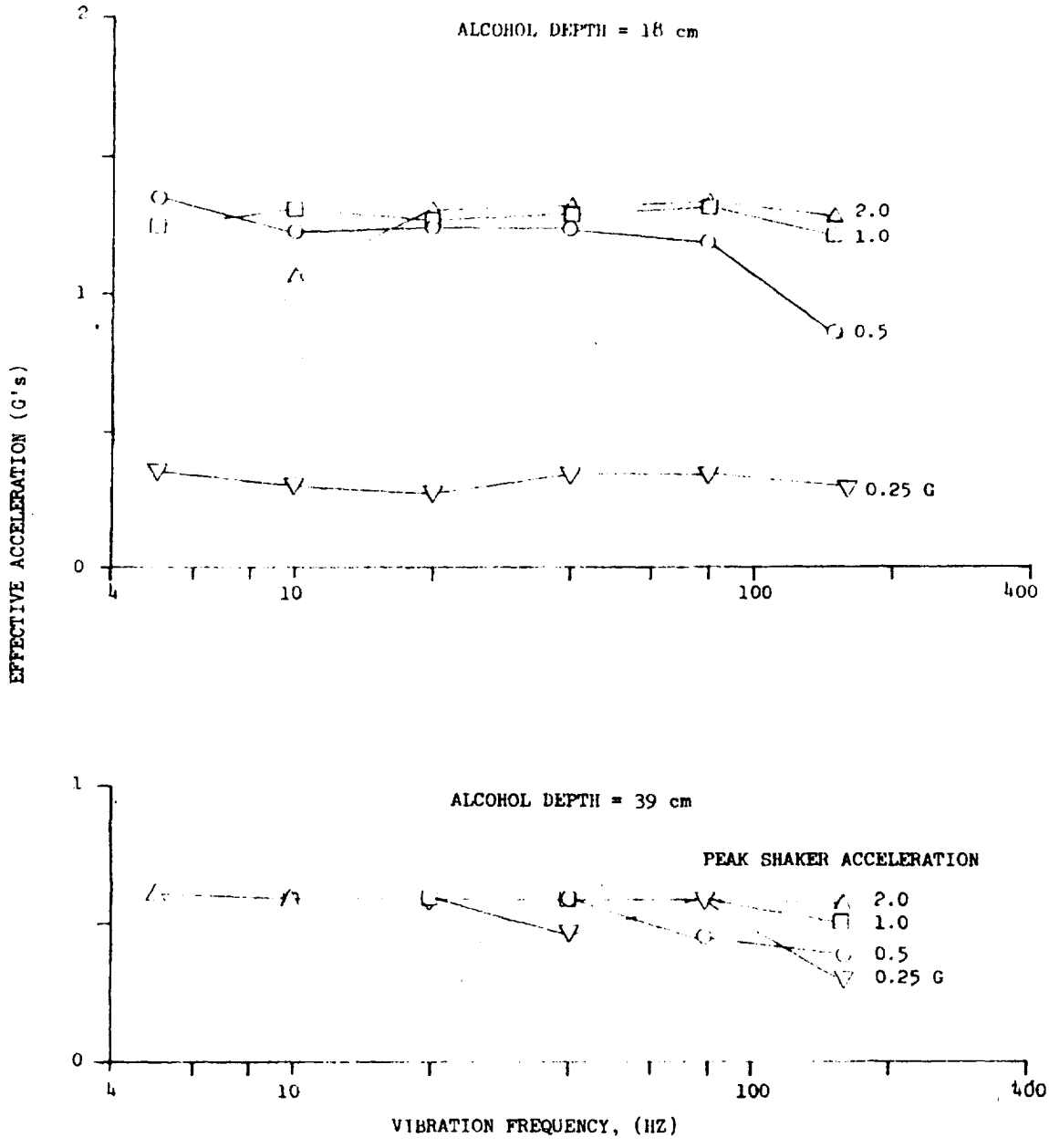

Figure 52. Vertical Sinusoidal Vibration – 200 X 600 Dutch Twill

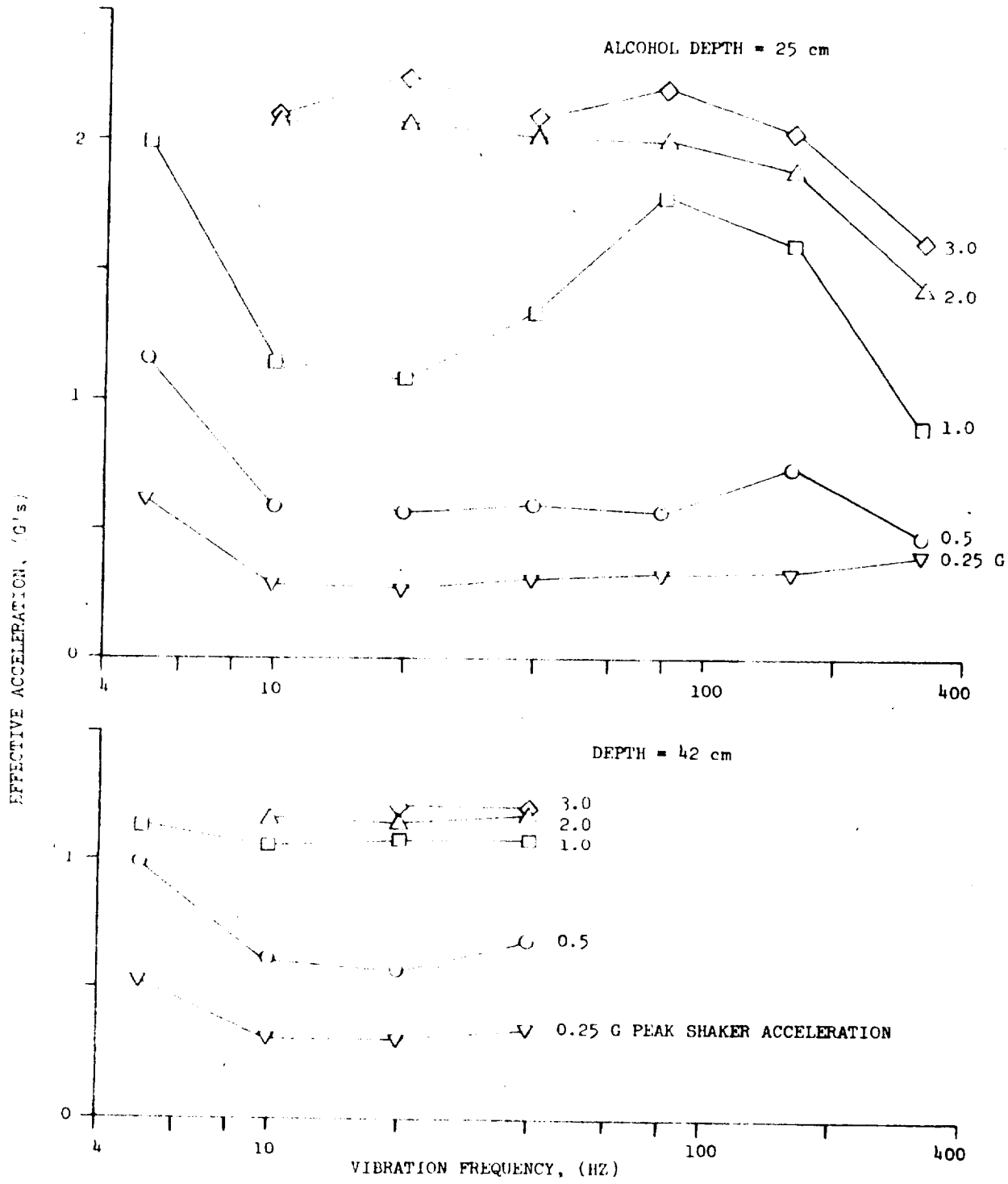

Figure 53. Vertical Sinusoidal Acceleration – 200 X 1400 Dutch Twill

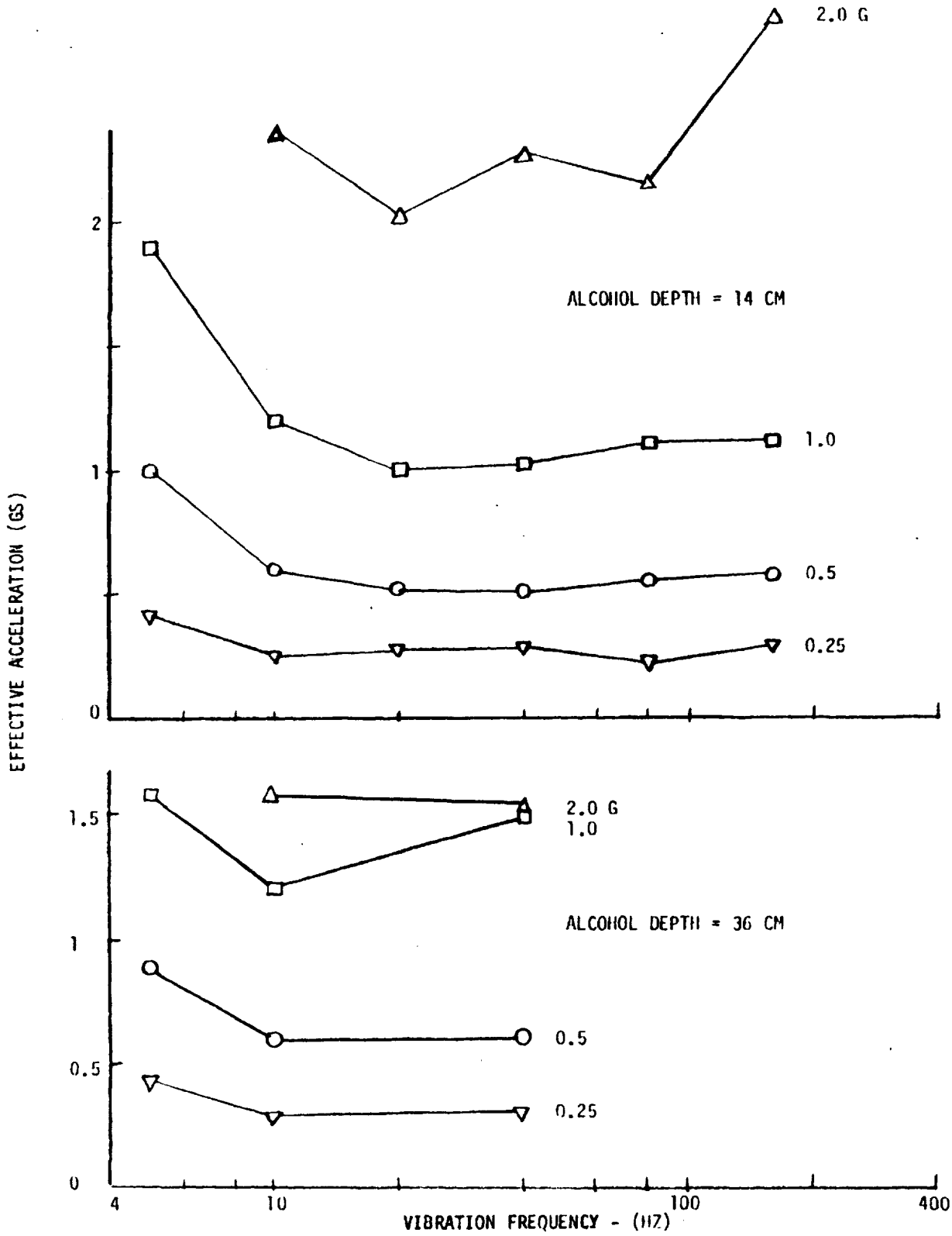

Figure 54. Vertical Sinusoidal Vibration (250 X 1370 Mesh)

The absolute pressure, P, at which bubbles break through into the liquid should exceed P_{screen} by an amount equal to an effective bubble point for the vibrating screen. Since

$$P = P_{atmos} + P_{manometer}$$

where $P_{manometer}$ is the gage pressure measured at bubble breakthrough, the effective bubble point is

$$P_{BP/_{effective}} = P - P_{screen} = P_{manometer} - gh - ahcos\,\omega t$$

It can be seen from the data that bubble breakthrough occurs most readily when the effective vibration acceleration is opposite to that of gravity. Assuming that breakthrough occurs when this adverse acceleration is maximum, and nondimensionalizing the previous equation with the static bubble point gives

$$\frac{P_{BP/_{effective}}}{P_{BP/_{static}}} = \frac{P_{manometer} - \rho gh + \rho ha}{P_{BP/_{static}}}$$

Figure 55 illustrates the predominant conclusions reached as a result of these preliminary vibration tests. Most of the data fall on or below a bubble point ratio of 1.0. It should be noted that in these vibration experiments the screen is used to support a column of liquid, and thus the pressure at the screen is higher than the atmospheric pressure. The pressure decrease resulting from the vibration, therefore, is subtracted from the hydrostatic level. With an actual screen device, the pressure in the liquid is a minimum at the top of the screen device. In effect, the static acceleration plus the maximum vibrational acceleration would impose a total head greater than the hydrostatic level. This condition would correspond, to first order, to the maximum pressure difference across the screen device, tending to cause breakthrough of the surrounding gas. If the data of Figure 55 were to cluster about a value of 1.0, it would be reasonable to assume that by adding the adverse vibration acceleration imposed on a screen device to the static g-level, the total acceleration obtained could then be used to determine the maximum height of liquid which could be supported. Unfortunately, much of our data fall significantly below a dimensionless bubble point of 1.0. Some of the data are as low as approximately 0.5, which implies that the column height supportable by a given screen with a total acceleration equal to that of the static acceleration plus the peak vibrational acceleration is decreased by as much as 50 percent from the predicted value. There is an effect of major importance tending to cause a premature screen failure.

Inspection of the data has shown that this effect is highly variable. Although most of the decreases in effective bubble point occur at a frequency of 5 cps, there is no apparent correlation with respect to vibrational acceleration or frequency. In some cases, increasing the vibrational acceleration from 0.25 to 1.0 causes an almost linear decrease in effective bubble point, especially at 5 cps, but this does not illustrate a general trend. Above 1.0g,

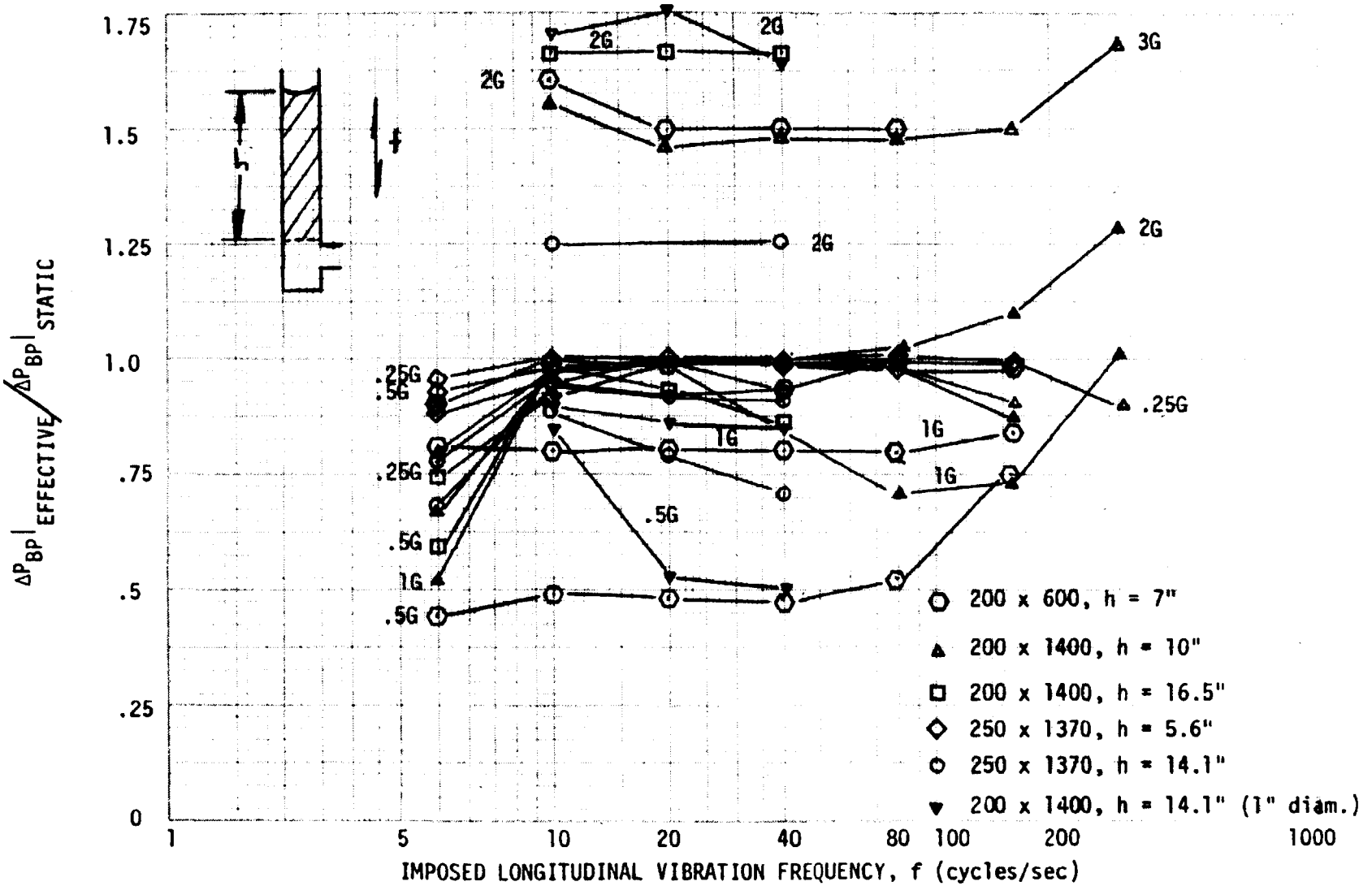

Figure 55. Longitudinal Vibration Effects on Bubble Point for Liquid Columns

the data indicate anomalous behavior. At 2g and 3g, most of the data indicate an improvement in the effective bubble point. It was observed that these data would cluster about the dimensionless bubble point value of 1.0 if the vibrational acceleration level effects above 1g were ignored.

It is not yet known how well the experimental conditions model the effects of a full-scale acquisition device. Several experimental conditions differ significantly from the vehicle conditions. The screen samples used were small and rigid, having natural vibration frequencies much greater than the maximum shaker frequency. The compliance of the tube, screen, and the air column beneath the screen differ greatly from practical vehicle conditions. The column heights used are much smaller than actual acquisition devices. Finally, the marked difference in the breakthrough data for the 2.54 cm diameter 200 x 1400 screen compared with the two nearly identical cases for the 0.95 cm diameter 200 x 1400 screen may be indicative of a scale effect based on screen and tube diameter.

In spite of these experimental limitations, a significant effect of vibration on screen breakthrough has been demonstrated. These effects must be conservatively accounted for in the acquisition device design, especially under conditions such as the vehicle boost phase with offloaded propellant tanks, vehicle docking in orbit, or operation of screen devices in the vicinity of equipment inducing significant vibration levels.

3. Multilayer Screen Flow Test. Multiple layers of closely-spaced screen mesh have been used to create a combined bubble point capability far in excess of that achievable with a single layer of mesh. This concept was investigated under MDAC IRAD (Reference 8). It was found that if the spacing of the individual layers is appropriate, the combined bubble point of a multilayer stack is proportional to the number of layers, thus offering apparently unlimited bubble point potential. This increase is achieved only when the region between the individual layers of screen is occupied by gas while the screens remain wetted. The pressure within the gas regions varies in a linear fashion through the stack, with the difference between successive gas regions being equal, approximately, to the bubble point pressure of the intervening screen.

The gas regions necessary to create a large overall bubble point pressure create a problem once liquid flow through the screen is to be established. Within the multilayer element, the gas can completely blanket each screen layer, thus blocking the liquid flow even with some portion of the multilayer screen in contact with the bulk propellant. This trapped gas must be disposed of, which leads to two consequences:

The trapped gas will be forced downstream into the propellant feed system with potentially unfavorable results.

In order to force the gas (or some portion of it) from between the screen, the differential pressure across the multilayer elements must exceed the overall bubble point.

The second item above can also result in gas breaking into the feed system through portions of multilayer screen exposed to the ullage in other portions of the tank.

The two features discussed have been demonstrated in a laboratory setup wherein alcohol was transferred between two clear plastic tanks via a multilayer screen element. Figure 56 illustrates the important features of this demonstration. The screen unit contained three layers of 30 x 250 plain dutch mesh which gave the unit an overall bubble point of 15.3 cm water column (W.C.) in isopropyl alcohol. Figure 56A shows that liquid was expelled from the supply to the receiver tank until the transfer line was cleared of all trapped gas. The liquid level was then lowered in the supply tank by draining from the bottom until the screen unit was surrounded by ullage. A pressure differential (ΔP) of 32.3 cm W.C. was imposed on the screen layers by this ΔP in the same fashion as might result from hydrostatic forces developed during lateral accelerations while a vehicle is in a coast mode. Next, the screen unit was covered by adding alcohol to the supply tank. Trapped gas still blanketed two of the three screen layers. A ΔP of 7.6 cm W.C. produced no liquid flow out of the supply tank. Increasing the ΔP to approximately 10 cm W.C. caused some of the interlayer gas to pass into the transfer line (see Figure 56C) at which point liquid transfer was established. The full bubble point of 15 cm W.C. was not required to purge the gas, because the lowermost screen layer was submerged in liquid rather than gas.

These tests point out that techniques must be developed to dispose of, or render harmless, the gas that enters between the screen layers. The high ΔP associated with the initial liquid flow through the entrapped gas layers is also undesirable in that it may cause portions of the screen acquisition device to fail. These two difficulties must be addressed before multilayer screen elements can be reliably used.

4. Film Bubble Point Procedure Feasibility Test. Bubble-point testing is usually accomplished by submerging the screen in fluid and then pressurizing one side of the screen. At the outset of this study, channel preliminary designs were evolved to permit this type of checkout test on the channel as installed in the completed cryogen tank with no tank access requirement. This led to the solid channel design with screen on only one face which would facilitate immersion bubble-point testing. However, the design studies have shown that a significant design improvement can be achieved with all-screen channels. This will require a new method of bubble-point testing which does not require access to or removal of the acquisition system and can be performed during the normal refurbishment of the vehicle. It was found during the bubble point testing of the interface demonstration unit (IDU) being fabricated by MDAC under NAS 8-27571, that the screen could be kept completely wet with alcohol simply by pouring alcohol over the screen. The thin film of liquid formed an individual meniscus at each pore of the screen, and excess liquid flowed off the screen. Since each pore was closed with its individual meniscus, there was no hydrostatic head exerted along the full height of screen, and the total wetted screen height exceeded the height which could be supported if the screen devices were full of liquid. Therefore, it was practical to determine the bubble point pressure of the screen without completely submerging the device in liquid.

The problem with the procedure, when applied to large-scale vehicles without direct access to the screen, is that the entire screen surface must be wetted and evaporation controlled. One solution, which has been successfully demonstrated in a recent bench test, involves flowing saturated vapor of

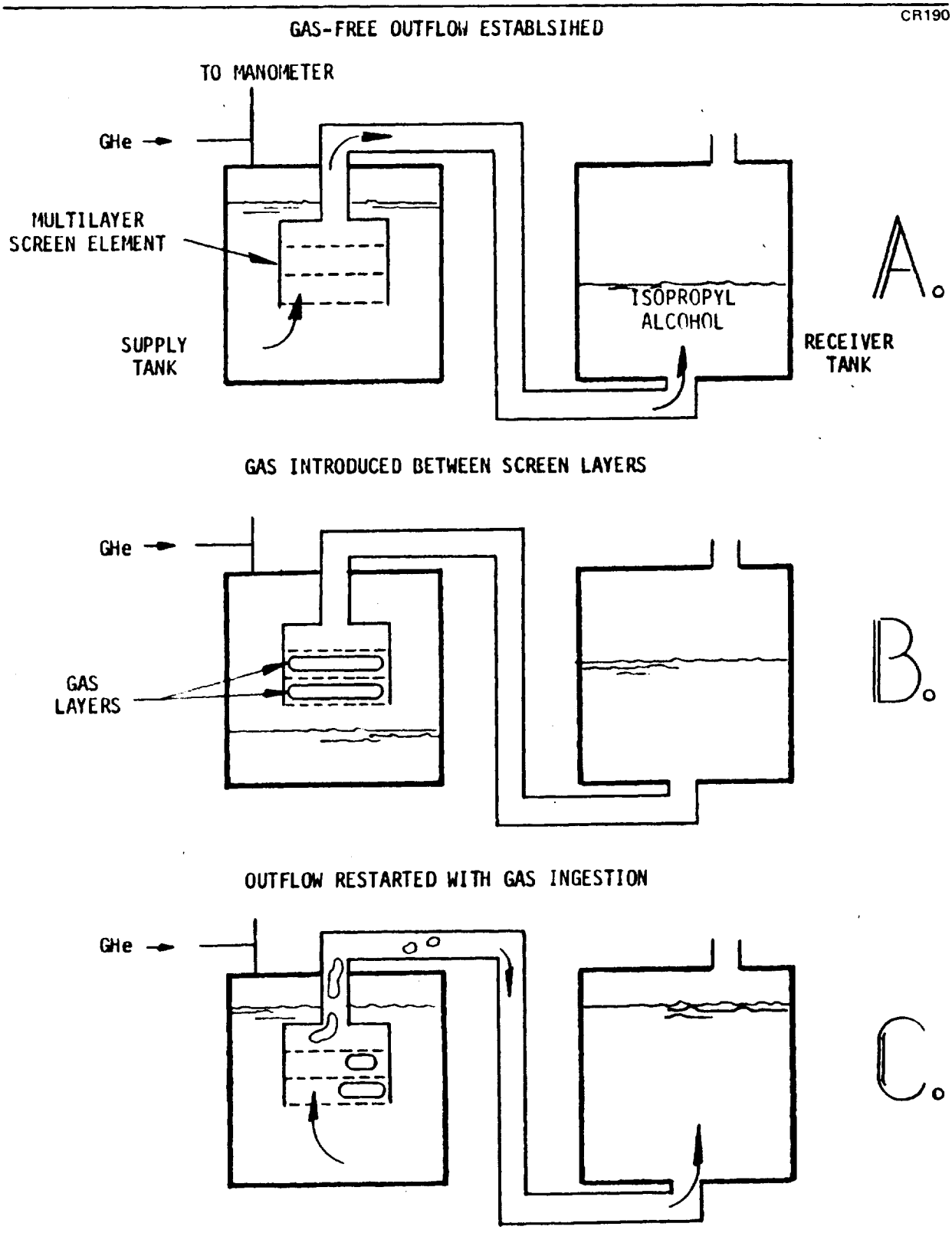

Figure 56. Multilayer Screen Flow Test

an appropriate bubble point test fluid (methanol, Freon 114, isopropyl alcohol, etc.) into the screen device and tank, which are maintained at a temperature below that required for condensation.

Vacuum-pumping the extraneous gases from the tank or purging the tank with the test vapor assures a one-component system; therefore, evaporation from the screen due to diffusion is alleviated. Maintaining the tank at a constant temperature assures that an equilibrium, steady-state condition is obtained in which the condensed film on the screen pores remains indefinitely. Bubble point measurements can then be taken.

The apparatus shown in Figure 57 was used to demonstrate that condensation would seal all of the pores of a screen. A cylindrical screen, 200 x 600 mesh, 3.2 cm diameter and 24 cm length, was supported in the center of a 2,000 ml vacuum test flask. Isopropyl alcohol was heated to the boiling point (82 °C) in a separate vapor supply flask. A vacuum pump was used to remove the air in the test flask. The vacuum pump was disconnected after closing the valve between the vacuum pump and test flask. The valve between the vapor supply flask and test flask was then opened, and vapor flowed into the cooler test flask, condensing on the screen and walls. A bubble point test was then made using nitrogen gas at room temperature, which demonstrated that approximately 15 cm of water column pressure was obtained, as had been observed in an earlier submerged bubble point test. Since the height of the screen device is 24 cm, whereas a column of alcohol only 15-18 cm high could be supported, this test further confirmed that a film of liquid blocking each pore in the screen could be used to test the bubble point of screens in 1-G with heights exceeding those obtainable with columns of liquid.

However, since the test flask was not insulated and was much warmer than room temperature (20 °C), a steady-state condition was not reached. As the flask cooled, the alcohol on the warmer screen began to evaporate, with condensation occurring on the walls of the flasks. The test flask pressure dropped, and the resulting pressure difference between the inner region of the screen and the flask, coupled with the evaporation of the liquid sealing the screen pores, led to breakdown within 10 to 15 seconds. The test was then repeated with the flask at room temperature, and it was found that by wetting the screen by shaking the flask, the film of liquid sealed the pores indefinitely; again, a bubble point of 15 cm of water column was achieved. This second test demonstrated that a steady-state condition could be achieved with the screen pores sealed, if the flask equaled the ambient temperature, or, in general, if the test flask were approximately adiabatic.

To assure that no pores were unsealed, leading to a low leakage rate and false bubble point reading, two procedures were used. First, the absolute pressure of the test flask was monitored during the adiabatic test and was found to be constant. A more precise proof that no pores leaked was achieved inadvertently, however. Some alcohol had drained into the transparent tube leading from the needle valve (used to control the nitrogen gas flow) into the cylindrical screen. Thus, any nitrogen gas flowing into the screen device first had to bubble through the alcohol. These bubbles were more easily observed than the escaping bubbles from the standard bubble-point test technique with the screen submerged in the test liquid. For the adiabatic

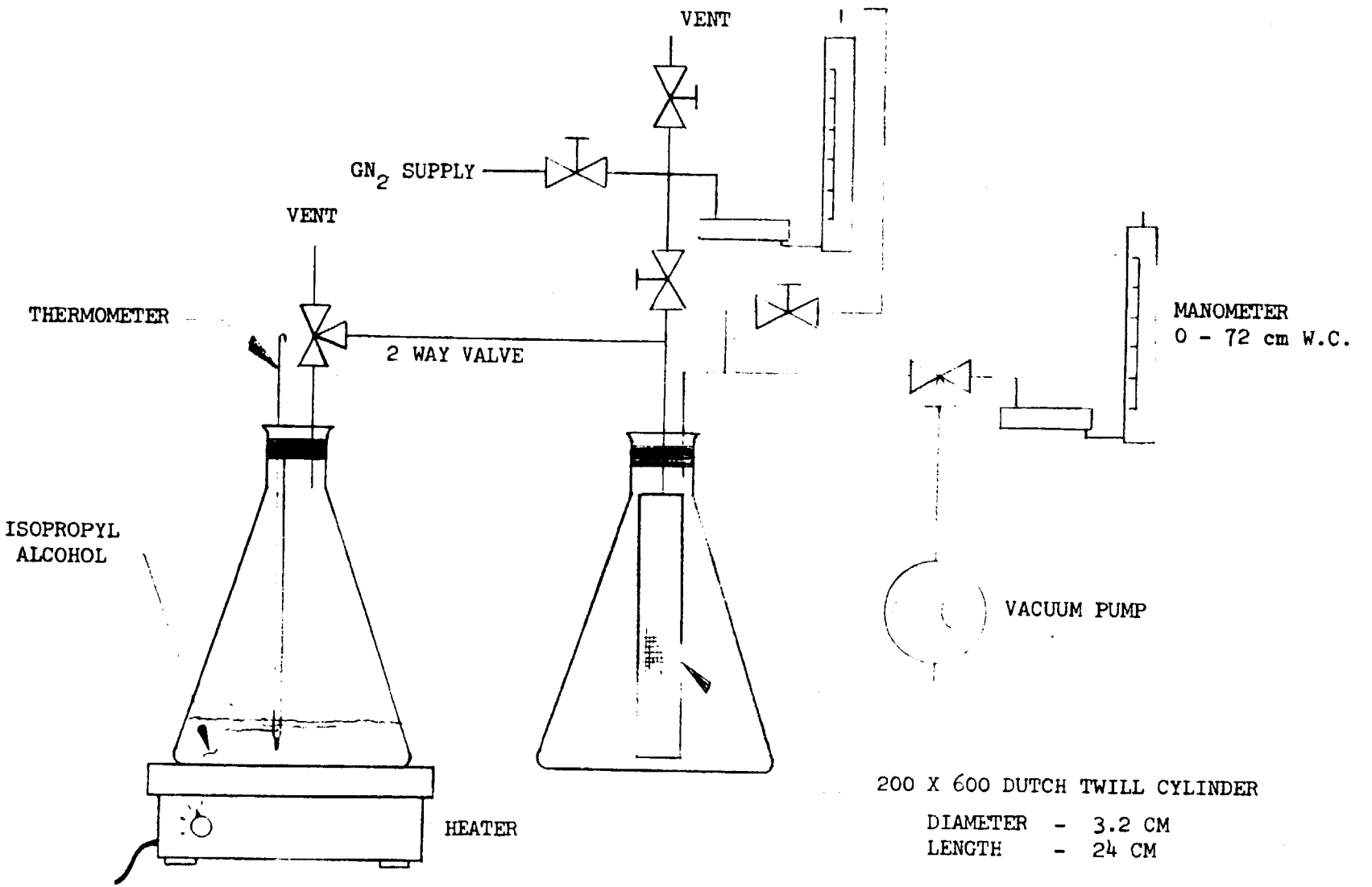

Figure 57. Film Bubble Point Evaluation Test Apparatus

test, it was found that a bubble point of 15 cm of water column was maintained for more than five minutes with no movement of any nitrogen bubbles through the alcohol.

The above bubble-point test was a rather simple demonstration of the principle of condensation sealing of a screen, and it is felt that more extensive tests are desirable. However, the implication for screen devices is clear: all screen channels or other such localized or distributed screen devices can be tested in one-g without disassembly and removal from the propellant tanks. For localized devices, such as the start tank, it is probably more practical to forego condensing of the bubble point test vapor and simply fill the tank with liquid, allow the liquid to drain off while replacing the liquid volume with saturated alcohol vapor, and then proceed with the bubble point test. With large tanks, the weight of the test fluid would be prohibitive and, therefore, the condensation technique would be used.

Based on the test results described above, as well as the bubble point test procedure used with the IDU under Contract NAS 8-27571, all screen channels can now be considered viable candidates for large, reusable vehicles without the additional costs and operational complexities of screen removal and testing prior to each flight. Only if the screens fail to meet the bubble point specification would removal and inspection be required.

5. Settling Tests With Screens. Tests to show the influence of screens or propellant settling were conducted using available plexiglas tank models. The tests were conducted with distilled, deionized water with a potassium permanganate dye. Three plexiglass tank models were used: 15.24 cm (6-inch), 20.3 cm (8-inch), and 30.5 cm (12-inch) diameter with horizontal 200 x 600 mesh screens across the tank, a few inches above the bottom. The 20.3 and 30.5 cm models had inverted hemispherical domes which simulated the integrated tankage tank bottom recommended in our designs. The horizontal screen simulated the main tank screens used to facilitate settlings. Figure 58 shows the test hardware which was used in earlier MDAC IRAD projects.

Settling was simulated by stretching a rubber diaphragm across the tank diameter and supporting the water above it; the region beneath the diaphragm was pressurized slightly, so that the initial shape simulated that of a liquid-vapor interface in a low-gravity environment. The diaphragm was then ruptured, allowing the liquid to fall to the bottom of the tank and impact the screen, A Millikan DBM camera at 64 frames per second was used to photograph the settling tests. Test procedures of this type were used by MDAC to study and characterize the liquid settling process under its IRAD program (see Reference 9). Figure 59 shows frames taken for the various test movies. Films of all tests have been provided to NASA.

The general results of the tests were as summarized below:

a. Liquid penetration through the screen at impact was much less than expected in all cases. Liquid initially impacting the screen penetrated slightly, but it appears that most of the liquid is deflected by the screen, flows along the screen, and thus wets it. Once the screen is wetted, there is little further penetration. In addition, the liquid supported by the screen dissipates the momentum of the remaining falling liquid, and quickly causes

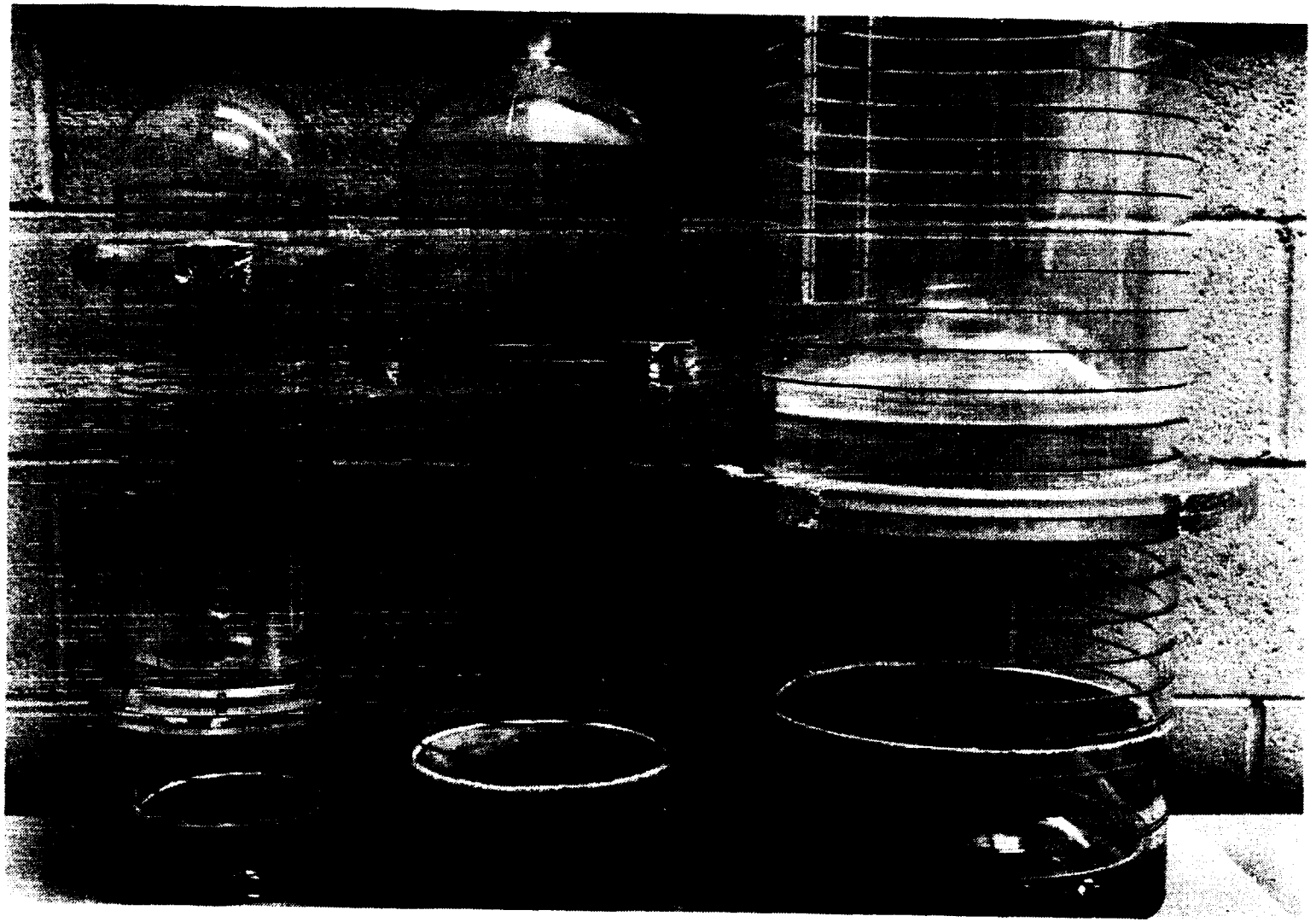

Figure 58. Tank Model for Settling Tests

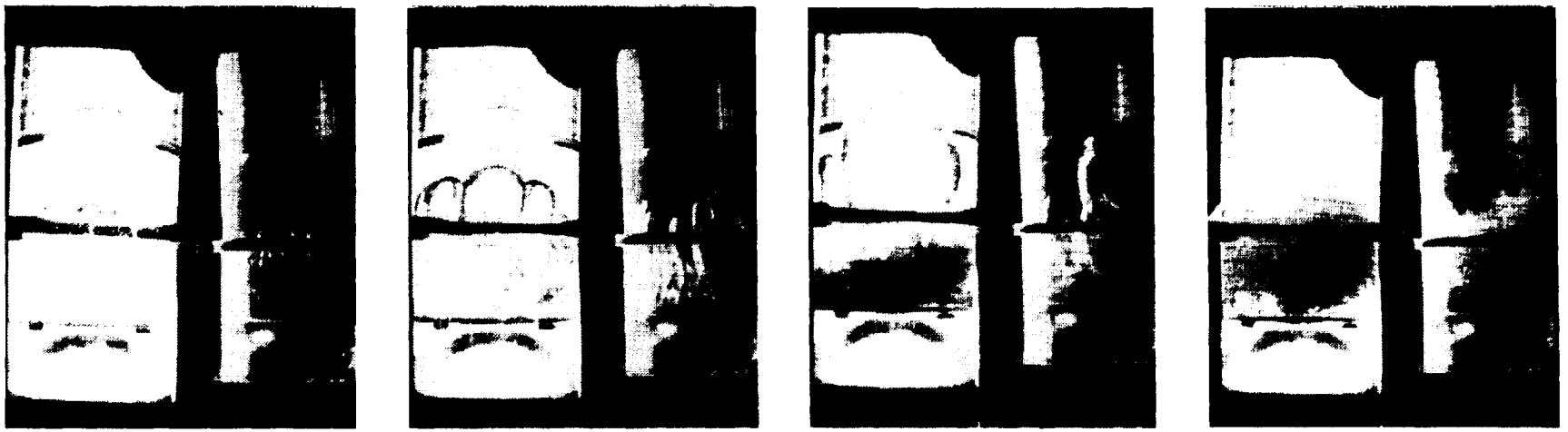

30 CM (12 IN.) DIAMETER TANK

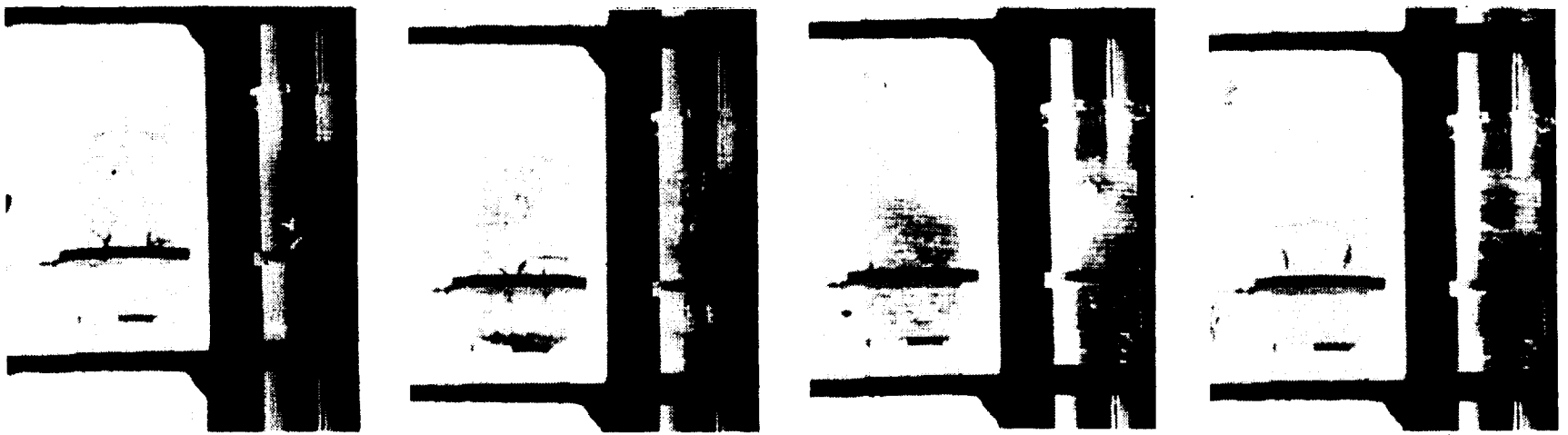

15 CM (6 IN.) DIAMETER TANK

Figure 59a. Settling Tests with Screen

15 CM (6 IN.) DIAMETER TANK (TILTED)

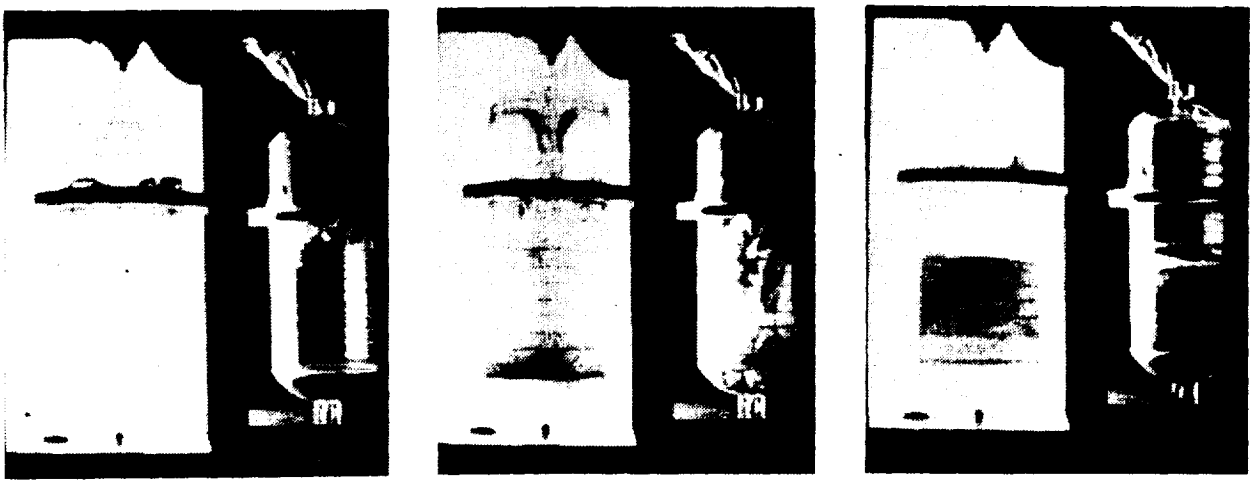

20 CM (8 IN.) DIAMETER TANK

30 CM (12 IN.) DIAMETER TANK

Figure 59b. Settling Tests with Screen

all penetration to cease. The liquid is then supported by the required gas pressure increase beneath the screen, and the screen stabilizes the liquid interface.

b. Bubble formation and turbulence above the screen is similar to that seen with similar tests with tanks having solid bottoms.

c. One test was performed with clean liquid held under the screen, and the dyed liquid supported by the diaphragm. The impact of the dyed liquid on the screen gave no indication of bubble penetration or liquid penetration and mixing.

These test results indicate that screen device refill rates due to liquid momentum will be reduced as a result of screen wetting and gas entrapment as the liquid falls. Further, the liquid dynamics for settling are best approximated by using the tank geometry with the main tank screen as an effectively solid membrane. If it is necessary to refill a region beneath a main tank screen, these test results indicate that positive means of venting this region are required, since liquid dynamics can quickly wet and effectively seal the screen, entrapping gas.

SECTION 3. SUMMARY AND CONCLUSIONS

The supporting experimental program proved to be of considerable value in exploring the critical design concepts and evaluating appropriate design criteria to be applied to the developed cryogenic feed systems. A number of important results and conclusions can be drawn from this work.

a. Minimum screen bubble points with LH_2 can be predicted within 10 percent by appropriately correcting, for density and surface tension, test data obtained with isopropyl alcohol. Test data indicate the predicted bubble point will be conservative.

b. Screen flow loss data were obtained for a broad range of screen mesh materials and were found to be less than that obtained using the standard Armour and Cannon correlation technique; in some cases, flow losses were half that predicted by the Armour and Cannon correlation. Robusta screens, however, generally have higher flow losses than predicted by the Armour and Cannon correlation.

c. To minimize screen mesh/backup plate pressure loss, a coarse mesh screen should be used as a separator between the fine mesh and the backup structure.

d. Conventional screen pleating, when carefully done, produces only a slight loss in bubble point performance (less than 20 percent) and no significant increase in flow loss.

e. Anticipated screen deflection does not appear to be a serious source of degradation for screen acquisition devices.

f. A variety of welding techniques is available for fabricating screen devices with no significant degradation in basic bubble point or retention performance.

g. Duct structures made from aluminum sheet as thin as 0.05 cm (0.020 inch) can be made with significant structural rigidity for practical systems. However, riveted structures which were tested did not provide leak-free joints. Mechanical attachments with sealing elements or welded joints are therefore recommended.

h. Conventional Marmon-type couplings provide a convenient attachment technique and, when used with Creavey-type O-ring seals, achieve more than adequate sealing for acquisition channels.

i. Although more work is required to develop LO_2-compatible repair techniques, polyurethane adhesive is a good material for repairing small flaws or imperfections in the completed acquisition device.

j. Large all-screen devices can be checked out for bubble point performances, as in a qualification test operation, using a liquid film technique rather than complete immersion.

k. Although multiple layer screens can be used to increase hydrostatic head retention in a flow system, the gas trapped between the screen layers will be ingested into the outlet flow and can therefore result in potential downstream problems, as well as requiring increased ΔP to initiate flow.

l. Screen vibration can result in alteration of the retention characteristics of the basic screen. Reliable prediction techniques are not currently available.

m. Direct heat transfer to a screen retaining LH_2 or thermal-induced tank pressure decay has been observed to cause premature breakdown of the screen.

n. Screen baffles retard liquid and ullage flow during propellant dynamic settling.

The tests conducted as part of this program were basically exploratory in nature, and several areas were uncovered which require more definitive experimental and analytical research. These primarily relate to environmental conditions imposed on the screen device and include the following:

a. The influence of ullage gas heating on basic screen retention.

b. The effects of vibration on screen breakdown.

In addition, the analysis of transient flow effects due to feedline valve operation and pump startup/shutdown dynamics (see Volume I) demonstrates the need for further experimental work in this area, and consideration of these effects in screen device designs.

APPENDIX A

SUPPLEMENTARY SCREEN FLOW LOSS DATA

Additional screen flow loss data are presented below. Figure A-1 shows flow loss, as expressed by the Poiseuille number (P_o), versus the Reynolds number for three screens supported directly on a 51 percent open area backup plate have 3/16 inch holes with 1/4 inch center spacings. Helium and GN_2 were used as the test fluids. Figure A-2 shows the flow loss versus Reynolds number for 250 x 1370 screen supported by seven different backup plates, and without a plate. This figure shows that the flow loss is increased by the use of backup plates without spacers, and that the flow loss increases as the flow area decreases, as expected.

Tests with three different spacer materials yielded identical results, as shown in Table A-1. Spacers used were a 1/16 inch cork spacer, to lift the 250 x 1370 screen off of the backup plate, a 10 x 10 x 0.025 wire spacer, and a 16 x 16 ("window screen") spacer. Pressure drops versus flow rates were equal within expected experimental accuracy.

Further, the pressure drop versus flow rate for a screen with spacers and a perforated backup plate is essentially equal to that due to the effective flow area through the screen being increased to that of the screen alone. Negligible additional flow loss occurs from flow through the spacer screen and between the fine mesh screen and backup plate solid area.

The friction factor correlation and geometrical properties of screens used in this study are presented in Tables A-2 and A-3.

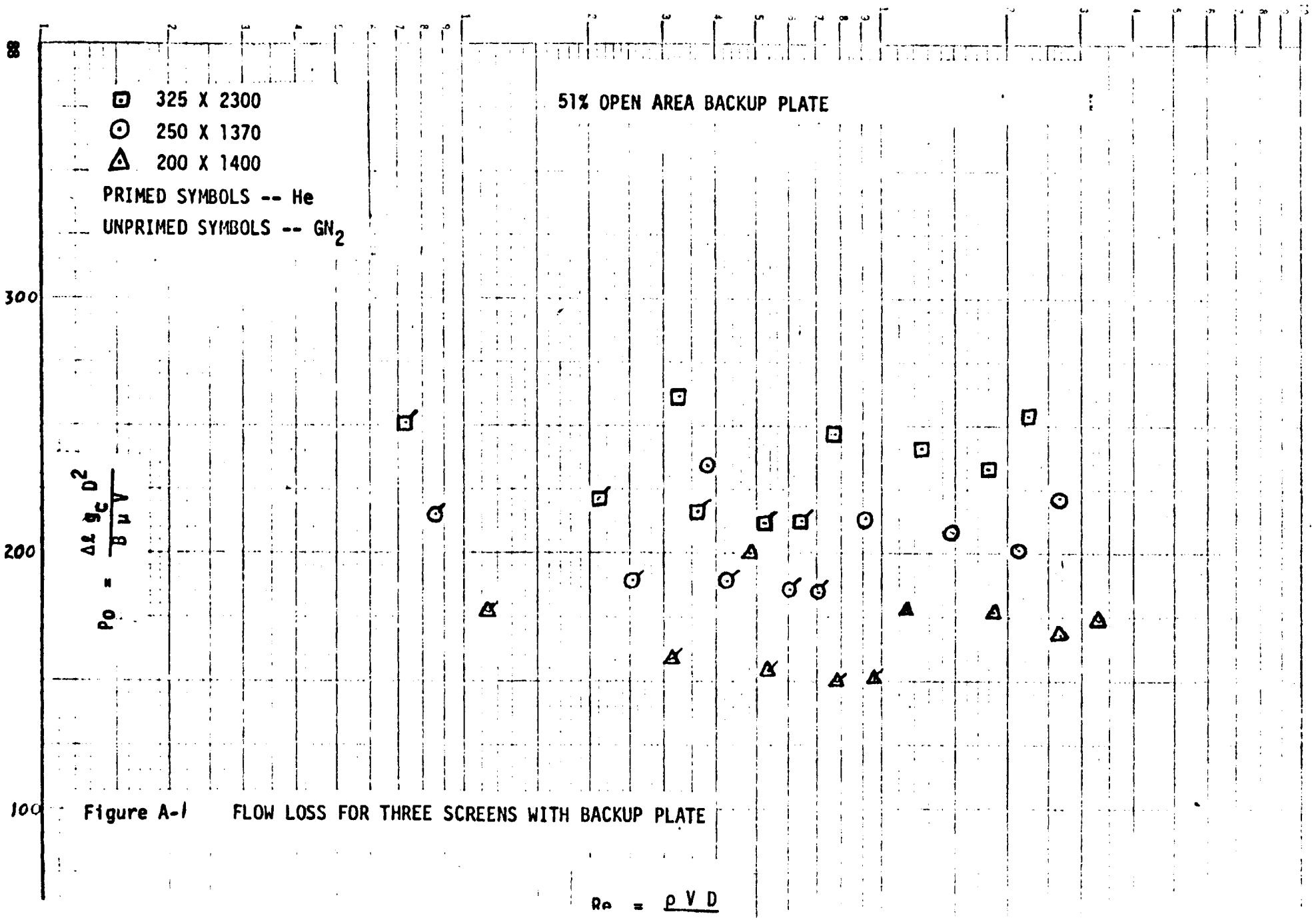

Figure A-1 FLOW LOSS FOR THREE SCREENS WITH BACKUP PLATE

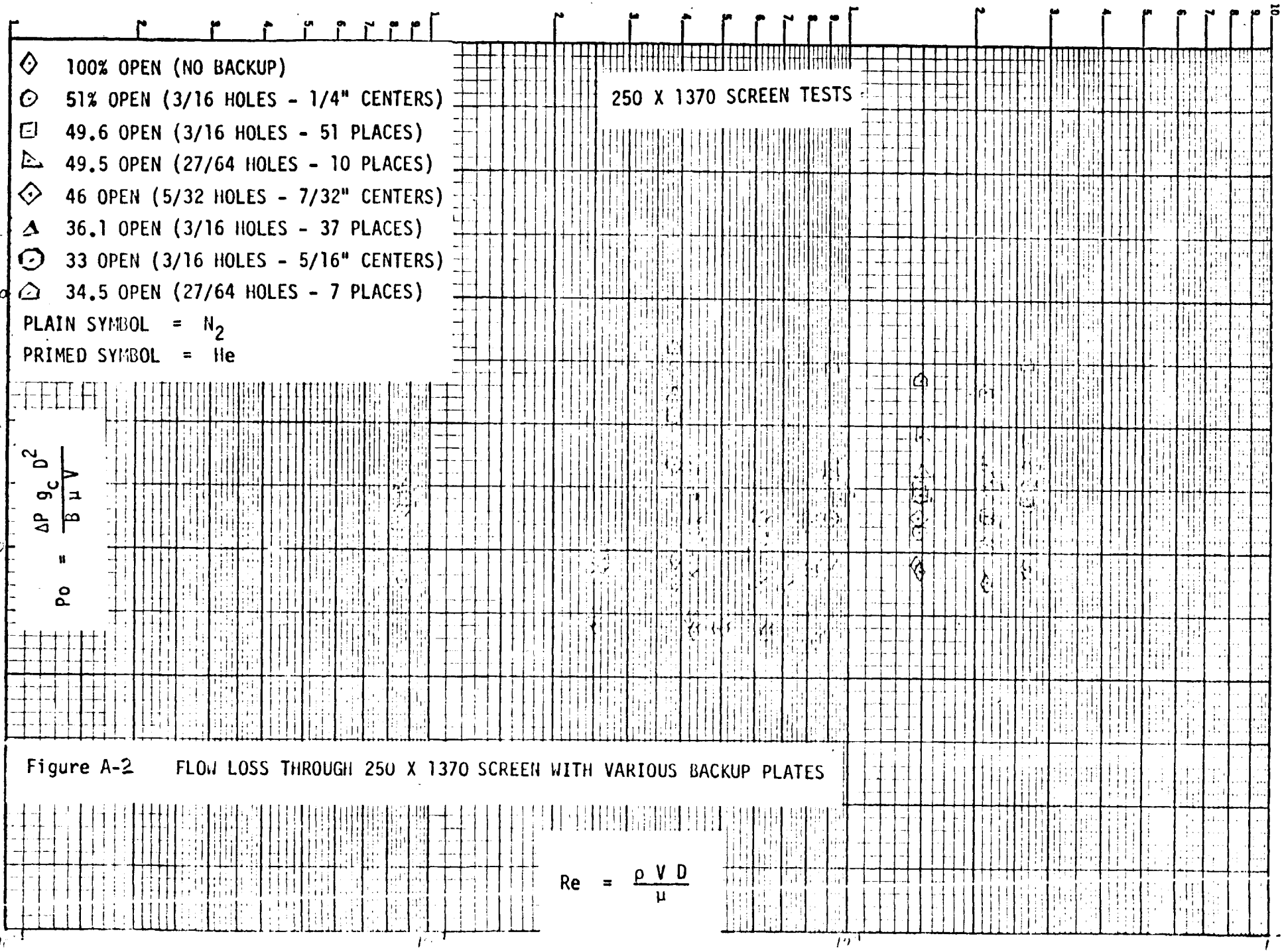

Figure A-2 FLOW LOSS THROUGH 250 X 1370 SCREEN WITH VARIOUS BACKUP PLATES

Table A-1

COMPARISON OF PRESSURE DROP/FLOW RATE FOR 250 X 1370 SCREEN WITH BACKUP PLATES AND VARIOUS SPACERS

Test No.	ΔP	P_{Static}	$\dot{W}$	Gas	Porous Material Code
272	.22	9.5	5	N_2	A
273	.49	20.3	10		
274	.78	24.9	15		
275	1.04	40.5	20		
276	1.31	47.5	25		
277	.23	13.8	5		B
278	.47	54.6	10		
279	.78	42.6	15		
280	1.07	47.6	20		
281	1.33	57.3	25		
282	.23	10.3	5		C
283	.51	23.3	10		
284	.78	50.5	15		
285	1.10	43.1	20		
286	1.37	52.3	25		

Porous Material		
A	B	C
250 x 1370 1/16 Inch Cork Spacer 27/64 - 7 holes	250 x 1370 10 x 10 x 0.025 Spacer 27/64 - 7 holes	250 x 1370 16 x 16 x Window Screen 27/64 - 7 holes

Table A-2

CALCULATION OF GEOMETRICAL PROPERTIES

TWILLED DUTCH

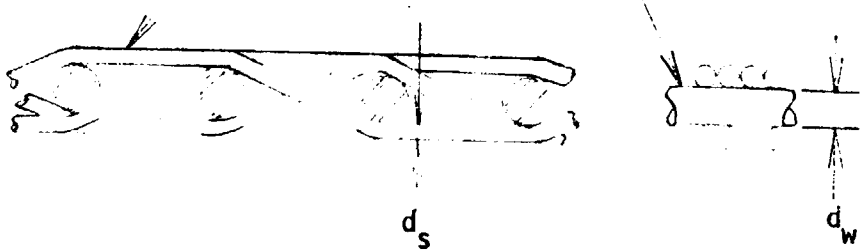

PLAIN WEAVE

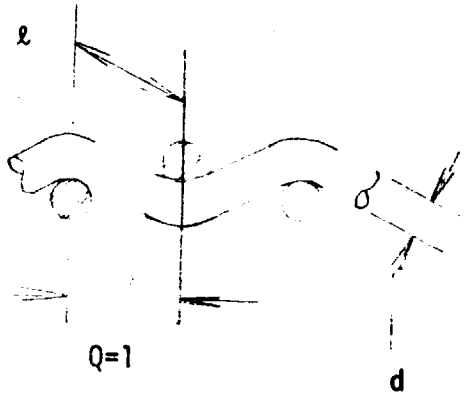

SCREEN	THICKNESS, B (FT)	SURFACE AREA TO VOLUME RATIO A (FT)	VOID FRACTION ϵ	PORE DIAMETER D (FT)
PLAIN WEAVE	2d/12	$\frac{2\pi N^2 d\ell}{B}$ WHERE $\ell = \left[d^2 + 1/N^2\right]^{1/2}$	$1 - \frac{2\pi N^2 d^2 \ell}{48B}$	$\left[\frac{1 - 2Nd + N^2d^2}{N^2}\right]^{1/2} \frac{1}{12}$
TWILLED DUTCH	$\frac{d_w + 2d_s}{12}$	$\frac{\pi}{B}\left[N_w d_w + 1/2\, N_s d_s + 1/2\, N_s N_w d_s \ell_1\right]$ WHERE $\ell_1 = \left[\left(d_s + d_w\right)^2 + 1/N_w^2\right]^{1/2}$	$1 - \frac{\Pi}{48B}\left[N_w d_w^2 + 1/2 N_s d_s^2 + 1/2 N_w N_s d_s^2 \ell_1\right]$	USE MANUFACTURE'S NOMINAL MICRON RATING

TABLE II

Table A-3

FRICTION FACTOR CORRELATION

$$f = \frac{8.6}{NR_e} + 0.52$$

f	Friction Factor, $\frac{\Delta P\ \epsilon^2 D}{QB\rho U^2}$
N_{Re}	Reynolds No., $\frac{U}{\nu a^2 D}$
ΔP	Pressure Drop (lbf/ft^2)
U	Fluid Approach Velcity (ft/sec)
B	Screen Thickness (ft)
ν	Fluid Kinematic Viscosity (ft^2/sec)
a	Surface Area to Unit Volume Ratio of Screen Wire (1/ft)
ϵ	Screen Volume Void Fraction
ρ	Fluid Density ($slug/ft^3$)
N	Mesh Count (wires/in.)
Q	Tortuosity Factor
	$Q = 1$ Plain Weave
	$Q = 1.3$ Dutch Weave
d	Wire Diameter (in.)
Subscripts:	
s	Shute
w	Warp

APPENDIX B

PRESSURE DECAY AND HEAT TRANSFER INDUCED BREAKDOWN WITH "MILK CARTON" SCREEN DEVICE

The liquid hydrogen breakdown data obtained using the milk-carton-shaped screen device are compiled in Table B-1. Particular attention should be given to tests 9a and b, 10a and b, and 12, since screen breakdown was observed with measured temperature differences between liquid and gas of the order of 10° to 20°R. These recorded screen breakdown results are further substantiated by direct observation, as noted in tests 2, 4, 5a and b, 7a, b, and c, and 8a, b, and c.

Table B-1

Test No.	Hold Pressure (psig)	Hold Time (min)	Temperature Beginning of Hold T_1 Top of Insulated Box	Temperature Beginning of Hold T_2 Bulk Liquid	Temperature End of Hold T_1	Temperature End of Hold T_2	Failure Pressure (psig)	Failure Temperature T_1	Failure Temperature T_2	Diffuser	L&N Record	Remarks
1.	Max 35 Starts Out Lower	2					14			Submerged	No	Hold period not constant so liquid level varies during test. Level not down at time of failure. Most GH_2 condenses in the LH_2 heat exchanger when used (plus excessive boiloff).
2.	35	0	63°R				55			Overhead	No	Screen fails at beginning of hold (probably due to warm gas).
3.	35	2	-403		-414		20	-418	-418	Overhead	Yes	Prepressurize with screen lowered (this now becomes standard procedure). Nonlinear pressure decay because of vent limitations.
4.	35	15	-400	-415	-400	-414	26	-416.5	-417	Overhead	Yes	Gas pocket forms during hold period (may have been caused by pounding on lid, more likely due to heat transfer-pocket grows from approximately 3/4" to 1-1/2" during test). Boiling at failure seems to come from screen sides but top can't be seen since light absorbed by surface fog.
5a.	35	0						-392		Overhead	No	Fails when set upright. } Result of warm gas due to shorter chill-down time.
b.	35	0						-392		Overhead	No	Fails when set upright.
c.	35	0	-414	-414			10	-420.5		Overhead	Yes	No hold period, immediate decay (non-linear) Did not fail when set upright. Failure point could not clearly be seen because of boiling in dewar. Probably no head difference.
6.	35	2	-409.6	-421.8	-414.1	-421.9				Overhead	Yes	No failure observed. Liquid level high in box.
7a.	35	0						-404.6		Overhead	No	Immediate failure due to gas impingement. } Gas was bled in as an attempt to hold box full of gas.
b.	35	0						-405.6		Overhead	No	
c.	35	0						-405.2	-415.8	Overhead	No	
d.	35	2	-412.3	-415.9	-404.7	-416.7				Overhead	Yes	Failed at beginning of decay period. Rising value for T_1 during hold is unexplained.
8a.	35	0						-405.6	-417.6	Overhead	No	Immediate failure with no gas impingement.
b.	35	0						-405.8	-416.5	Overhead	No	Immediate failure with no gas impingement.
c.	35	0						-405.8		Overhead	No	Immediate failure with no gas impingement.
d.	35	2	-406.7	-419.8			20	-414.2	-419.6	Overhead	Yes	Failure not seen clearly.
9a.	35	145	-408.1	-422.2	-414.2	-421.8				Overhead	Yes	On film. Carton inverted, set upright during first hold because of suspected failure. No gas inflow and immediate failure in both cases.
b.	35	145	-414.2	-421.8	-414.2	-421.9				Overhead	Yes	
10a.	10		-408.4	-422.2						Overhead	No	On film. Two repeated failures when carton set up into gas.
b.	10	120 sec	-408.8									
11.	35	15	-405		-417.6			-410.4		Overhead	Yes	No observed failure. Liquid level rose out of sight. Little or no head difference.
12.	0	0						-410.4		Overhead	No	Fails after 7 seconds due to impingement.
13.	0	0								Overhead	No	No failure. Max $\Delta T \approx 10°R$, with low head difference.

REFERENCES

1 J. N. Castle, "Cryogenic Bubble Point Testing of Selected Screens," MDAC Report MDC G2389, August 1971.

2 J. C. Armour and J. N. Cannon, "Fluid Flow Through Woven Screens," AIChE Journal, May 1968, pp 415-420.

3 "Low Gravity Propellant Control Using Capillary Devices in Large Scale Cryogenic Vehicles," related IRAD Studies, Contract NAS 8-21465, Report No. GDC-DDB70-009, August 1970.

4 J. N. Castle, "Heat Transfer Effects on Bubble Point Tests in Liquid Nitrogen," MDAC Report MDC G2653, January 1972.

5 E. G. Brentari, et. Al. "Boiling Heat Transfer for Oxygen, Nitrogen, Hydrogen and Helium," NBS TN No. 317, September 1965.

6 "Design Analysis of Cryogenic Tankage Concepts," NAR Report SD72-SA-0025,

7 G. F. Orton, "Simulated Flight Vibration Testing of a Surface Tension Propellant Expulsion Screen," MDAC Report MDC E0091, January 1970.

8 B. R. Heckman, "Bubble Point Characteristics of Multi-Layer Screen Elements," MDAC Report MDC G2656, December 1971.

9 G. W. Burge, J. B. Blackmon, R. A. Madsen, "Analytical Approaches for the Design of Orbital Refueling Systems," AIAA Paper No. 69-567, June 1969.

U.S. DEPARTMENT OF COMMERCE
Technology Administration
National Technical Information Service
Springfield, VA 22161 (703) 605-6000